ABSTRACT

Name: John E. Carr

Department: Chemistry & Biochemistry

Title: Investigation of Inductively Coupled Plasma Mass Spectrometry with Ultrasonic Nebulization and Membrane Desolvation Sample Introduction as a Liquid Chromatography Detector for Heteroatom-Containing Pharmaceutical Compounds

Major: Chemistry

Degree: Doctor of Philosophy

Approved by:

Jon W. Carnahan

Dissertation Director

Date:

3/21/07

NORTHERN ILLINOIS UNIVERSITY

ABSTRACT

Inductively coupled plasmas (ICPs) efficiently excite and ionize metals and semi-metals allowing for their detection by atomic emission spectroscopy (AES) or mass spectrometry (MS). Nonmetal analytes are more difficult to detect due to their higher excitation and ionization energies. The sensitive detection of nonmetal analytes is becoming increasingly important in the pharmaceutical industry as new drug compounds and impurities containing nonmetals are being developed. These compounds are typically detected after they are separated by high performance liquid chromatography (HPLC). The research presented in this dissertation investigates the application of ultrasonic nebulization and membrane desolvation (USN-MD) with ICP-MS and ICP-AES as detectors for nonmetal analytes speciated by HPLC.

A study identified which HPLC mobile phases and buffers lead to sensitive determinations for a phosphorus-containing analyte with ICP-AES and ICP-MS detection. For ICP-AES detection, neither large signal enhancements nor degradations were observed for the buffers and mobile phase combinations tested. It was determined that gradient elution could be performed with USN-MD-ICP-AES detection. For ICP-MS detection, effects of these buffers were more significant. A large decrease in sensitivity was noted when the mobile phase included organic solvents. Isocratic elution conditions are suggested when USN-MD-ICP-MS detection is utilized.

The addition of supplemental gases to the nebulizer gas flow of an ICP-MS was also investigated. For oxygen addition, signal degradation was noted for sulfur-, phosphorus-, and chlorine-containing analytes. It was determined that 6% oxygen in the nebulizer gas flow yielded efficient removal of carbon while not appreciably increasing detection limits. With nitrogen addition, a large increase in the background signal was found for phosphorus determinations. A decrease in sensitivity was found when determining sulfur. Helium addition did not produce significant deviations from standard argon ICP behavior, indicating that it is not being significantly ionized.

A final study utilized ICP-MS as a detector for the separation of several model analyte systems. It was found that significant band broadening occurred for several volatile analytes, reducing sensitivity and negatively affecting chromatographic figures of merit. However, nonvolatile analytes yielded sensitive determinations.

NORTHERN ILLINOIS UNIVERSITY

INVESTIGATION OF INDUCTIVELY COUPLED PLASMA MASS SPECTROMETRY WITH ULTRASONIC NEBULIZATION AND MEMBRANE DESOLVATION SAMPLE INTRODUCTION AS A LIQUID CHROMATOGRAPHY DETECTOR FOR HETEROATOM-CONTAINING PHARMACEUTICAL COMPOUNDS

A DISSERTATION SUBMITTED TO THE GRADUATE SCHOOL
IN PARTIAL FULFILLMENT OF THE REQUIREMENTS
FOR THE DEGREE
DOCTOR OF PHILOSOPHY

DEPARTMENT OF CHEMISTRY & BIOCHEMISTRY

BY

JOHN E. CARR

DEKALB, ILLINOIS

MAY, 2007

UMI Number: 3272146

INFORMATION TO USERS

The quality of this reproduction is dependent upon the quality of the copy submitted. Broken or indistinct print, colored or poor quality illustrations and photographs, print bleed-through, substandard margins, and improper alignment can adversely affect reproduction.

In the unlikely event that the author did not send a complete manuscript and there are missing pages, these will be noted. Also, if unauthorized copyright material had to be removed, a note will indicate the deletion.

UMI®

UMI Microform 3272146

Copyright 2007 by ProQuest Information and Learning Company.

All rights reserved. This microform edition is protected against unauthorized copying under Title 17, United States Code.

ProQuest Information and Learning Company
300 North Zeeb Road
P.O. Box 1346
Ann Arbor, MI 48106-1346

Certification:

In accordance with departmental and Graduate School policies, this dissertation is accepted in partial fulfillment of degree requirements.

Dissertation Director

3/21/07

Date

ANY USE OF MATERIAL CONTAINED
HEREIN MUST BE DULY ACKNOWLEDGED.
THE AUTHOR'S PERMISSION MUST BE OBTAINED
IF ANY PORTION IS TO BE PUBLISHED OR
INCLUDED IN A PUBLICATION.

ACKNOWLEDGEMENTS

I would like to extend my gratitude to several individuals who made this work possible. Dr. Jon Carnahan has been a great teacher and advisor. Your hard work, support, and understanding these past few years is greatly appreciated. Thank you to the members of my dissertation committee. Critically reading a 200-plus-page document represents a significant investment of time and effort. Thank you for taking this time to help me complete my studies at Northern Illinois. I greatly appreciate the support, advisement and friendship of Dr. Victor Ryzhov. Special thanks to Larry Gregerson, Dan Edwards, Charlie Caldwell, Larry Metcalf and all the other departmental support staff whose help made this research possible. I'd like to acknowledge Dr. Gregory Webster for contributing his time, effort, and critical thinking on collaborative projects over the past few years.

I'd like to thank my brothers and sisters for their love, support and understanding. I am grateful for the support and encouragement from my mother-, father- and brother-in-law. Finally, I want to thank my beautiful wife and best friend, Mariangela. You kept us focused and on task. I couldn't have done this without you. We make quite a team. I love you.

TABLE OF CONTENTS

Page

LIST OF TABLES vii

LIST OF FIGURES ix

Chapter

1. INDUCTIVELY COUPLED PLASMA ATOMIC SPECTROMETRY FOR PHARMACEUTICAL ANALYSIS..... 1

Introduction to Elemental Analysis and Common Atomization, Excitation, and Ionization Sources......... 1

Inductively Coupled Plasma Atomic Emission Spectrometry.. 9

Inductively Coupled Plasma Mass Spectrometry......... 14

Considerations for Pharmaceutical Analysis............... 18

Sample Introduction Techniques............................ 24

Research Considerations.................................... 37

2. STUDY OF SELECTED BUFFER AND MOBILE PHASE COMBINATIONS ON ANALYTICAL FIGURES OF MERIT FOR USN-MD SAMPLE INTRODUCTION FOR ICP-AES AND ICP-MS.. 38

Buffers in Reversed Phase HPLC.......................... 38

Pharmaceutical Application of Examining Chromatographic Buffer and Mobile Phase Combinations for Heteroatom Detection by ICP-AES and ICP-MS...................................... 39

Chapter Page

Experimental.... 44

Sample Introduction.... 50

ICP-AES Results.... 50

ICP-MS Results.... 60

Comparison of ICP-AES and ICP-MS Results.... 71

Conclusion.... 73

3. EFFECT OF SUPPLEMENTAL NEBULIZER GAS ON ANALYTICAL FIGURES OF MERIT FOR USN-MD-ICP-MS DETECTION OF VARIOUS HETEROATOM-CONTAINING PHARMACEUTICAL COMPOUNDS.... 77

Introduction to Nebulizer Gas Doping Experiments.... 77

Experimental.... 92

Results and Discussion for Oxygen Addition.... 97

Oxygen Study Conclusions.... 127

Results and Discussion for Nitrogen Addition.... 128

Nitrogen Study Conclusions.... 165

Results and Discussion for Helium Addition.... 167

Conclusion.... 181

4. APPLICATION OF ICP-MS AS A DETECTOR FOR HPLC: SELECTED EXAMPLES AND VOLATILITY CONSIDERATIONS.... 182

Chapter Page

Background.. 182

Experimental.. 185

HPLC-ICP-MS Detection of IPMS and Methyl-Methionine.................................... 191

IPMS and Methyl Methionine Conclusions................ 198

HPLC-USN-MD ICP-MS Analyte Volatility Concerns: DFBC, DFBB, Vitamin B_{12}, and a Bromine-Containing API.................................... 198

Results and Discussion.................................... 199

Conclusion.. 208

5. CONCLUSIONS AND FUTURE DIRECTIONS 210

Overall Summary.. 210

HPLC Mobile Phase and Buffer Study Conclusions and Suggested Future Directions............................ 210

Supplemental Nebulizer Gas Addition Conclusions and Future Directions.. 211

HPLC-USN-MD-ICP-MS Experiment Conclusions and Future Directions.. 213

REFERENCES 215

LIST OF TABLES

Table Page

1. Temperatures for common chemical flames........................ 5
2. Atomization efficiency of selected elements in an air-acetylene and N_2O-acetylene flame.. 6
3. Ionization energy of selected metals and non-metals............... 17
4. Detection limits obtained for several heteroatom-containing antibiotics using USN-MD-ICP-MS................................ 32
5. Common HPLC buffers... 41
6. ICP-AES operating parameters...................................... 47
7. ICP-MS operating parameters....................................... 49
8. Solvents and buffers utilized...................................... 51
9. Phosphorus figures of merit in methanol mobile phases for ICP-AES.. 53
10. Phosphorus figures of merit in acetonitrile mobile phases for ICP-AES.. 54
11. Phosphorus figures of merit in methanol mobile phases for ICP-MS... 62
12. Phosphorus figures of merit in acetonitrile mobile phases for ICP-MS... 63
13. Operating parameters for oxygen addition experiments............ 94
14. Operating parameters for nitrogen addition experiments........... 95
15. Operating parameters for helium addition experiments............ 96

Table Page

16. Analytical figures of merit for sulfur as amoxicillin.............. 98

17. Analytical figures of merit for phosphorus as phosphomycin..... 99

18. Analytical figures of merit for chlorine as chlorpropamide......... 100

19. Analytical figures of merit for fluorine as olfoxacin............... 101

20. Common interferents for elements of interest........................ 116

21. Tolerable nitrogen flow rates at forward powers utilized............ 131

22. Table of nitrogen flow rates yielding the lowest detection limit for phosphorus at each forward power utilized...................... 151

23. Table of nitrogen flow rates yielding the lowest detection limit for sulfur at each forward power utilized............................ 166

24. Operating parameters for separation of IPMS and methyl-methionine.. 188

25. Operating parameters for the separation of DFBC and DFBB from a bromine-containing API...................................... 189

26. Physical properties of select organohalides......................... 203

27. Comparison of select HPLC figure of merit for 2,6-DFBB......... 206

LIST OF FIGURES

Figure Page

1. Infrared spectrum of diethyl parathium.................................. 2

2. Infrared spectrum of triphenyl phosphine............................... 3

3. Quartz torch utilized to contain plasmas................................. 8

4. Temperature profile of an inductively coupled plasma................. 9

5. Atomic emission energy level diagram showing atomic excitation and emission transitions.. 11

6. Schematic of an ICP-AES instrument.................................... 12

7. Schematic of an ICP-MS instrument and the interface region.......... 15

8. Tailing factor calculation.. 22

9. Ultrasonic nebulizer and membrane desolvator.......................... 27

10. Membrane desolvator... 28

11. Isopropyl methanesulfonate.. 30

12. Structures of phosphomycin, amoxicillin, chlorpropamide, and olfoxacin.. 31

13. Calibration plot for phosphorus as phosphomycin....................... 33

14. Calibration plot for sulfur as amoxicillin.................................. 34

15. Calibration plot for chlorine as chlorpropamide.......................... 35

16. Calibration plot for fluorine as ofloxacin.................................. 36

17. Buffer capacity for phosphoric acid....................................... 40

Figure Page

18. Methanol background emission spectrum with and without membrane desolvation in a He-MIP...................................... 43

19. Schematic diagram of experimental setup for ICP-AES................ 46

20. Schematic diagram of experimental system............................. 48

21. Atomic emission spectrum of phosphomycin........................... 52

22. ICP-AES phosphorus sensitivity as a function of methanol composition... 57

23. ICP-AES phosphorus sensitivity as a function of acetonitrile composition.. 58

24. ICP-MS mass spectrum of background and phosphomycin at $^{31}P^{+}$.... 61

25. ICP-MS phosphorus detection limits as a function of methanol concentration with various buffers....................................... 64

26. ICP-MS phosphorus detection limits as a function of acetonitrile concentration with various buffers....................................... 65

27. ICP-MS phosphorus sensitivity as a function of methanol concentration for selected buffers... 66

28. ICP-MS phosphorus sensitivity as a function of acetonitrile concentration for selected buffers... 67

29. ICP-MS phosphorus detection limits as a function of methanol concentration for selected buffers... 68

30. ICP-MS phosphorus detection limits as a function of acetonitrile concentration for selected buffers... 69

31. Glass T-junction utilized in nitrogen and helium supplementary gas studies.. 86

Figure Page

32. Graph of signal to background ratio vs. applied forward power for a 100 ppb solution of phosphorus as phosphomycin................ 88

33. Graph of raw signal and background counts vs. applied forward power for a 100 ppb solution of phosphorus as phosphomycin........ 89

34. Mass spectrum of a 10 ppb Sr aqueous solution at a forward power of 350 watts.. 90

35. Mass spectrum of a 10 ppb Sr aqueous solution at a forward power of 750 watts.. 91

36. Analytical signal trends for sulfur as a function of oxygen nebulizer gas composition... 102

37. Background signal intensity for sulfur as a function of oxygen nebulizer gas composition... 103

38. Detection limits for sulfur as a function of oxygen nebulizer gas composition.. 104

39. Analytical signal trends for phosphorus as a function of oxygen nebulizer gas composition... 105

40. Background signal intensity for phosphorus as a function of oxygen nebulizer gas composition.. 106

41. Detection limits for phosphorus as a function of oxygen nebulizer gas composition.. 107

42. Analytical signal trends for chlorine as a function of oxygen nebulizer gas composition... 108

43. Background signal intensity for chlorine as a function of oxygen nebulizer gas composition.. 109

44. Detection limits for chlorine as a function of oxygen nebulizer gas composition.. 110

Figure Page

45. Analytical signal trends for fluorine as a function of oxygen nebulizer gas composition.. 111

46. Background signal intensity for fluorine as a function of oxygen nebulizer gas composition.. 112

47. Detection limits for fluorine as a function of oxygen nebulizer gas composition.. 113

48. Mass spectrum of the m/z = 48 for a 1000 ppb sulfur solution of 50:50 (ACN:Aqueous).. 117

49. Mass spectrum of aqueous background and a 100 ppb solution of phosphorus as phosphomycin.. 118

50. Plot of analytical and background signals for phosphorus at an applied forward power of 450 watts.. 133

51. Plot of analytical and background signals for phosphorus at an applied forward power of 550 watts.. 134

52. Plot of analytical and background signals for phosphorus at an applied forward power of 650 watts.. 135

53. Plot of analytical and background signals for phosphorus at an applied forward power of 750 watts.. 136

54. Plot of analytical and background signals for phosphorus at an applied forward power of 850 watts.. 137

55. Plot of analytical and background signals for phosphorus at an applied forward power of 950 watts.. 138

56. Plot of analytical and background signals for phosphorus at an applied forward power of 1050 watts.. 139

Figure Page

57. Plot of analytical and background signals for phosphorus at an applied forward power of 1150 watts.................................... 140

58. Plot of analytical and background signals for phosphorus at an applied forward power of 1250 watts.................................... 141

59. Plot of analytical and background signals for phosphorus at an applied forward power of 1350 watts.................................... 142

60. Plot of nitrogen flow rate that yields the largest analytical signal at all forward powers.. 144

61. Plot of maximum analytical signal observed for all forward powers... 145

62. Plot of nitrogen flow rate that yields the largest background signal at all forward powers.. 147

63. Plot of maximum background signal observed for all forward powers.. 148

64. Surface contour displaying S/B trends for phosphorus against applied power and nitrogen flow rate added to the nebulizer gas......... 149

65. Plot of analytical and background signals at an applied forward power of 450 watts... 153

66. Plot of analytical and background signals at an applied forward power of 550 watts... 154

67. Plot of analytical and background signals at an applied forward power of 750 watts... 155

68. Plot of analytical and background signals at an applied forward power of 1050 watts.. 156

69. Plot of analytical and background signals at an applied forward power of 1250 watts.. 157

Figure Page

70. Plot of analytical and background signals at an applied forward power of 1350 watts... 158

71. Plot of nitrogen flow rate that yields the largest analytical signal at all forward powers... 159

72. Plot of maximum analytical signal observed for all forward powers... 160

73. Plot of nitrogen flow rate that yields the largest background signal at all forward powers... 162

74. Plot of maximum background signal observed for all forward powers.. 163

75. Surface contour displaying S/B trends for sulfur against applied power and nitrogen flow rate added to the nebulizer gas................ 164

76. Plot of analytical and background signals at an applied forward power of 450 watts... 170

77. Plot of analytical and background signals at an applied forward power of 490 watts... 171

78. Plot of analytical and background signals at an applied forward power of 550 watts... 172

79. Plot of analytical and background signals at an applied forward power of 590 watts... 173

80. Plot of analytical and background signals against applied forward power with no helium added to the nebulizer gas flow.................... 174

81. Plot of analytical and background signals against applied forward power with 10 mL/min helium added to the nebulizer gas flow.......... 175

82. Plot of analytical and background signals against applied forward power with 30 mL/min helium added to the nebulizer gas flow.......... 176

Figure Page

83. Plot of S/B ratio against helium gas flow rate at an applied forward power of 450 W....... 177

84. Plot of S/B ratio against helium gas flow rate at an applied forward power of 550 W....... 178

85. Structures of 2,4-difluorobenzyl bromide, 2,6-difluorobenzyl bromide, vitamin B_1, and methyl methionine....... 186

86. Structure of vitamin B_{12} where X is a C≡N group....... 187

87. UV-VIS trace of a mixture of 5 ppt IPMS and 400 ppm methyl-methionine....... 192

88. HPLC-ESI-MS trace of a mixtue of methyl methionine and IPMS....... 193

89. Mass spectrum obtained from direct injection of IPMS into the ESI-MS....... 195

90. HPLC-ICP-MS trace monitoring $^{34}S^+$ for a 5 μL injection of a 25 ppt solution of IPMS....... 196

91. HPLC-ICP-MS trace monitoring $^{34}S^+$ for a 5 μL injection of a 400 ppm solution of methyl methionine....... 197

92. HPLC-UV-VIS trace for a 5 μL injection of a 1000 ppm mixture of the bromine-containing API and 2, 6-DFBB....... 200

93. HPLC-ICP-MS trace monitoring $^{79}Br^+$ for a 5 μL injection of a 1000 ppm mixture of the bromine-containing API and 2, 6-DFBB....... 201

94. HPLC-ICP-MS trace of a 5 μL injection of a 1000 ppm mixture of the bromine-containing API and DFBC....... 202

95. HPLC-ICP-MS trace monitoring $^{31}P^+$ for a 5 μL injection of a 45 ppm phosphorus solution of vitamin B_{12}....... 204

Figure Page

96. HPLC-ICP-MS trace monitoring $^{79}Br^{+}$ for a 5 μL injection of a 1 ppt solution of the bromine-containing API........................ 206

CHAPTER 1

INDUCTIVELY COUPLED PLASMA ATOMIC SPECTROMETRY FOR PHARMACEUTICAL ANALYSIS

Introduction to Elemental Analysis and Common Atomization, Excitation, and Ionization Sources

Elemental analysis is an essential field of analytical chemistry with the objective of identification and quantification of the constituent atoms of a sample. The utility of such analyses is in their reliance on characteristic responses of the individual atoms within a molecule rather than the response of the entire molecule. For example, the atomic emission spectrum of phosphorus is characteristically unchanged whether it is present as the insecticide diethyl parathion ($C_{10}H_{14}NO_5PS$) or the nucleophilic reagent triphenyl phosphine ($P(C_6H_5)_3$). A consistent atomic line emission signal at 253.5 nm will be evident for both compounds. Contrast this with an analytical technique such as infrared spectroscopy that measures the absorption of infrared radiation corresponding to rotational and vibrational energies between the covalently bonded atoms of a molecule. Figures 1 and 2 illustrate infrared spectra of diethyl parathion ($C_{10}H_{14}NO_5PS$) and triphenyl phosphine ($P(C_6H_5)_3$). While the

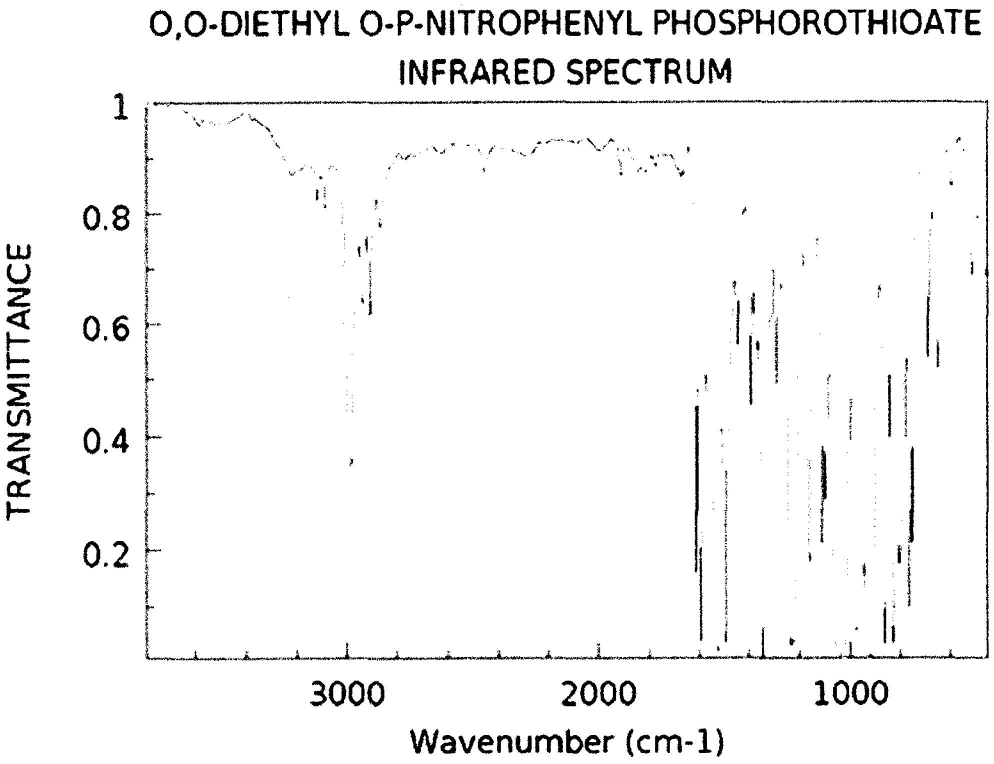

Figure 1. Infrared spectrum of diethyl parathium (adapted from NIST Chemistry WebBook[1]).

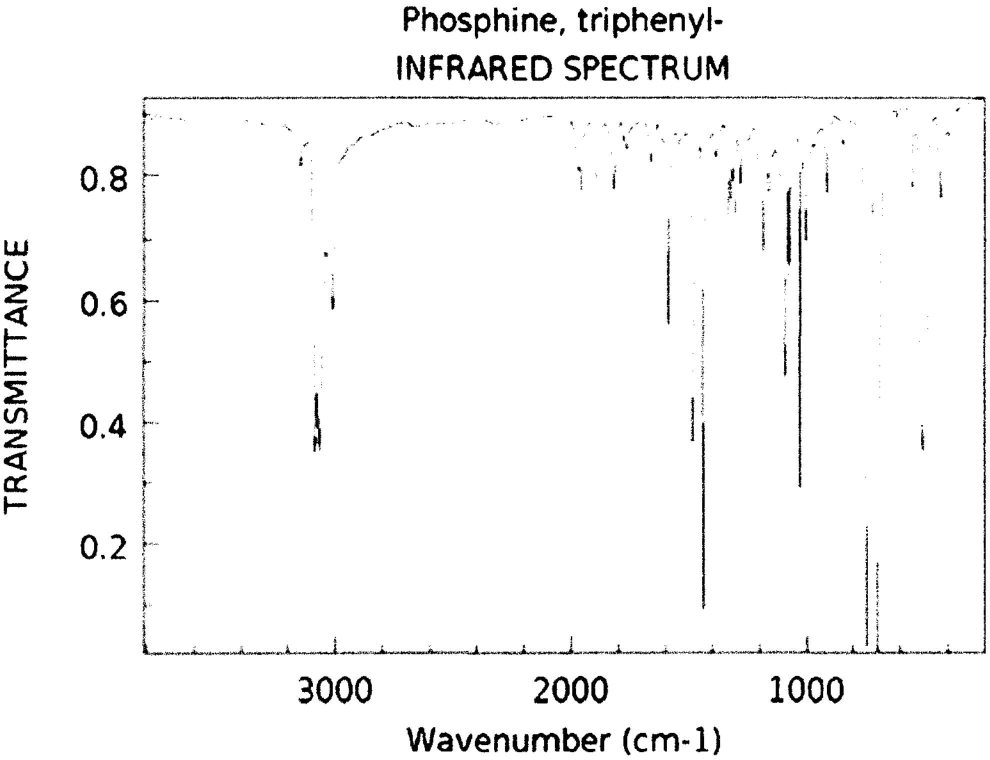

Figure 2. Infrared spectrum of triphenyl phosphine (adapted from NIST Chemistry WebBook[1]).

spectra are substantially different and make qualitative identification straightforward, it is not difficult to imagine that a sample with several compounds would yield an over-lapping spectrum making sample analyses difficult, or even impossible. Reducing a molecule into constituent atoms for identification and quantification provides atomic spectrometric techniques with unique advantages compared to other analytical methods.

There are several atomic spectrometric techniques available to the analytical chemist. All require complete atomization of the analyte molecule to obtain a useful analytical signal. The most common of these techniques are atomic absorption, emission, fluorescence, and mass spectrometry. Whereas the production of the monitored species may differ from one technique to another, the conversion of the analyte molecule to analyte atoms requires comparable atomization steps.

Atomic absorption and fluorescence techniques typically utilize atmospheric pressure flames as an atomization source. These flames are composed of a fuel, such as acetylene, and an oxidant, such as air or nitrous oxide. The energy of the flames is utilized to break intramolecular bonds to produce free atoms that may be interrogated with incident light for absorption or fluorescence measurements. These flames can achieve temperatures in excess of 3000 K (Table 1) and yield high atomization efficiencies dependent on the fuel-oxidant type (Table 2)[2].

Atomic emission and mass spectrometry require atomization of the analyte molecule. Atom excitation is necessary for emission spectroscopy. Ionization is required for mass spectrometric analysis. Ideal sources for these

Table 1. Temperatures for common chemical flames (adapted from Ingle, Crouch[2]).

Fuel – oxidant	Theoretical stoichiometric temperature (K)
C_3H_8 – air	2267
H_2 – air	2380
C_2H_2 – air	2540
H_2 – O_2	3080
C_3H_8 – O_2	3094
C_2H_2 – N_2O	3150
C_2H_2 – O_2	3342

Table 2. Atomization efficiency (N_m/N_t) of selected elements in an air-acetylene and N_2O-acetylene flame. N_m is the total number density of free metal atoms and N_t is the total number density of metal-containing species. Some species efficiencies are relative to Cu for which $N_m/N_t = 1.00$ was assigned (adapted from Ingle, Crouch)[2].

Element	**C_2H_2-air flame**	**C_2H_2-N_2O flame**
Al	$<10^{-5}$	0.42-0.59
Ba	0.0011-0.009	0.15-0.30
Ca	0.066-0.14	0.69-1.4
Cu	0.87-1.00	0.69-1.4
Fe	0.38-0.66	-
Li	0.21-0.26	0.44
Mg	0.59-.084	1.5-2.3
Mn	0.45-0.93	0.76-0.80
Na	0.50-1.00	0.33-0.65
Sn	$<10^{-4}$-0.078	0.71-0.76
Zn	0.45-1.10	0.91-1.00

techniques should have the following characteristics: a high atomization efficiency, sufficient energy to excite or ionize analyte atoms, a chemical environment conducive to background signal minimization, sufficient energy to ionize or electronically excite the element of interest, robustness with a variety of experimental conditions, stability to maintain accuracy and reproducibility, capability for simultaneous multi-element analysis, and simple operation[2]. Potential sources for atomic emission include flames, inductively coupled plasmas (ICPs), microwave-induced plasmas (MIPs), and direct current plasmas (DCPs). Due to their superior ionization and excitation capabilities, plasmas are the preferred atom sources for atomic emission (AES) and atomic mass spectrometry (MS).

Direct current plasmas are typically used only for emission spectroscopy. DCPs typically consist of two or three electrodes that provide a direct current discharge to a stream of partially ionized gas. These plasmas can attain temperatures up to 6000 K[2]. Argon gas is used to deliver the analyte as nebulized aerosol to the plasma where it is desolvated, atomized, and excited. The DCP provides an electron-rich environment lessening ionization interferences, is able to tolerate high solids in solution and organic solutions, and has power requirements less than 1 kilowatt. Disadvantages of the DCP include short residence time of the analyte within the plasma and a small optimum analytical zone cross-section for analyte detection[2].

Microwave induced plasmas typically utilize a focused microwave field to maintain the discharge. The plasma is contained in a quartz torch as shown in Figure 3. MIPs have been formed with argon, helium, and nitrogen gases, providing microwave powers from 25 to 3000 watts[3-6]. Microwave plasmas provide for gas temperatures up to 3000 K and excitation temperatures up to 5000 K. Due to the lower temperatures compared to DCPs atomization efficiency, solvent tolerance, and interference effects are more significant with MIPs. However, helium MIPs have been shown to excite non-metals and halogens due to the high excitation temperature as well as through charge transfer[2,7].

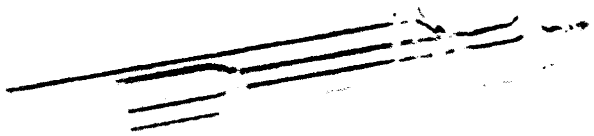

Figure 3. Quartz torch utilized to contain plasmas[3].

Inductively coupled plasmas (ICPs) were introduced in the mid-1960s in the works of Greenfield, Berry, and Jones[8] and Wendt and Fassel[9]. ICPs are maintained by an electromagnetic field sustained with an induction coil. The plasma is also contained within a quartz torch (Figure 3). Temperatures of up to 10,000 K can be attained with argon ICPs. Figure 4 details the temperature zones within a typical argon ICP. Advantages of an argon plasma include high gas temperatures leading to efficient atomization, excitation, and ionization as well as a chemical environment which reduces interference effects. The residence time of the analyte is typically on the order of milliseconds. Argon plasmas accept analytes as nebulized solutions and gases. Drawbacks to ICP behavior may include atomic emission spectral overlaps and high operating costs due to the high volume of argon used[2]. ICPs may also become unstable or be extinguished when the matrix contains an organic solvent. Desolvation of the analyte stream prior to introduction into the ICP is often necessary to analyze samples with these matrices.

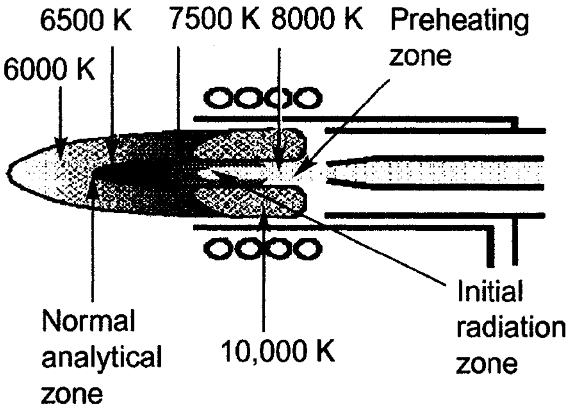
6500 K
7500 K
8000 K
Preheating zone
6000 K
Normal analytical zone
10,000 K
Initial radiation zone

Figure 4. Temperature profile of an inductively coupled plasma[10].

The research presented in this dissertation utilizes an argon ICP as a source for atomic emission and mass spectrometry. The following sections will briefly detail the pertinent theories and instrumental apparatus utilized in atomic emission and mass spectrometry employing ICP as the source.

Inductively Coupled Plasma Atomic Emission Spectroscopy

Atomic emission spectroscopy involves the radiative relaxation of a population of atoms from an excited to a lower energy level. The process is illustrated in Figure 5. An excited state population density, the number of atoms per cm^3 existing in the ith excited state, (n_i), can be calculated using the Boltzmann distribution[2]:

$$n_i = \frac{n_t g_i e^{-\frac{E_i}{kT}}}{Z(T)} \tag{1.1}$$

where n_t is the total number of atoms per cm^3, g_i is the degeneracy of state i, E_i is the energy of the state above the electronic ground state, k is Boltzmann's constant, T is the absolute temperature, and Z(T) is the partition function.

The emission intensity (Φ_{ij}) of an electronic transition from the ith to the jth state is expressed in the following equation[2]:

$$\Phi_{ij} = A_{ij} h v_{ij} n_i \mathrm{V} \tag{1.2}$$

where A_{ij} is the transition probability of an atom from state i to state j, h is Planck's constant, v_{ij} is the frequency of photons emitted, n_i is the population density of excited state atoms, and V is the observed volume element in cm^3. A linear correlation between Φ_{ij} and the analyte concentration in the sample is desired in atomic emission spectrometry. This relationship is observed over several orders of magnitude with ICP-AES.

Figure 6 illustrates the pertinent ICP-AES components. The figure shows a lateral plasma viewing configuration although an axial configuration may also be

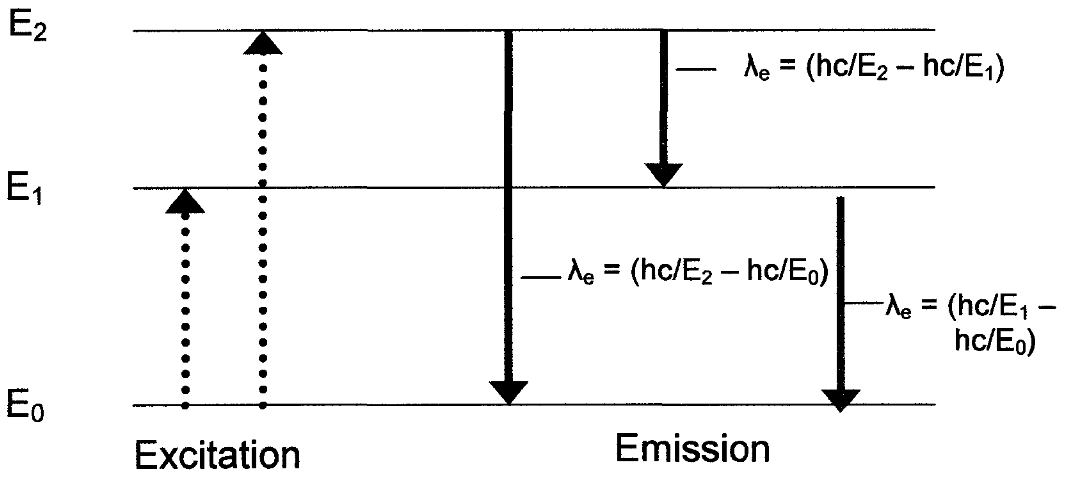
E2
E1
E0
λe = (hc/E2 – hc/E1)
λe = (hc/E2 – hc/E0)
λe = (hc/E1 – hc/E0)
Excitation
Emission

Figure 5. Atomic emission energy level diagram showing atomic excitation and emission transitions. λ_e is the wavelength of emission, h is Planck's constant, c is the speed of light in a vacuum, and E is the energy of the state an atom is in.

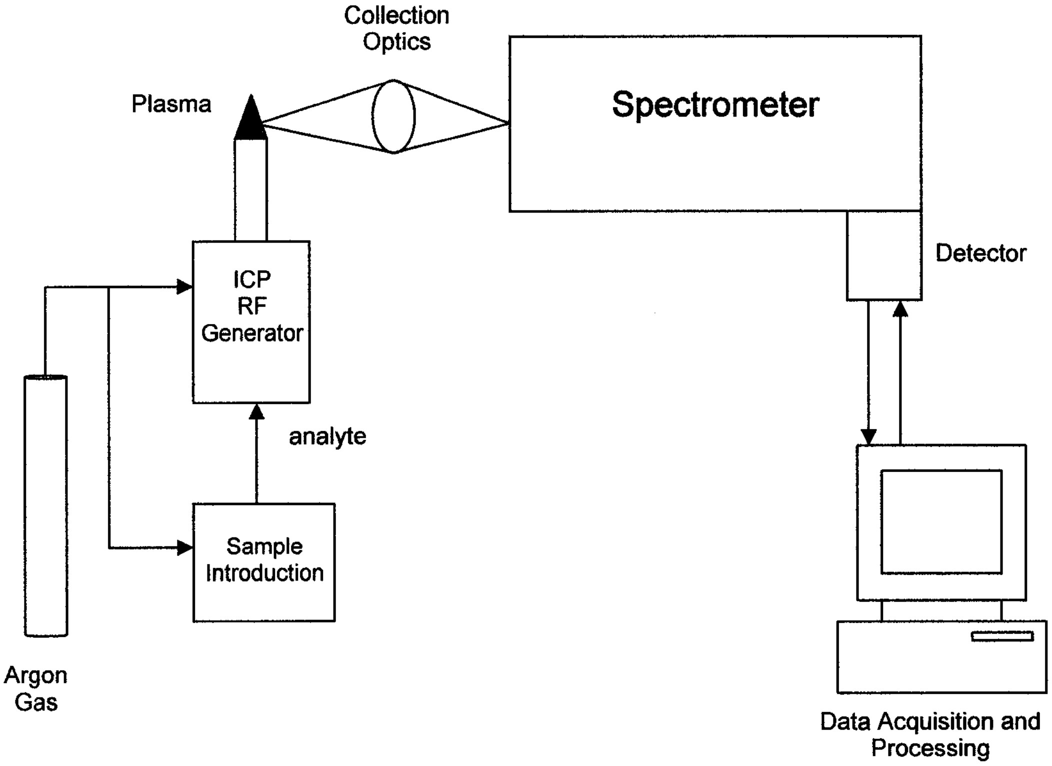
Collection
Optics
Plasma
Spectrometer
Detector
ICP
RF
Generator
analyte
Sample
Introduction
Argon
Gas
Data Acquisition and
Processing

Figure 6. Schematic of an ICP-AES instrument.

utilized. The sample introduction step will be discussed in a separate section. Optics are used to focus an image of the ICP spectrometer. The spectrometer disperses and isolates radiation of the analytical zone of the plasma. The spectrometer may be scanned to acquire the background and analyte atomic emission signal. For ultraviolet and visible regions of the spectrum, a photo-emissive detector such as a photomultiplier tube (PMT) is utilized.

ICP-AES is generally utilized to analyze samples in solution, although the analysis of solids may be accomplished via special sample introduction techniques such as electrothermal vaporization and spark ablation. The lowest limits of detection are typically obtained for metals because they have lower excitation energies compared to nonmetals. Nonmetals are not sufficiently excited in an argon plasma to yield ultraviolet or visible emission lines of sufficient intensity to be analytically useful.

Advantages of ICP-AES include sub-part per billion metal detection limits, large dynamic ranges, high reproducibility, and resistance to matrix interferences. However, the technique is not without problems. As noted earlier, atomic emission spectra can produce spectral overlap interferences due to the large number of atomic emission lines present. Calibration curve rollover may also occur at high analyte concentrations. Lastly, multi-element analysis may be time consuming if a scanning monochromator is used.

Inductively Coupled Plasma Mass Spectrometry

With inductively coupled plasma mass spectrometry (ICP-MS), analyte ions formed in the plasma are sampled and separated based on their mass-to-charge ratio (m/z) with a mass analyzer. While doubly ionized atoms may be formed in the plasma, the majority of analyte ions will be singly charged and present at their nominal isotopic masses. Figure 7 shows a diagram of a typical ICP-MS instrument and the interface region. Like ICP-AES spectrometers, ICP-MS instruments typically accept nebulized liquid analytes, although gas and solid samples may be analyzed as well[11,12]. The interface between the atmospheric plasma and the high vacuum mass spectrometer is accomplished by a staged transition beginning in the interface region. Sample and skimmer cones extract analyte ions formed in the plasma and transfer the ions into the intermediate region of the ICP-MS. The gas orifices of the sample and skimmer cones typically have diameters of 1.0 and 0.7 mm, respectively. The intermediate region contains a series of conducting discs called ion lenses. The ion lenses focus the ions from the interface region for transmission to the mass analyzer. Turbomolecular pumps provide the gas extraction necessary to achieve pressures down to 10^{-7} mbars. The mass analyzer is typically a quadrupole with a resolution of approximately 300. This is sufficient for discrimination of ions based on unit mass differences. Higher resolution mass analyzers such as double focusing sector analyzers or time of flight analyzers have been employed to isolate the analyte ions of interest in special applications. Common detectors include the Faraday cup, discrete dynode detector, and channel electron multiplier. Argon gas flow rates and plasma

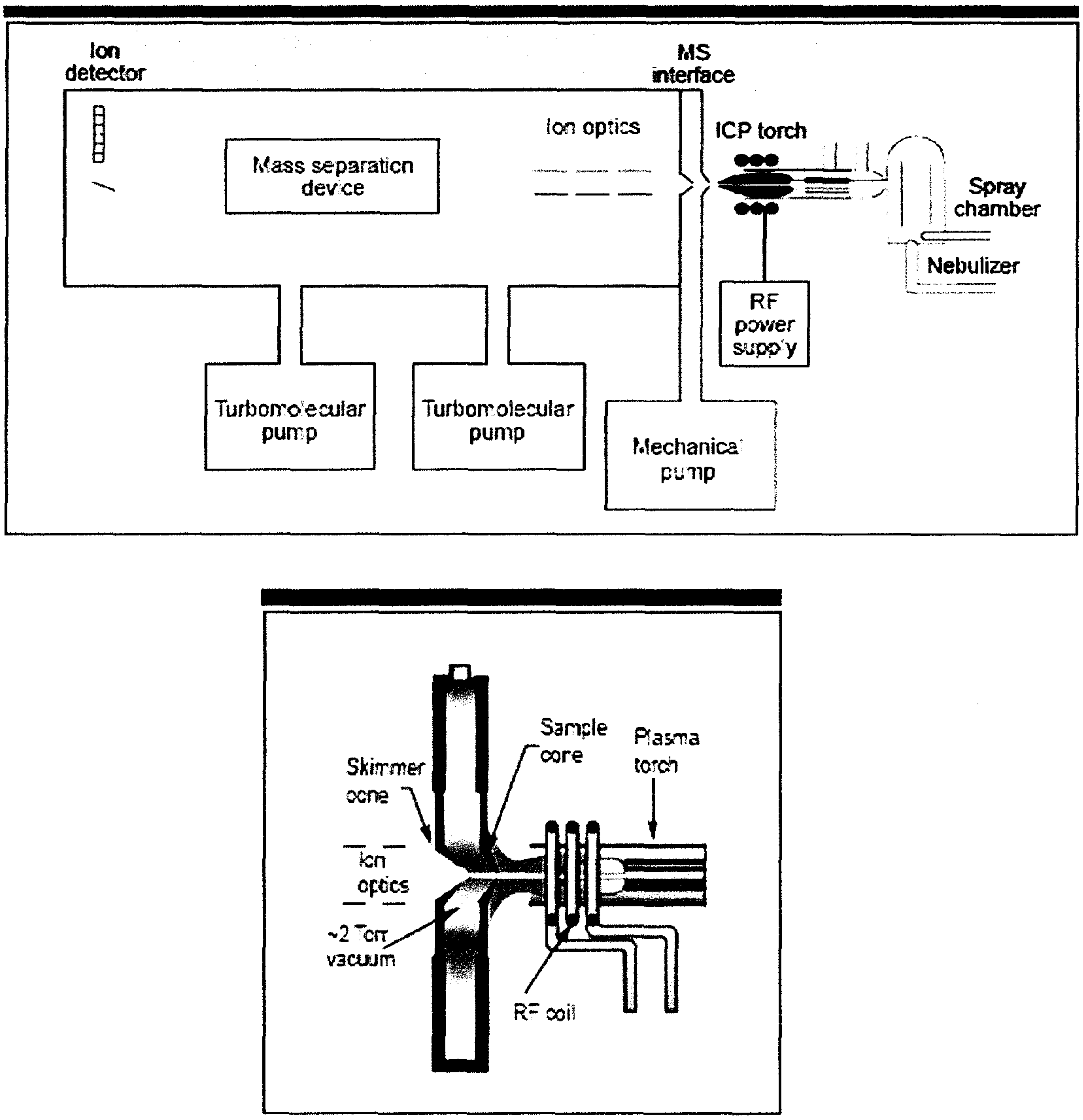
Ion detector
MS interface
Ion optics
Mass separation device
ICP torch
Spray chamber
Nebulizer
RF power supply
Turbomolecular pump
Turbomolecular pump
Mechanical pump
Sample cone
Plasma torch
Skimmer cone
Ion optics
~2 Torr vacuum
RF coil

Figure 7. Schematic of an ICP-MS instrument and the interface region[10].

forward power levels greatly influence the position of this analytical zone and careful optimization is necessary when instrumental parameters are changed.

The analytical signal output from the detector is directly proportional to the concentration of analyte ions formed in the plasma. The fraction of atoms ionized can be calculated using the Saha equation[2]:

$$\log K_i = 15.684 + \log\left[\frac{Z_{M^+}}{Z_M}\right] + \frac{3}{2}\log(T) - \frac{5040E_{ion}}{T} \tag{1.3}$$

Here K_i is the ionization constant defined as the ratio of ions (n_{M^+}) and electrons (n_{e^-}) to ground state atoms (n_M):

$$\frac{n_{M^+} n_{e^-}}{n_M} \tag{1.4}$$

Z_M^+ and Z_M are partition functions for the ion and ground state atom, and E_{ion} is the ionization energy in units of eV. Houk[13] calculated the ionization efficiency for elements in the periodic table with a 7500 K plasma and an electron density of $10^{15}/cm^3$. These results indicate that most metals are ionized greater than 90%. Table 3 lists some of the ionization energies for select metals, semi-metals, and nonmetal elements.

Advantages of ICP-MS are superior sensitivity and a large dynamic range for a large number of elements. Detection limits in the part per trillion range have been reported for a number of elements[14]. Interferences present at an analyte's isotopic mass raise the background ion current, negatively affecting the sensitivity of the

Table 3. Ionization energy of selected metals and non-metals.

Element	Ionization Energy (eV)
Li	5.39
In	5.79
Cr	6.76
Cu	7.72
As	9.78
P	10.48
Br	11.81
Cl	12.96
F	17.42

instrument. Careful matrix matching and sample preparation are necessary to ensure optimal performance.

Considerations for Pharmaceutical Analysis

Atomic Spectrometry of Nonmetals

The sensitivity and robustness of ICP-AES and ICP-MS to a number of elements have been utilized in a number of environmental[15,16], regulatory[17], industrial[18-20], and pharmaceutical[21-23] applications. A majority of the applications have been directed at monitoring samples and determining concentrations based on the metal content of an analyte. This is due primarily to the greater sensitivity of these techniques towards metals. The recent incorporation of nonmetal heteroatoms such as phosphorus, sulfur, chlorine, and fluorine into pharmaceutical drugs has brought renewed interest for designing nonmetal selective detection methods.

Specific applications of interest to the pharmaceutical industry include impurity profiling, monitoring of degradation products, and regulatory compliance issues. A starting point in designing an instrumental method for sensitive non-metal detection is identifying the selectivity and sensitivity requirements of the system.

ICP-AES and ICP-MS Utilizing High Performance Liquid Chromatography

ICP-AES and ICP-MS are element-specific detection techniques. They respond to the presence of a specific element within a nebulized solution regardless of its source. The presence of two compounds or more with similar elemental composition occurs frequently in a pharmaceutical synthesis environment. The active pharmaceutical ingredient (API) may contain the same heteroatoms as an impurity, as a degradation byproduct, or as a result of side reactions during or following API synthesis.

High performance liquid chromatography (HPLC) has become a standard separation method in the pharmaceutical industry due to its ability to separate non-volatile polar and non-polar compounds.[24-30] Separation of polar compounds is typically performed using reverse phase chromatography. Separation of non-polar compounds is often accomplished using normal phase chromatography. Volatile compounds may be separated utilizing gas chromatography[31-33]. A large number of pharmaceutical compounds are non-volatile in nature and contain heteroatoms. This research focuses on the development of ICP-AES and ICP-MS as an element-specific nonmetal detector for HPLC with applications in the pharmaceutical industry.

Standard detection systems for HPLC include ultraviolet detectors (UV) and electrospray mass spectrometry (ESI-MS). Both have proven to be robust and sensitive detection methods for pharmaceutical analysis. However, drawbacks to these detection methods exist. Detection by UV absorption requires the presence of a chromophoric moiety. Response factors are different for all analytes, requiring calibration standards for each. Detection by ESI-MS suffers when the analyte molecules possess poor ionization characteristics. Additionally, ESI-MS requires a volatile matrix. This factor limits the range of chromatographic buffers that can be used. ICP-AES and ICP-MS detection has the potential to be a complementary detection technique when ESI-MS or UV detection is not feasible.

Interfacing ICP-AES and ICP-MS to HPLC can be achieved by connecting the outflow of liquid from the HPLC column to the sample introduction system. A low volume connection is used to limit post-column chromatographic band broadening of the analyte. ICP-AES and ICP-MS may be used in tandem with UV detection.

Analytical figures of merit pertinent for chromatographic systems include the number of theoretical plates (N) given by the following equation[34]:

$$N = \frac{5.54 t_r^2}{{w_{0.5}}^2} \tag{1.5}$$

where t_r is the retention time of the analyte peak and $w_{0.5}$ is the width of the peak at half the peak maxima . The number of theoretical plates is an indication of column efficiency. The minimum number of plates required for regulatory purposes in the pharmaceutical industry is 2000[35].

Adequate separation of one component from another is necessary and is measured by the resolution (R_s) calculated between two chromatographic peaks. The standard resolution equation is given below:

$$R_s = \frac{(t_{r2} - t_{r1})}{\frac{(w_{b1} + w_{b2})}{2}} \quad (1.6)$$

where t_{r2} and t_{r1} are the retention times of the two components and w_{b1} and w_{b2} are the baseline widths of the peaks. A minimum resolution of 0.8 is required for the pharmaceutical industry[35].

Peak tailing factors are an additional figure of merit monitored by regulatory agencies. Figure 8 illustrates the method by which tailing factors are calculated.

Tailing factors between 0.5 and 2.0 are required in the pharmaceutical industry for acceptable HPLC peak shape.

Interference Considerations for ICP-AES and ICP-MS

Interferences are of great concern with all analytical instrumental techniques. Plasma sources generally have lower chemical and matrix-based interferences compared with other atomizing techniques. For ICP-AES, the principal concern when operating near the instrumental detection limit arises from the high background due to blackbody radiation and broad molecular spectral features from solvent recombination of argon or other matrix ions that create broad molecular emission lines[37]. Spectral overlap is also of great concern due to the numerous atomic lines present for many elements in the periodic table. Judicious choice of the proper

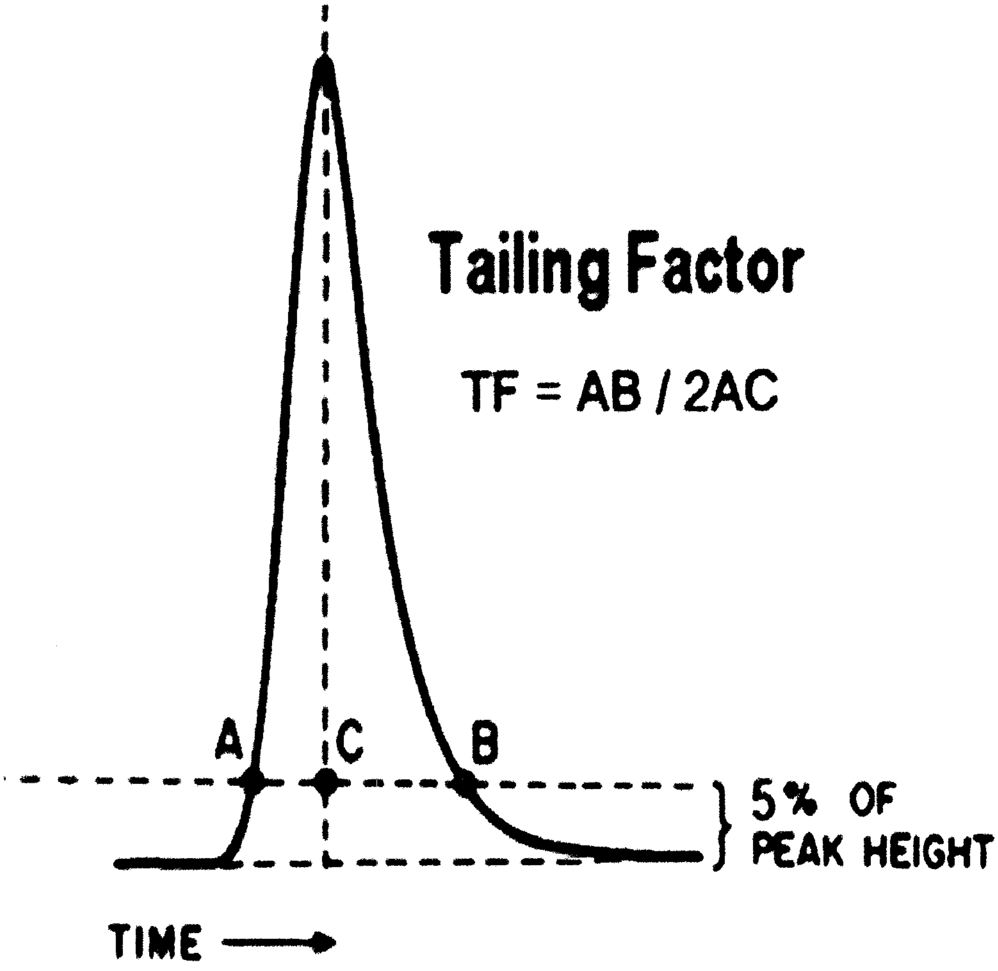
Tailing Factor
TF = AB / 2AC
A
C
B
5% OF PEAK HEIGHT
TIME

Figure 8. Tailing factor calculation[36].

atomic line for the element of interest and careful control of the matrix are necessary to ensure that no spectral overlap is present.

Due to the enhanced sensitivity of ICP-MS compared to ICP-AES, interference considerations take on added import. Spectroscopic interferences for ICP-MS arise due to the presence of interfering ionic species. Typical ICP-MS spectrometers utilize a quadrupole mass analyzer with resolutions of approximately 300. These lower resolution instruments make differentiating an analyte ion of phosphorus at mass 30.974 and a background interferent such as $^{14}N^{17}O^+$ at mass 31.002 impossible.

There are three principal types of interferences that will be of concern in this research discussion. The above-mentioned interference of phosphorus is an example of a polyatomic ion interference. Polyatomic ion interferences, such as those mentioned in the previous paragraph, are generally formed in the cooler or post-plasma regions. The sources of these interferences are sample matrix species and the atmospheric entrainment. Tables of polyatomic interferences are available in the literature[38-40]. Isobaric interferences for a quadrupole mass analyzer occur when two elements have isotopes that have less than a mass unit difference between each other. This is the case for $^{40}Ca^+$ (96.94% abundant) at mass 40.078 and the ^{40}Ar ion at mass 39.948. The determination of calcium would have to be performed at another one of its isotopes such as $^{44}Ca^+$ (2.09% abundant), to avoid the large background from the argon ions present to sustain the plasma. The formation of oxides and hydroxides ions with the analyte or matrix is another potential interference that can either cause spectral overlap or the shifting of the analyte ion of interest to a different mass[41].

There are several methods available to the analytical atomic spectroscopist to attempt to mitigate the effects of the interferences. Meticulous matrix matching allows blank subtraction. Careful optimization of gas flow rates, ICP power levels, and sample introduction conditions can significantly reduce the formation of polyatomic interferences and oxide formation[37]. Instrumental solutions are available for ICP-MS. The use of high resolution mass analyzers[41,42] can be employed to successfully isolate an analyte ion from an interferent. Collision or reaction cells[43,44] positioned prior to the quadrupole region allow for removal of polyatomic ions formed after the plasma by collision with an inert gas such as helium. This affords the removal of polyatomic interferences from the analytes mass to isolate the analyte mass of interest or remove polyatomic interferences. The utilization of non-standard sample introduction systems that provide additional solvent removal yields a cost-effective means to limit spectroscopic interferences and enhance sensitivity.

Sample Introduction Techniques

Membrane Desolvation, Pneumatic Nebulization, and Ultrasonic Nebulization

One of the most important aspects in elemental plasma techniques is the sample introduction step. The research presented in this dissertation deals with the aspiration of liquid sample via a nebulizer. Consequently, the focus for this discussion of sample introduction will be on the comparison of standard pneumatic nebulizers that appear on a majority of ICP-AES and ICP-MS instruments with ultrasonic nebulizers.

Inductively coupled plasmas benefit from the introduction of an efficiently nebulized and desolvated analyte within a narrow and homogenous droplet size distribution. This allows the thermal energy of the plasma to be effectively utilized for the analyte atomization and excitation or ionization of the pure analyte sample. Desolvation of the analyte stream will aid in limiting the formation of polyatomic and oxide based interferences in the plasma.

Pneumatic nebulizers utilize the Bernoulli effect, where a gas flow at high pressure draws a liquid solution through a capillary where it is converted into a mist of droplets at the capillary tip. Liquid uptake rates using standard pneumatic nebulizers are generally between 1 and 3 mL per minute. The aspirated liquid is sent to a spray chamber that excludes large droplet diameters (>10 μm) and may also be cooled to aid in desolvating the analyte stream. It has been shown that standard pneumatic nebulizers and spray chambers suffer from poor transport efficiency and memory effects[45,46].

Ultrasonic nebulizers accept liquid sample at an uptake rate between 0.5 to 3.0 mL/min. The liquid is directed onto a quartz faceplate that oscillates via the piezoelectric effect producing a nebulized aerosol with a droplet diameter described by the Lang equation[47]:

$$D = 0.34\sqrt[3]{\frac{8\pi\sigma}{\rho v^2}} \tag{1.7}$$

where D is the mean droplet diameter, σ is the surface tension of the liquid, ρ is the liquid density, and ν is the transducer frequency. The ultrasonic nebulizer creates a dense and homogeneous aerosol that has high transport efficiency to the plasma. After nebulization, the analyte stream is carried by an argon gas flow through a heated J-tube where water and solvent are volatilized from the analyte. Subsequent passage through a cooled condenser region allows condensation of the solvent. Ultrasonic nebulizers efficiently nebulize both analyte and matrix elements. Additional desolvation is sometimes utilized and is often accomplished with a membrane desolvator. The membrane desolvator removes additional solvent by osmotic pressure-induced diffusion through a microporous PTFE membrane to a region continuously swept by a dry external countercurrent gas stream. The dry analyte stream exits the membrane desolvator (MD) and is sent to the plasma for atomization and ionization. Figures 9 and 10 illustrate the USN-MD sample introduction system and additional desolvation in the MD, respectively.

Advantages of USN-MD Sample Introduction

There are several advantages to utilizing a USN-MD sample introduction system as compared to the standard pneumatic nebulizers. The USN is more efficient than pneumatic nebulizers. This allows a greater flux of analyte to reach the plasma[47-49]. The dual desolvation step removes matrix elements, helping to reduce the background ion counts by limiting potential interferences[50,51]. The desolvation also benefits ionization of the analyte by removing solvent that may cool the plasma

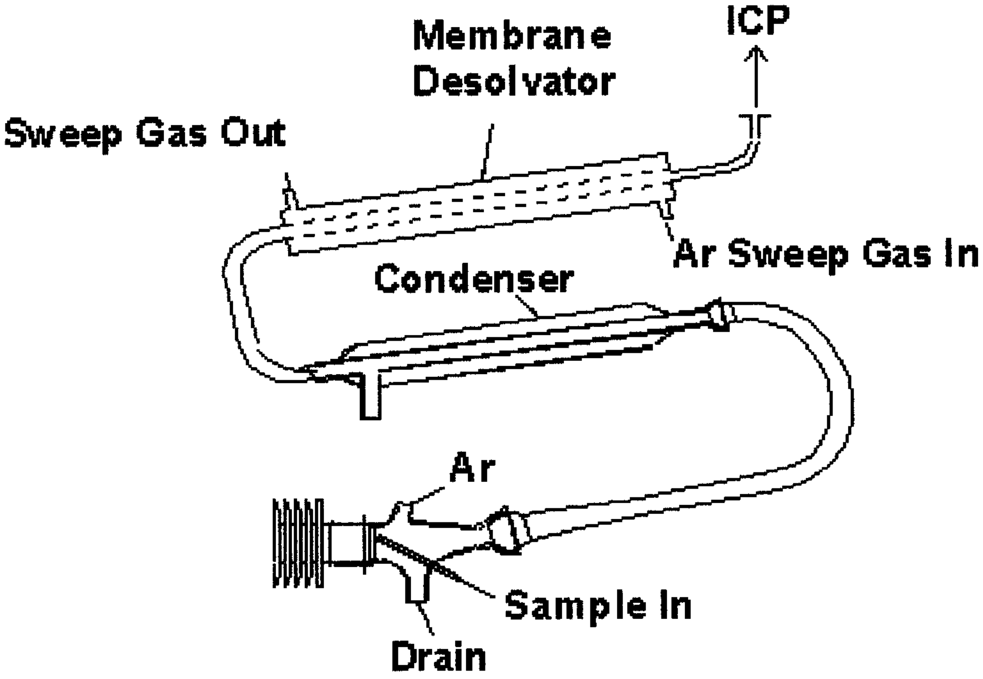
Membrane Desolvator
ICP
Sweep Gas Out
Ar Sweep Gas In
Condenser
Ar
Sample In
Drain

Figure 9. Ultrasonic nebulizer and membrane desolvator (adapted from Cetac Technologies[52]).

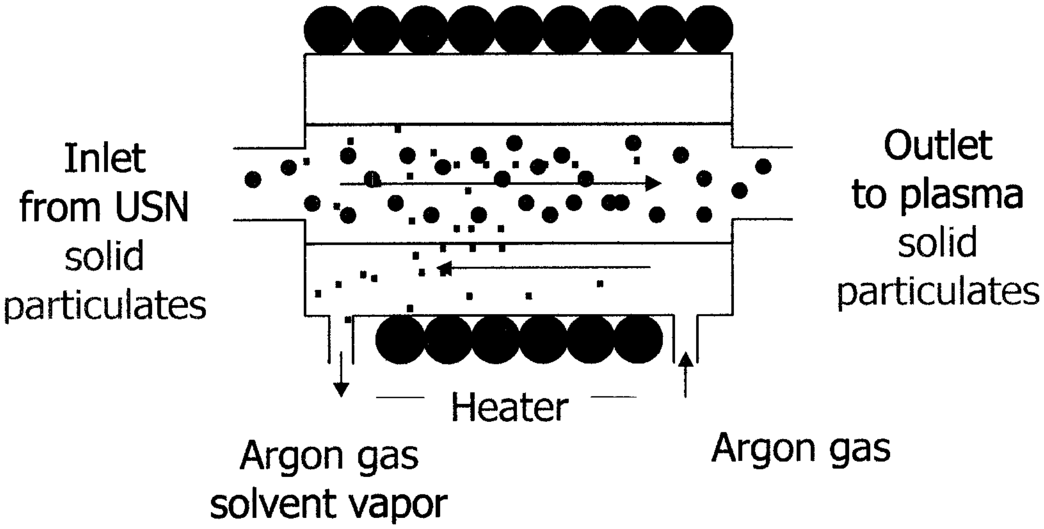
Inlet
from USN
solid
particulates
Outlet
to plasma
solid
particulates
Heater
Argon gas
solvent vapor
Argon gas

Figure 10. Membrane desolvator (adapted from Cetac Technologies[52]).

and inhibit efficient excitation or ionization. Lastly, USN-MD allows for the determination of analytes in organic solvents. Plasmas may become unstable or extinguish when there is excessive solvent load necessitating the addition of oxygen to the nebulizer gas or additional desolvation. The ability to analyze samples in solvent-based matrices greatly extends the applicability of ICP-AES and ICP-MS as a detector for HPLC.

Additional Considerations Concerning USN-MD Sample Introduction

USN-MD sample introduction systems introduce heating and cooling elements that may have deleterious effects on volatile analytes. Montaser, Kahen, and Jorabchi[53] noticed non-linearity in the calibration plot of ammonium bromide with membrane desolvation, determining that analyte loss occurred principally in the membrane desolvation step. Optimization of USN-MD temperature and gas flow rates may aid in limiting analyte loss. Encapsulating the analyte as a thermally stable particulate has been demonstrated by Carnahan and Das[54], allowing retention of an analyte through the membrane by post-column addition of H_2SO_4. Lastly, standard ultrasonic nebulizers can accommodate flow rates down to a minimum of 500 µL/min, limiting their application to standard analytical columns and flow rates.

Sensitivity Considerations and Example Analyte Compounds

It has been stated previously that the analytical detection methods used in this research are not as sensitive toward non-metal elements. The most stringent detection requirements in the pharmaceutical industry pertain to impurity analysis such as the detection of isopropyl methanesulfonate (IPMS) shown in Figure 11. This compound and other impurities need to be detected in a range of 5 to 500 parts per million relative to the API. This corresponds to a detection level of 10-1,000 ppb for the impurity if the API is present at a concentration of 2 parts per thousand.

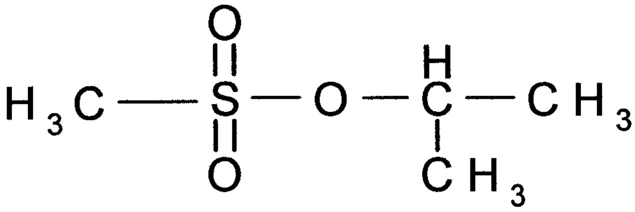

$H_3C-S(=O)_2-O-CH(CH_3)-CH_3$

Figure 11. Isopropyl methanesulfonate.

To ascertain whether these detection limits are obtainable, our research group performed an ICP-MS detection limit study on the model heteroatom-containing compounds shown in Figure 12. The results are summarized in Table 4. Sensitive nonmetal detection was obtained for sulfur-, phosphorus-, and chlorine-containing analytes. The sensitivity of the instrumental method towards fluorine was markedly lower, yet this detection limit is one of the lowest reported in the literature for fluorine[55]. Calibration curves with a high degree of linearity have been obtained for these compounds utilizing USN-MD-ICP-MS (Figures 13-16).

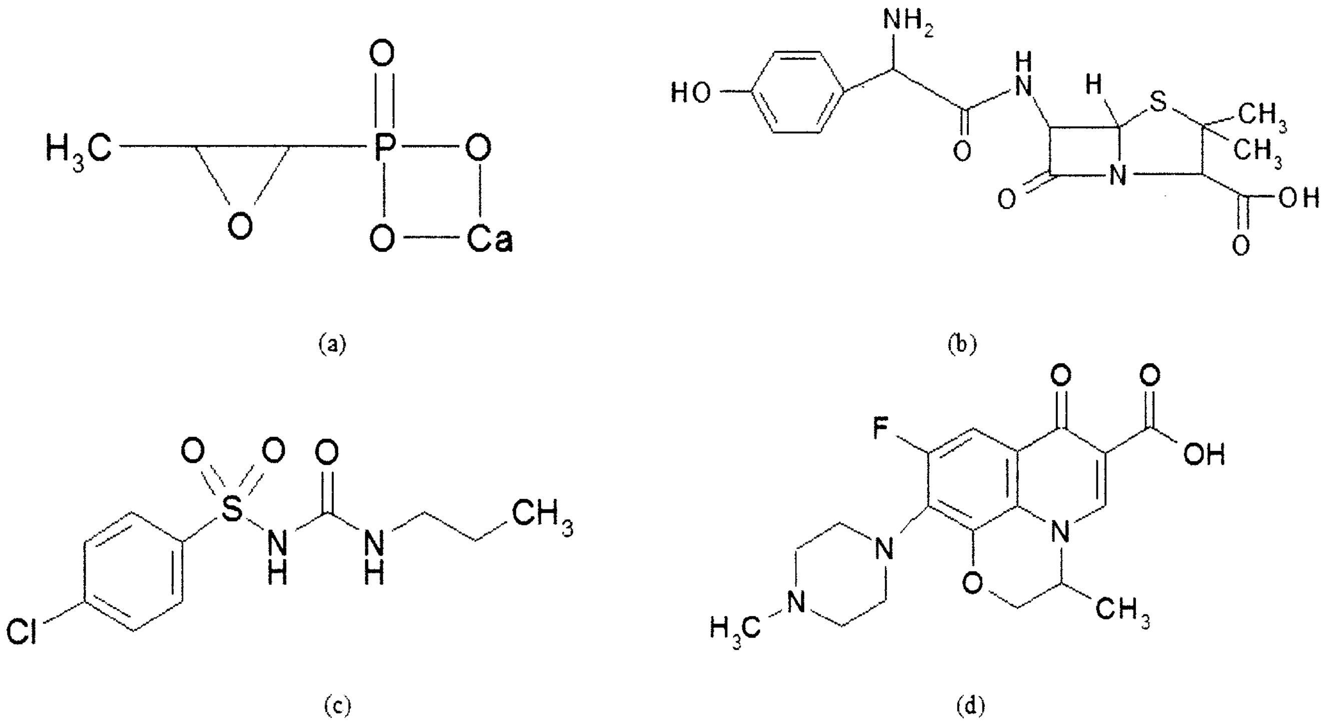
H$_3$C
O
P
Ca
HO
NH$_2$
H
N
S
CH$_3$
OH
Cl
F
(a)
(b)
(c)
(d)

Figure 12. Structures of (a) phosphomycin, (b) amoxicillin, (c) chlorpropamide, and (d) olfoxacin[34].

Table 4. Detection limits obtained for several heteroatom-containing antibiotics using USN-MD-ICP-MS[55].

Compound	**Monitored Isotope**	**Detection Limit (ng)**	**Detection Limit (ng/mL)**
Phosphomycin	$^{31}P^+$	0.3	2
Amoxicillin	$^{34}S^+$	0.3	3
Chlorpropamide	$^{35}Cl^+$	9	90
Ofloxacin	$^{19}F^+$	1000	3000

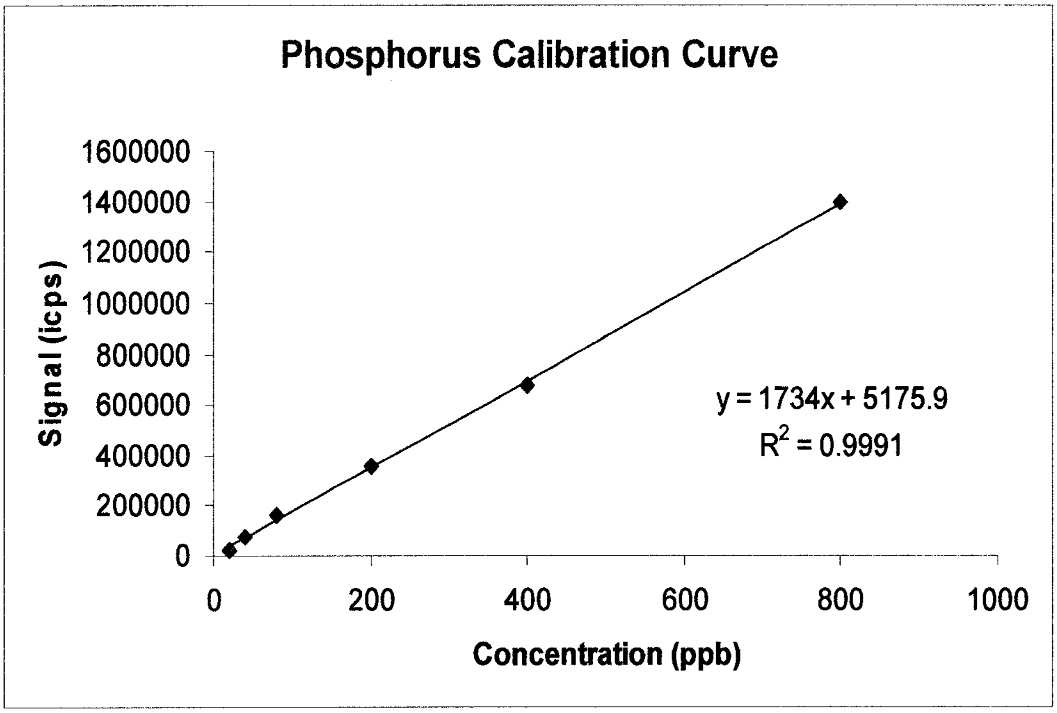

Figure 13. Calibration plot for phosphorus as phosphomycin.

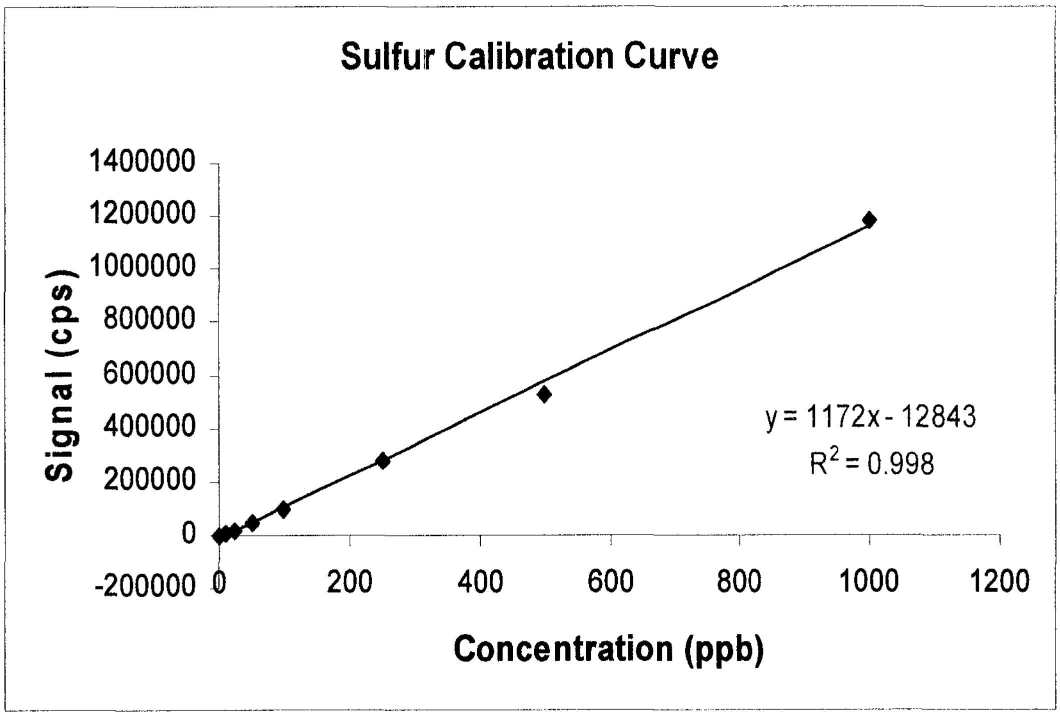

Figure 14. Calibration plot for sulfur as amoxicillin.

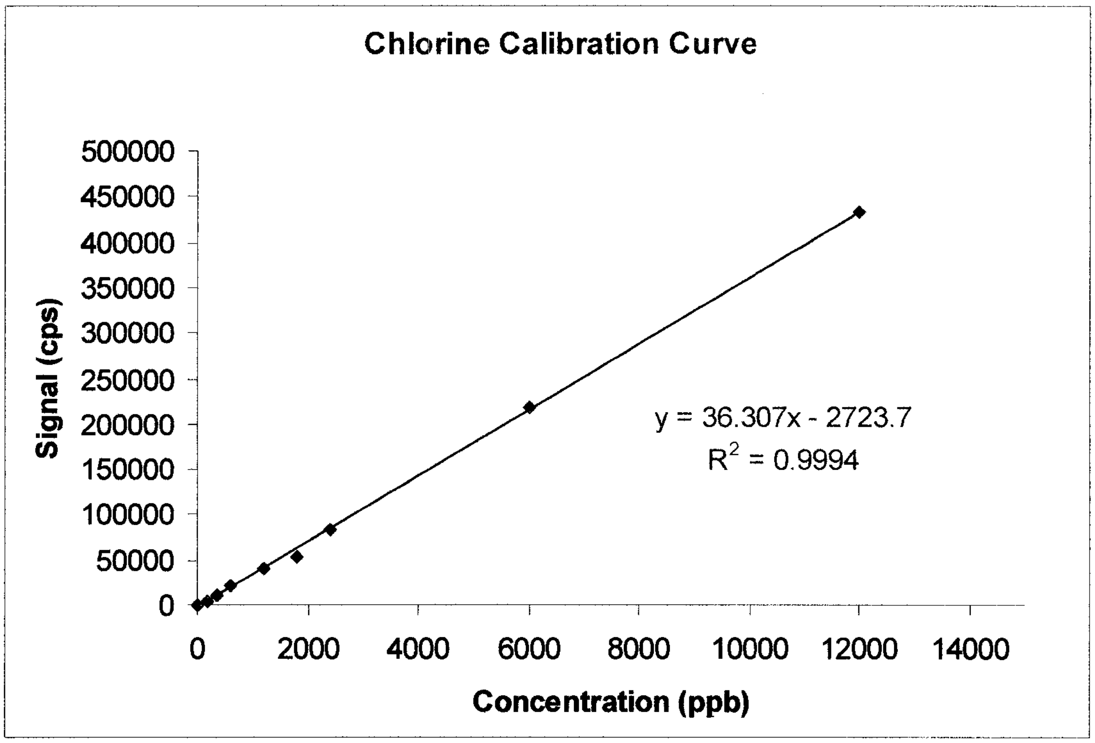

Figure 15. Calibration plot for chlorine as chlorpropamide.

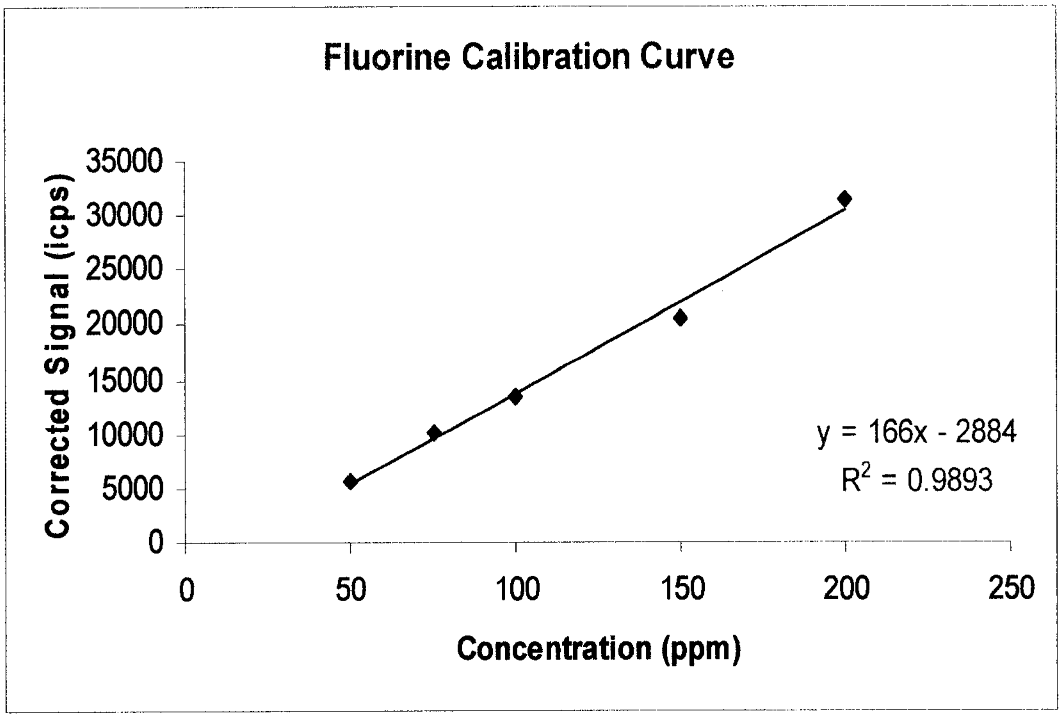

Figure 16. Calibration plot for fluorine as ofloxacin.

Research Considerations

Sensitive non-metal detection has been demonstrated utilizing ICP-MS toward sulfur-, phosphorus-, chlorine- and, fluorine-containing analytes[55]. Applicability of this technique toward analysis of mixtures of pharmaceutical products can be investigated by a systematic study of the effect of mobile phase additives and solvent combinations on the analytical figures of merit for a representative nonmetal-containing analyte. Studies will be performed with ICP-AES and ICP-MS on the phosphorus-containing antibiotic phosphomycin. The purpose of this initial investigation is to define what mobile phase solvent combinations and additives lead to the most robust and sensitive non-metal determinations for plasma-based detection. Additionally, the effect of doping the nebulizer gas flow with oxygen, nitrogen, and helium will be examined. Oxygen is commonly added to the nebulizer gas flow stream to mitigate the formation of carbon deposits on the sample cone when organic matrices are nebulized. The effect on the sensitivity towards nonmetal analytes was quantified when USN-MD was the method of sample introduction. The addition of nitrogen and helium to the argon gas flows has been reported to enhance the sensitivity towards nonmetal-containing analytes. A plurality of experiments bleeds these dopants into the auxiliary and coolant gas flows. The effect on the analytical figures of merit of bleeding nitrogen and helium into the nebulizer gas stream was experimentally determined. Finally, the application of USN-MD-ICP-MS as a detector for HPLC will be demonstrated. Several ongoing experiments will be highlighted.

CHAPTER 2

STUDY OF SELECTED BUFFER AND MOBILE PHASE COMBINATIONS ON ANALYTICAL FIGURES OF MERIT FOR USN-MD SAMPLE INTRODUCTION FOR ICP-AES AND ICP-MS

Buffers in Reversed Phase HPLC

Separation in reversed phase HPLC is dependent on the hydrophobicity of the analyte. Analytes with a greater degree of hydrophobicity will be retained longer than another analyte. If the analyte molecule is ionizable, small changes in the pH of the solution may greatly affect the elution time. For example, an analyte molecule that is acidic in nature will lose a proton and be ionized when the pH of the solution is raised to a sufficient level. The ionized analyte molecule is less hydrophobic, leading to a reduced retention time. A large number of molecules separated in reversed phase HPLC are ionizable, thus the incorporation of buffers into the mobile phase allows for reproducibility and control of retention times and resolution.

Proper selection of an HPLC buffer is dependent on a number of variables, including the desired pH of the mobile phase solution. Buffering capacity is greatest at the pK_a of the buffer (Figure 17)[56]. If a highly selective method for the separation of a component mixture required a pH of 7.0 for the mobile phase, a buffer with a pK_a value near 7.0 would be desired. The pK_{a2} value of phosphoric acid is 7.2 and would be a proper choice of buffer for this pH level. Selecting a buffer with a pK_a value within 1 pH unit of the desired mobile phase pH will yield an acceptable buffering capacity[62]. Table 5 lists some common HPLC buffers with their associated pK_a values and useful pH ranges.

The pK_a and pH values of the buffer/mobile phase are not the only criteria for proper buffer selection. The compatibility of the detection method with the buffer and mobile phase must be taken into consideration. For example, when utilizing UV detection of HPLC separated analytes, it is important to consider the cutoff wavelength where the buffer/mobile phase begins to strongly absorb UV light. Obtaining sensitive detection for an analyte that has a chromophore absorbing at 210 nm is not possible if the buffer in the matrix strongly absorbs at wavelengths less than 215 nm. Additionally, as noted previously, ESI-MS only accepts buffers that are volatile. Using nonvolatile buffers such as phosphates would not be feasible.

Pharmaceutical Application of Examining Chromatographic Buffer and Mobile Phase Combinations for Heteroatom Detection by ICP-AES and ICP-MS

Many pharmaceutical compounds are comprised of small molecules containing carbon, hydrogen, oxygen and nitrogen. The vast majority of these

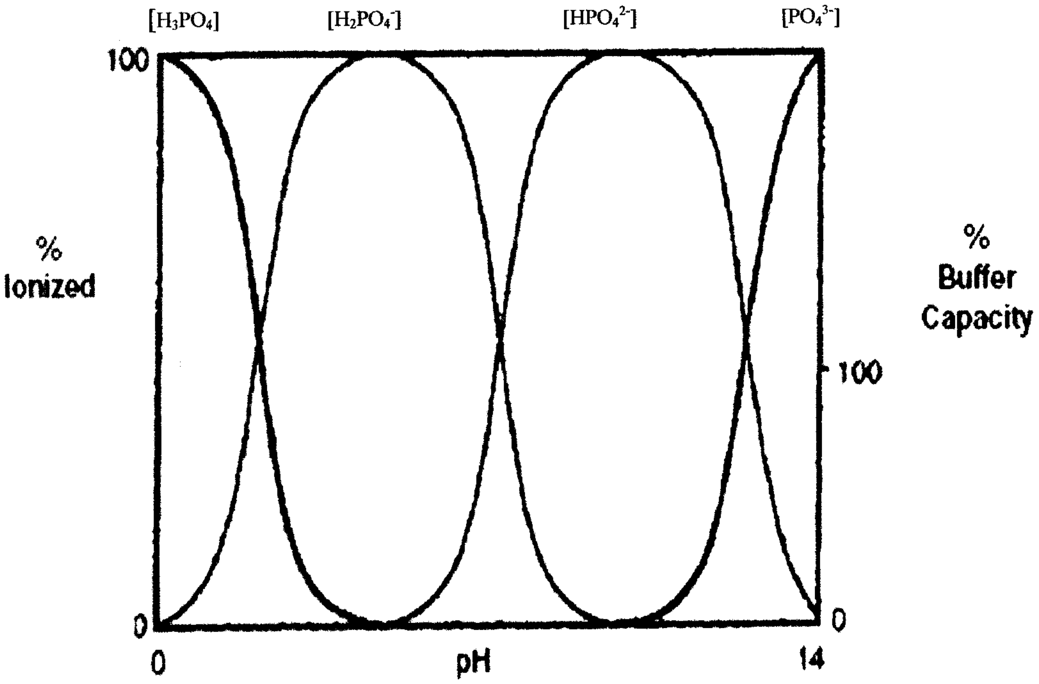

Figure 17. Buffer capacity for phosphoric acid[56].

Table 5. Common HPLC buffers[57].

Buffer	**pK_a**	**Buffer Range**
Phosphate	2.1 7.2 12.3	1.1-3.1 6.2-8.2 11.3-13.3
Formic acid	3.8	2.8-4.8
Acetic acid	4.8	3.8-5.8
Citrate	3.1 4.7 5.4	2.1-4.1 3.7-5.7 4.4-6.4
Tris	8.3	7.3-9.3
Triethylamine	11.0	10.0-12.0
Pyrrolidine	11.3	10.3-12.3

analytes speciated with reverse phase HPLC may be detected with classical liquid chromatography detectors such as UV or ESI-MS. Research and development initiatives, brought on by the drive for new medications, have seen the incorporation of heteroatoms such as sulfur, phosphorous, chlorine and fluorine into pharmaceutical compounds and impurities. Plasma-based detection methods offer an alternative approach to detecting these compounds.

However, analytical chemists in the pharmaceutical industry may approach the coupling of HPLC to ICP-AES or ICP-MS from an HPLC-UV or HPLC-MS detection scheme perspective. For example, users of traditional HPLC-ESI-MS systems must use volatile mobile phase buffers such as trifluoroacetic acid or formic acid. Would adding a less volatile salt such as perchlorate to an ICP-based system be an issue, as it would be with HPLC-ESI-MS? The possible effects of the mobile phase and buffer composition, such as ionization and/or emission quenching, deserve investigation.

With ICP techniques, it has been previously shown that a large percentage of organic solvent is successfully removed utilizing membrane desolvation. Figure 18 shows the background emission spectrum for a methanol solution nebulized into a He-MIP. The top spectrum is without membrane desolvation and shows prominent solvent emission features of C_2, CN, OH, and C(I). With membrane desolvation, these features are greatly reduced, indicating efficient desolvation. However, desolvation is not 100%. Any remaining organic solvent and buffer may have a

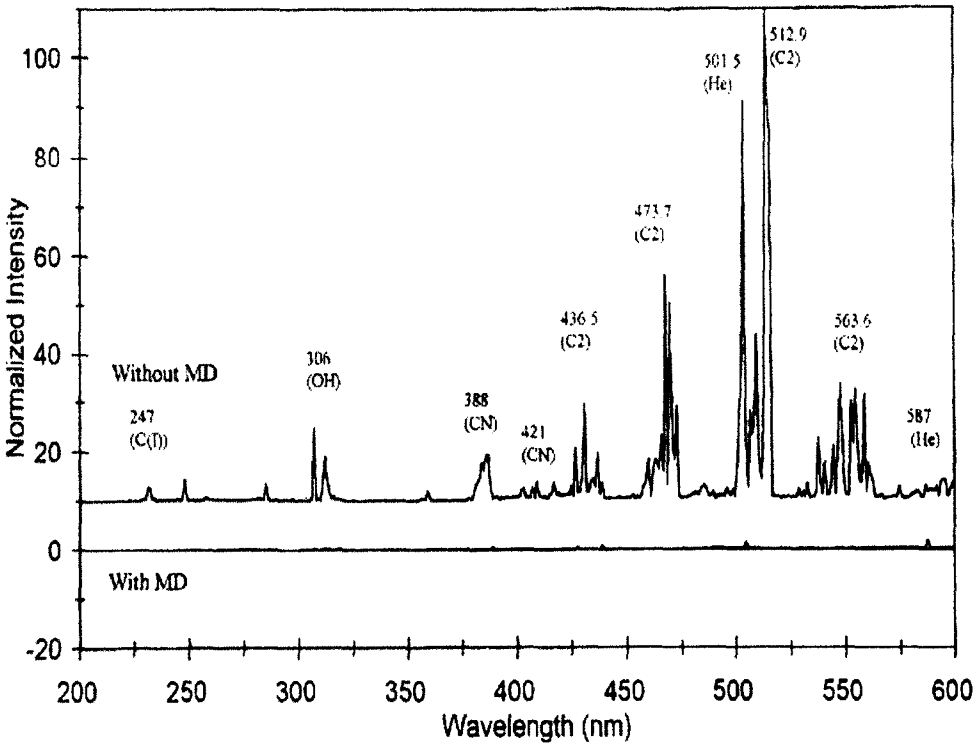

Figure 18. Methanol background emission spectrum with (top) and without (bottom) membrane desolvation in a He-MIP[54].

measurable impact on plasma stability and background signal intensity. This is especially true for ICP-MS since it is a much more sensitive technique.

Finally, it is important to establish the sensitivity trend across a range of organic mobile phase compositions. HPLC separations take advantage of gradient programming that allows the chromatographer to change the eluting power of the mobile phase. A large change in detector sensitivity across a gradient is not desirable, as either multiple calibration standards would be required for different mobile phase compositions or only isocratic elution would be possible.

The study presented here is designed to determine which mobile phase and buffer solvent systems lead to sensitive nonmetal determinations. The results of such a study will allow the chromatographer to design an HPLC method utilizing a buffer and mobile phase that is ICP-AES and/or ICP-MS friendly and yields sensitive determinations. Phosphorus as phosphomycin was examined both by ICP-AES and ICP-MS. Phosphorus was chosen as the model analyte based on the ability to detect it by both AES and MS.

Experimental

ICP-AES Instrumentation

Nebulized and desolvated analyte was directed to a Model 2.5 Leeman Laboratories (Hudson, NH) 27 MHz ICP. The image of the ICP was laterally focused upon a Model 1000 SPEX (Edison, NJ) 1 m focal length monochromator equipped with a 1200 groove/mm grating. Entrance and exit slits were set at 25 μm. Phosphorus emission at 253.8 nm was monitored with a Hamamatsu (Middlesex, NJ) R928 photomultiplier tube biased at −850 V and SPEX DataScan2 hardware with software Version 1.5.4.0. Integration time was 250 ms. A schematic of the ICP-AES experimental system is shown in Figure 19. The operating parameters are detailed in Table 6.

ICP-MS instrumentation

A Fisons (Thermo Electron) Instruments PlasmaQuad II 27 MHz ICP-MS was used. Ion signals from a Burle (Sturbridge, MA) Channeltron 4870V were acquired utilizing Thermo Electron PlasmaLab software (Version 1.06.007, Ionflight, Boston, MA). Mass spectra were obtained to confirm the peak position for ^{31}P. Single ion monitoring of peak intensities was used for quantification and the dwell time was set for 250 ms. A schematic diagram of the ICP-MS experimental system is shown in Figure 20. Detailed operating parameters are listed in Table 7.

Reagents and sample preparation

Phosphorus-containing solutions were prepared by dilution of a stock solution containing phosphomycin calcium salt in 18 MΩ deionized water. Solvents included aqueous–organic mixtures containing methanol or acetonitrile. The nine buffer salts,

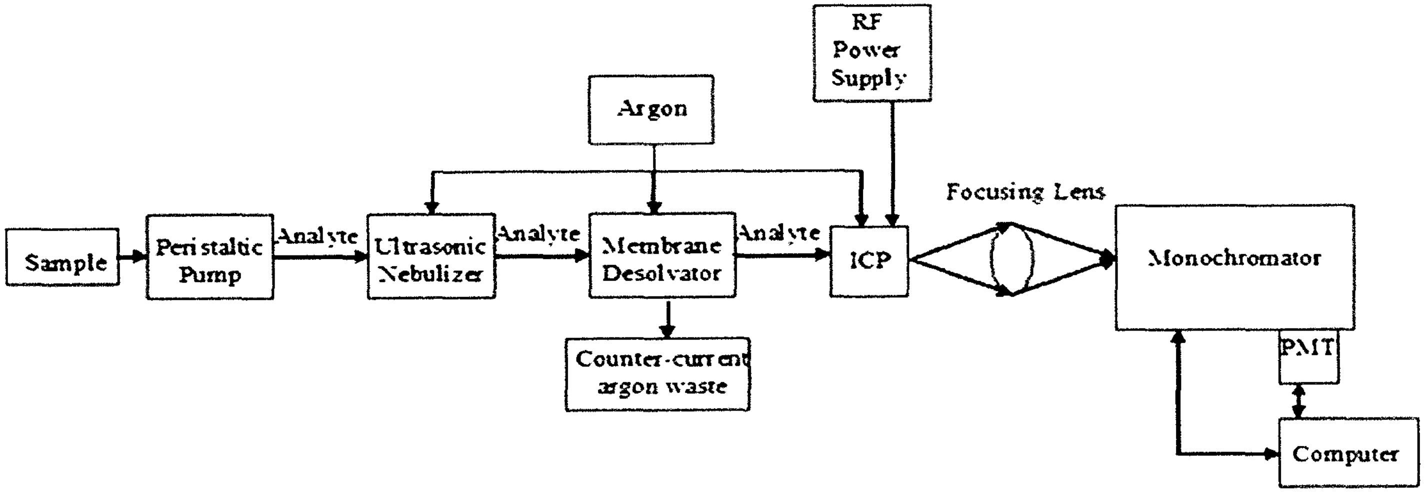
RF
Power
Supply
Argon
Focusing Lens
Sample
Peristaltic Pump
Analyte
Ultrasonic Nebulizer
Analyte
Membrane Desolvator
Analyte
ICP
Monochromator
Counter-current argon waste
PMT
Computer

Figure 19. Schematic diagram of experimental setup for ICP-AES.

Table 6. ICP-AES operating parameters.

Operating Parameters	
Peristaltic pump flow rate (mL/min)	1.0
Nebulizer flow rate (L/min)	0.78
Nebulizer heater temperature (°C)	140
Nebulizer condenser temperature (°C)	3
Membrane desolvator temperature (°C)	140
Membrane desolvator countercurrent gas flow rate (L/min)	0.51
Argon plasma gas flow rate (L/min)	13.0
Argon intermediate gas flow rate (L/min)	0.1
Applied plasma power (W)	1250

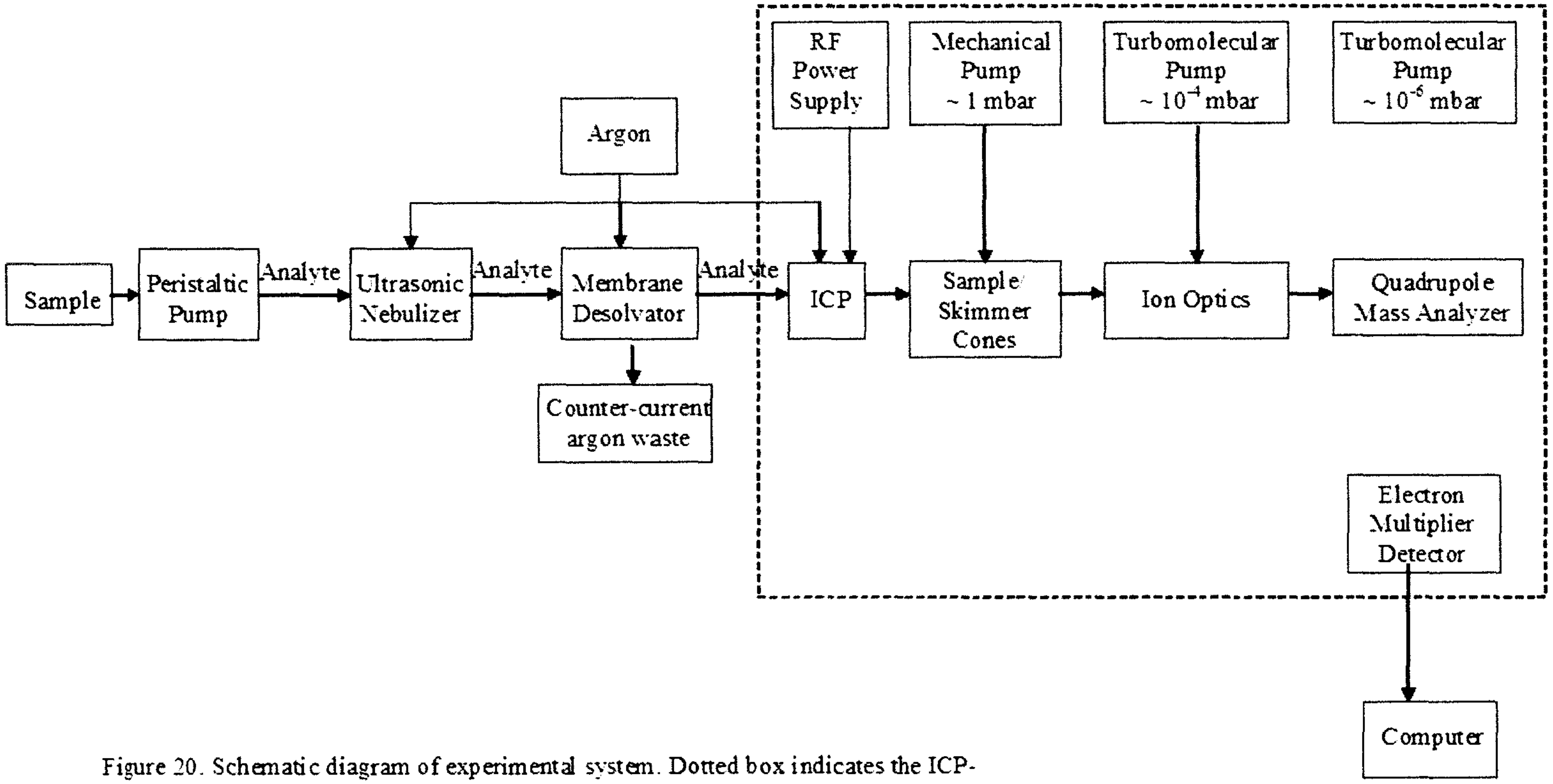
Sample
Peristaltic Pump
Analyte
Ultrasonic Nebulizer
Analyte
Argon
Membrane Desolvator
Analyte
Counter-current argon waste
RF Power Supply
Mechanical Pump ~ 1 mbar
Turbomolecular Pump ~ 10^{-4} mbar
Turbomolecular Pump ~ 10^{-6} mbar
ICP
Sample/ Skimmer Cones
Ion Optics
Quadrupole Mass Analyzer
Electron Multiplier Detector
Computer

Figure 20. Schematic diagram of experimental system. Dotted box indicates the ICP-MS unit.

Table 7. ICP-MS operating parameters.

Operating Parameters	
Peristaltic pump flow rate (mL/min)	0.9
Nebulizer flow rate (L/min)	0.62
Nebulizer heater temperature (°C)	140
Nebulizer condenser temperature (°C)	3
Membrane desolvator temperature (°C)	160
Membrane desolvator countercurrent gas flow rate (L/min)	1.9
Argon plasma gas flow rate (L/min)	14.0
Argon intermediate gas flow rate (L/min)	0.8
Applied plasma power (W)	1000
Flow injection volume (mL)	0.1-0.2

their formulations, applicable acronyms, concentrations and other reagent data are listed in Table 8.

Sample Introduction

Liquid samples were nebulized using a CETAC U5000 USN (CETAC Technologies, Omaha, NE) introduced by a Gilson Minipulse 3 peristaltic pump (Gilson, Inc., Middleton, WI). Upon exiting the USN condensation apparatus, the nebulized mist was directed through a CETAC MDX-100 polytetrafluroethylene (PTFE) membrane desolvator. The desolvated samples were then transported to the plasma.

ICP-AES Results

Solutions containing phosphorus (4 ppm) as phosphomycin were directed to the USN. The atomic emission spectrum of phosphomycin is shown in Figure 21. Phosphorus emission signals, background intensities and background noise were measured for aqueous solutions containing 0, 20, 50 and 80% organic mobile phases and each buffer. Results are reported as the average of triplicate runs. Detection limits (DL) and limits of quantification (LQ) were defined as analyte concentrations producing signals 3 and 10 times the standard deviation of the background noise, respectively. Results are summarized for methanol and acetonitrile mobile phases in Tables 9 and 10, respectively.

Table 8. Solvents and buffers utilized.

Compound (acronym); aqueous solution concentrations	**Formula**	**Grade**	**Manufacturer**
Methanol (MeOH)	CH_3OH	HPLC Grade	Fisher Scientific (Pittsburgh, PA)
Acetonitrile (ACN)	CH_3CN	HPLC Grade	Fisher Scientific (Pittsburgh, PA)
0.1% formic acid	$HCOOH$	>99%	Acros Organics (Pittsburgh, PA)
0.1% ammonium formate	$HCOONH_4$	99%	Acros Organics (Pittsburgh, PA)
0.1% acetic acid	CH_3COOH	Analytical Grade	Mallinckrodt, Inc. (Paris, KY)
0.1% ammonium acetate	CH_3COONH_4	Reagent Grade	Sigma-Aldrich (Milwaukee, WI)
0.1% trifluoroacetic acid (TFAA)	CF_3COOH	99%	Acros Organics (Pittsburgh, PA)
7.5mM tetrabutylammonium hydroxide (TBAH)	$(C_4H_9)_4NOH$	HPLC Grade	Acros Organics (Pittsburgh, PA)
0.2% perchloric acid	$HClO_4$	Reagent Grade	J.T. Baker Chemicals (Phillipsburg, NJ)
0.1% triethylamine (TEA)	$(C_2H_5)_3N$	Reagent Grade	Fisher Scientific (Pittsburgh, PA)
15mM 1-heptane sodium sulfonate (HEPS)	$NaSO_3C_7H_{15}$	HPLC Grade	Acros Organics (Pittsburgh, PA)

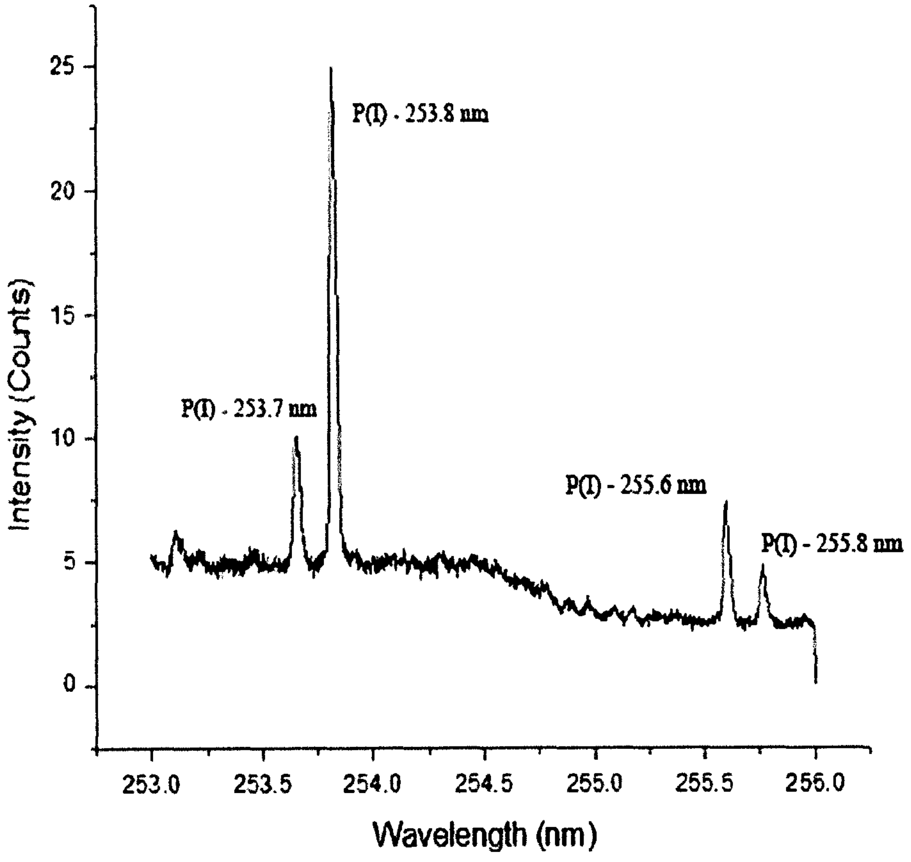

Figure 21. Atomic emission spectrum of phosphomycin.

Table 9. Phosphorus figures of merit in methanol mobile phases for ICP-AES.

Buffer	Sensitivity (S/ppm)	DL (ppb)	LQ (ppb)	Buffer	Sensitivity (S/ppm)	DL (ppb)	LQ (ppb)
0% MeOH				50% MeOH			
None	55	150	500	None	53	170	570
0.1% CH_3COOH	53	150	500	0.1% CH_3COOH	53	180	600
0.1% CH_3COONH_4	54	150	500	0.1% CH_3COONH_4	54	190	630
0.1% HCOOH	53	150	500	0.1% HCOOH	52	190	630
0.1% TFA	54	150	500	0.1% TFA	54	170	570
0.1% TEA	45	200	670	0.1% TEA	25	410	1400
0.2% $HClO_4$	49	160	530	0.2% $HClO_4$	52	180	600
0.1% $HCOONH_4$	51	160	530	0.1% $HCOONH_4$	54	170	570
7.5 mM TBAH	46	260	870	7.5 mM TBAH	50	200	670
15 mM HEPS	44	190	630	15 mM HEPS	42	230	770
20% MeOH				80% MeOH			
None	59	180	600	None	60	170	570
0.1% CH_3COOH	59	180	600	0.1% CH_3COOH	57	180	600
0.1% CH_3COONH_4	58	200	670	0.1% CH_3COONH_4	56	200	670
0.1% HCOOH	58	180	600	0.1% HCOOH	56	190	630
0.1% TFA	60	180	600	0.1% TFA	58	180	600
0.1% TEA	53	210	700	0.1% TEA	34	300	1000
0.2% $HClO_4$	56	180	600	0.2% $HClO_4$	56	180	600
0.1% $HCOONH_4$	58	180	600	0.1% $HCOONH_4$	59	180	600
7.5 mM TBAH	56	240	800	7.5 mM TBAH	41	390	1300
15 mM HEPS	55	200	670	15 mM HEPS	49	250	830

Table 10. Phosphorus figures of merit in acetonitrile mobile phases for ICP-AES.

Buffer	**Sensitivity (S/ppm)**	**DL (ppb)**	**LQ (ppb)**	**Buffer**	**Sensitivity (S/ppm)**	**DL (ppb)**	**LQ (ppb)**
0% CAN				50% CAN			
None	55	150	500	None	65	160	530
0.1% CH_3COOH	53	150	500	0.1% CH_3COOH	66	160	530
0.1% CH_3COONH_4	54	150	500	0.1% CH_3COONH_4	66	170	570
0.1% HCOOH	53	150	500	0.1% HCOOH	64	160	530
0.1% TFA	54	150	500	0.1% TFA	67	170	570
0.1% TEA	45	200	670	0.1% TEA	43	260	870
0.2% $HClO_4$	49	160	530	0.2% $HClO_4$	71	150	500
0.1% $HCOONH_4$	51	160	530	0.1% $HCOONH_4$	62	170	570
7.5 mM TBAH	46	260	870	7.5 mM TBAH	28	440	1500
15 mM HEPS	44	190	630	15 mM HEPS	62	180	600
20% CAN				80% ACN			
None	40	240	800	None	61	130	430
0.1% CH_3COOH	40	230	770	0.1% CH_3COOH	67	130	430
0.1% CH_3COONH_4	39	260	870	0.1% CH_3COONH_4	13	660	2200
0.1% HCOOH	40	230	770	0.1% HCOOH	65	140	470
0.1% TFA	40	250	830	0.1% TFA	65	140	470
0.1% TEA	27	340	1100	0.1% TEA	54	150	500
0.2% $HClO_4$	39	230	770	0.2% $HClO_4$	69	110	370
0.1% $HCOONH_4$	40	240	800	0.1% $HCOONH_4$	54	160	530
7.5 mM TBAH	48	240	800	7.5 mM TBAH	49	170	570
15 mM HEPS	37	260	870	15 mM HEPS	57	150	500

Detection limits in the range of 150 ppb were obtained when phosphomycin was introduced in pure aqueous solution, without any buffer salts. With the 100% aqueous solutions, the presence of most buffers did not significantly affect the detection limits. Detection limits with six of the buffers remained within 15% of 150 ppb and are not considered statistically different. For HEPS, TBAH and TEA, the detection limits were degraded slightly more. Because these buffers were prepared at concentrations normally used in HPLC, the concentrations of HEPS and TBAH (15 and 7.5 mM) had mass percentages three and two times that of the other buffers (0.1%). This mass loading factor may negatively affect the plasma, inhibiting excitation, contributing to the detection limit increases seen with those buffers. In general, the intensities of the background remained constant, regardless of the solution composition.

In most cases, the addition of buffers caused signal depression. This depression is probably caused by a combination of "de-tuning" of the plasma caused by organic loading and effects of analyte nebulization and transport through the sample introduction system. Membrane desolvation works well for lower boiling point solvents and buffers such as methanol and formic acid. Higher boiling point buffer salts tend to be retained through the desolvation process. However, the suppression is moderate and was greatest when HEPS, TBAH and TEA buffers were utilized.

To examine the response factors as a function of solvent composition, analytical sensitivity was examined over a range of organic:aqueous solvent concentrations. A plot of sensitivity versus organic phase content for methanol:water solutions is shown in Figure 22. Sensitivity data is tabulated in Table 9 for all methanol:water mobile phase combinations. Figure 22 shows a general trend of signal depression for the 20% methanol solutions compared to the 100% aqueous mobile phase. For most buffers, phosphorus signals increase as the mobile phase organic content increases to 50%. Greater enhancement is found with 80% methanol mobile phases. It is likely that depression and enhancement effects are caused by differences in solution viscosity, surface tension and the ability of the USN to nebulize these solvents with varying methanol compositions. Except for the solutions containing TEA, ammonium formate and perchloric acid, signals remained within 10% of the signal with the buffer and 100% water. The signal with TEA was depressed by 25% with 80% methanol and the signal with perchloric acid was enhanced by 14% with 80% methanol. The relative stability of sensitivity factors across a range of organic mobile phase compositions indicates that solvent programming should be possible, in most cases, while retaining the response integrity of the system.

The corresponding study with water:acetonitrile mixtures is listed in Table 10. Sensitivity as a function of acetonitrile mobile phase composition is shown in Figure 23 with three of the nine buffers. In general, as with the water:methanol solutions there is a trend that the 20% organic:water solutions produces a signal suppression. However, the suppression is noted to be much larger than with the 20% methanol:water solutions, averaging 23%. Compared to solutions with no acetonitrile, signals with 50 and 80% acetonitrile exhibit sensitivity enhancements of an average of 18 and 10%, respectively. Within these groups are several outliers. For

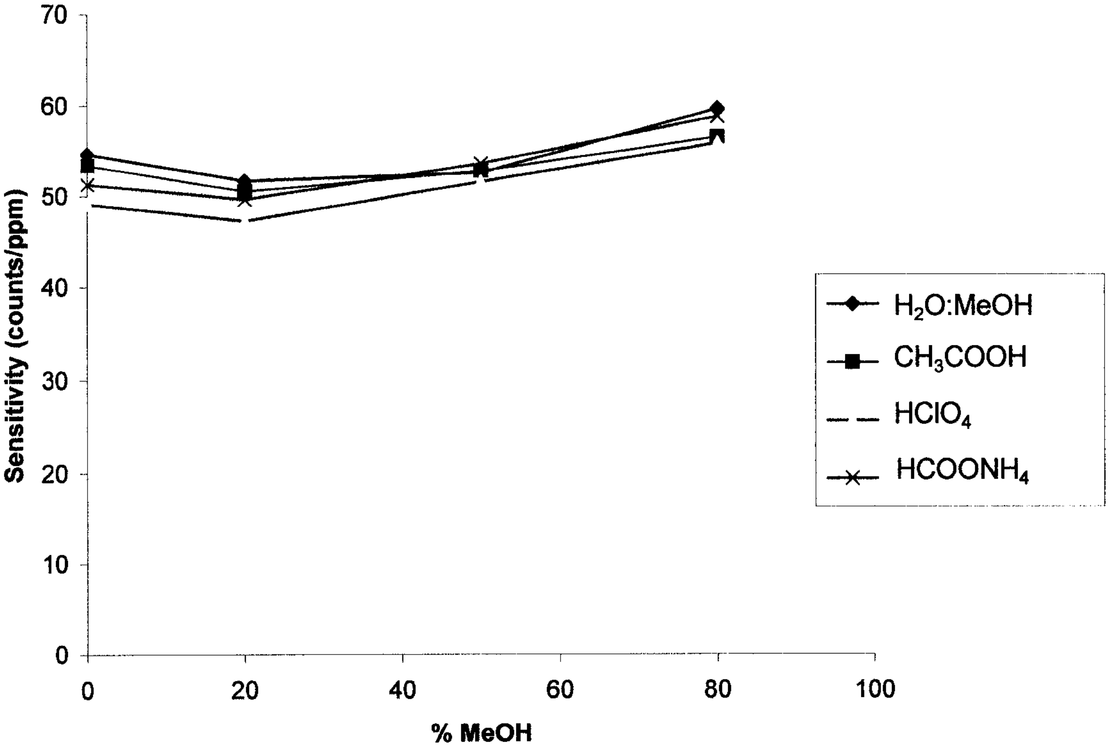

Figure 22. ICP-AES phosphorus sensitivity as a function of methanol composition.

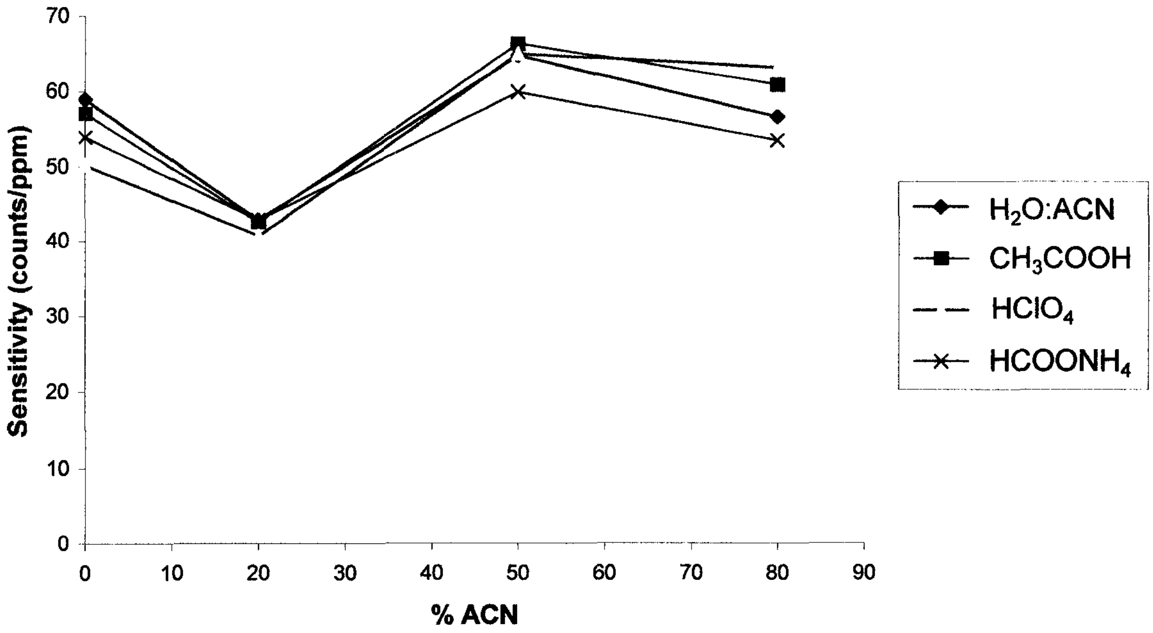

Figure 23. ICP-AES phosphorus sensitivity as a function of acetonitrile composition.

example, perchloric acid and HEPS produce exceptionally large enhancements (61–73%) with 50 and 80% acetonitrile. It is likely that these prominent differences between methanol and acetonitrile are caused by significant changes in nebulization characteristics. Higher acetonitrile mobile phase compositions nebulized very efficiently, evidenced by visual inspection of the USN spray chamber. In comparison, higher methanol mobile phase compositions were not nebulized as efficiently, creating a mist that was visibly less dense within the spray chamber.

In summary, detection limits for phosphorus as phosphomycin utilizing ICP-AES are on the order of 140–200 ppb, with a variety of buffers and solvent compositions. Buffers, in general, have a tendency to produce a depression in sensitivity. The most significant sensitivity effects are found with TEA, ammonium formate and perchloric acid buffered solutions. Effects of the methanol:water composition upon signal intensity are minimal. Although solvent gradient response varies significantly with the 0.1% TEA buffer, the average standard deviation for the remaining buffers is 6.1% and less than 5% for four of the buffers. It is likely, then, that LC solvent programming can be done without the need for recalibrating the response of the instrument as a function of the methanol:water ratio. Effects of the acetonitrile:water composition upon signal intensity are more significant. The average standard deviation of the sensitivity for all buffers in acetonitrile mobile phases is 26%. The standard deviation for solutions with no buffer is 20%. It is unlikely that LC solvent programming can be done reliably without the need for recalibrating the response of the instrument as a function of the acetonitrile:water ratio.

ICP-MS Results

Solutions containing the appropriate buffer and aqueous:organic solvent were nebulized. The phosphorus signal at *m/z* 31 was monitored and recorded to obtain the analyte signal, background and associated background noise. Figure 24 displays a typical mass spectrum obtained when deionized water background (blue) and phosphorus as phosphomycin (green) is nebulized. Results are reported as averages of triplicates. Using flow injection, 0.1–0.2 mL of phosphomycin-containing solutions were nebulized and desolvated. Tables 11 and 12 summarize the results for the methanol and acetonitrile-containing mobile phases, respectively. The absolute (mass) detection limits obtained for all buffers in each aqueous:organic solvent mixture for methanol and acetonitrile are graphically presented in Figure 25 and 26, respectively.

Sensitivity as a function of mobile phase composition for all buffers was examined as in ICP-AES experiments. Figures 27 and 28 demonstrate the effect on sensitivity for methanol and acetonitrile concentration gradients, respectively. A significant decrease in sensitivity was noted for both organic phases; however, detection limits, shown in Figures 29 and 30 did not similarly degrade. This is especially true for the acetonitrile mobile phases.

Table 11 indicates a significant loss of sensitivity once methanol is introduced in the solvent system. Figure 25 illustrates a large range of absolute detection limits for each buffer. Buffers that most negatively affected detection limits for all mobile

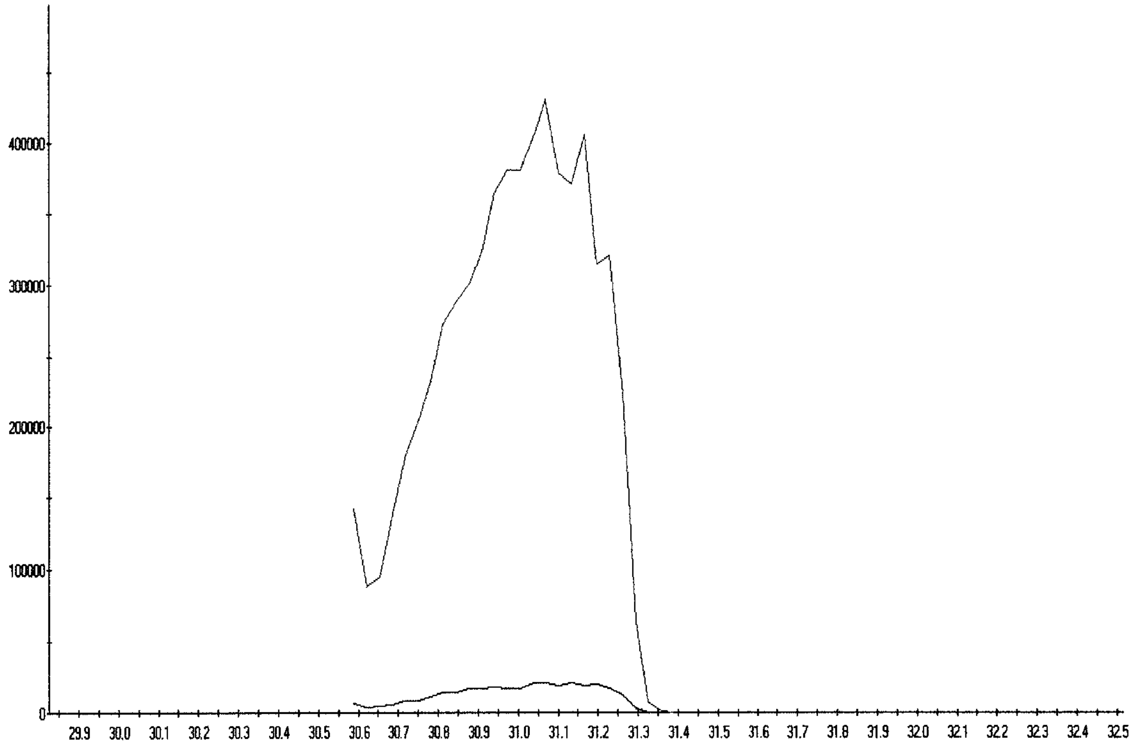

Figure 24. ICP-MS mass spectrum of background (blue) and phosphomycin (green) at $^{31}P^{+}$.

Table 11. Phosphorus figures of merit in methanol mobile phases for ICP-MS.

Buffer	Sensitivity (icps*/ng)	DL (ng)	LQ (ng)	Buffer	Sensitivity (icps*/ng)	DL (ng)	LQ (ng)
0% MeOH				50% MeOH			
None	23000	0.54	1.8	None	220	12	40
0.1% CH3COOH	77000	0.29	1	0.1% CH3COOH	210	13	43
0.1% CH$_3$COONH4	7300	3.5	12	0.1% CH3COONH$_4$	270	23	78
15 mM HEPS	n.d.	n.d.	n.d.	15 mM HEPS	34	63	210
0.1% HCOOH	55000	0.49	1.6	0.1% HCOOH	340	6	20
0.1% TFA	8200	9.1	30	0.1% TFA	240	11	38
0.1% TEA	23000	2.9	9.6	0.1% TEA	200	24	81
0.2% HClO$_4$	97000	0.64	2.1	0.2% HClO$_4$	220	8.8	29
0.1% HCOONH$_4$	42000	0.46	1.5	0.1% HCOONH$_4$	330	10	33
7.5 mM TBAH	4600	53	180	7.5 mM TBAH	310	150	500
20% MeOH				80% MeOH			
None	22000	0.36	1.2	None	800	3.8	13
0.1% CH3COOH	3600	2.4	8.1	0.1% CH3COOH	910	5.7	19
0.1% CH$_3$COONH$_4$	1500	4.2	14	0.1% CH3COONH$_4$	710	6.5	22
15 mM HEPS	130	33	110	15 mM HEPS	1000	25	82
0.1% HCOOH	1500	14	45	0.1% HCOOH	800	3.8	13
0.1% TFA	1000	26	86	0.1% TFA	750	11	35
0.1% TEA	1500	15	49	0.1% TEA	400	29	95
0.2% HClO$_4$	1300	16	53	0.2% HClO$_4$	650	3.2	11
0.1% HCOONH$_4$	1000	8.1	27	0.1% HCOONH$_4$	630	5.8	19
7.5 mM TBAH	560	68	230	7.5 mM TBAH	480	110	370

n.d.: not detectable under these conditions.
* Ion counts per second.

Table 12. Phosphorus figures of merit in acetonitrile mobile phases for ICP-MS.

Buffer	Sensitivity (icps*/ng)	DL (ng)	LQ (ng)	Buffer	Sensitivity (icps*/ng)	DL (ng)	LQ (ng)
0% CAN				50% ACN			
None	23000	0.54	1.8	None	830	0.88	2.9
0.1% CH_3COOH	77000	0.29	1	0.1% CH_3COOH	1000	1.2	4.1
0.1% CH_3COONH_4	7300	3.5	12	0.1% CH_3COONH_4	1300	1.2	4.1
0.1% HCOOH	55000	0.49	1.6	0.1% HCOOH	1500	0.54	1.8
0.1% TFA	8200	9.1	30	0.1% TFA	1400	0.95	3.2
0.1% TEA	23000	2.9	9.6	0.1% TEA	2200	0.48	1.6
0.2% $HClO_4$	97000	0.64	2.1	0.2% HClO4	1500	1.7	5.6
0.1% $HCOONH_4$	42000	0.46	1.5	0.1% $HCOONH_4$	1900	0.63	2.1
7.5 mM TBAH	4600	53	180	7.5 mM TBAH	2800	2.3	7.6
20% CAN				80% ACN			
None	5500	1.2	4.1	None	8900	0.54	1.8
0.1% CH_3COOH	21000	0.69	2.3	0.1% CH_3COOH	4900	0.54	1.8
0.1% CH_3COONH_4	4400	4.6	15	0.1% CH_3COONH_4	6200	0.86	2.9
0.1% HCOOH	3400	1.3	4.2	0.1% HCOOH	9800	0.43	1.4
0.1% TFA	3700	1.9	6.2	0.1% TFA	5800	0.72	2.4
0.1% TEA	3400	1	3.5	0.1% TEA	3600	0.41	1.4
0.2% $HClO_4$	49000	1.2	4	0.2% $HClO_4$	6300	0.69	2.3
0.1% $HCOONH_4$	8600	1	3.5	0.1% $HCOONH_4$	6200	0.51	1.7
7.5 mM TBAH	ND	ND	ND	7.5 mM TBAH	2100	3.7	12

ND: not detectable under these conditions.
* Ion counts per second.

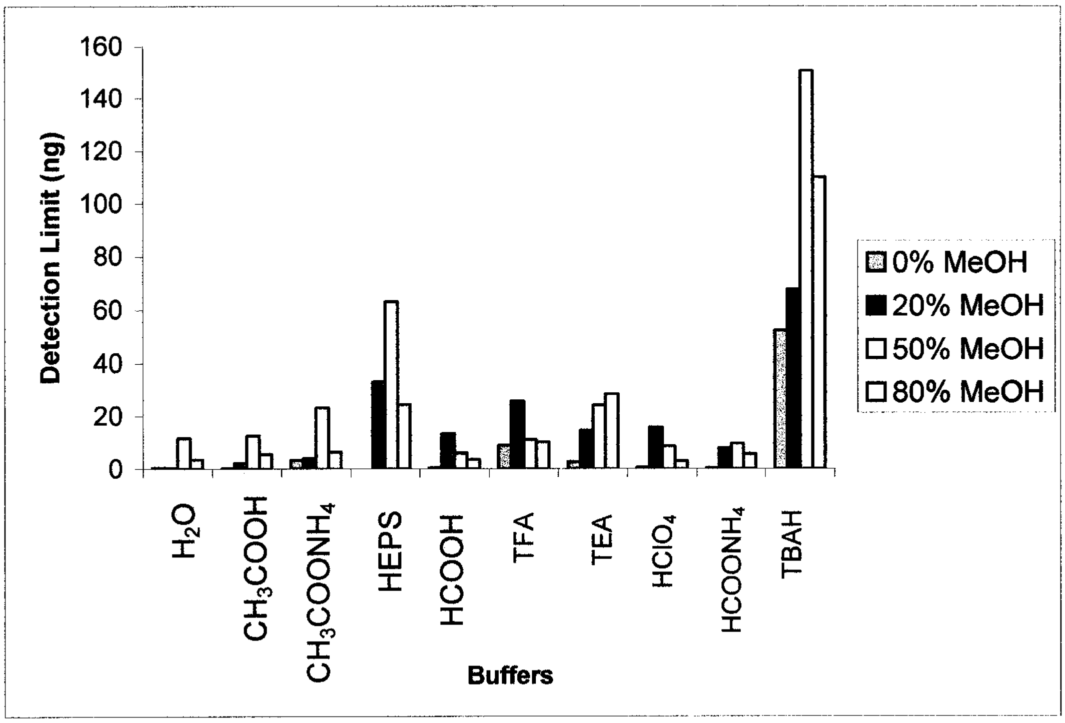

Figure 25. ICP-MS phosphorus detection limits as a function of methanol concentration with various buffers.

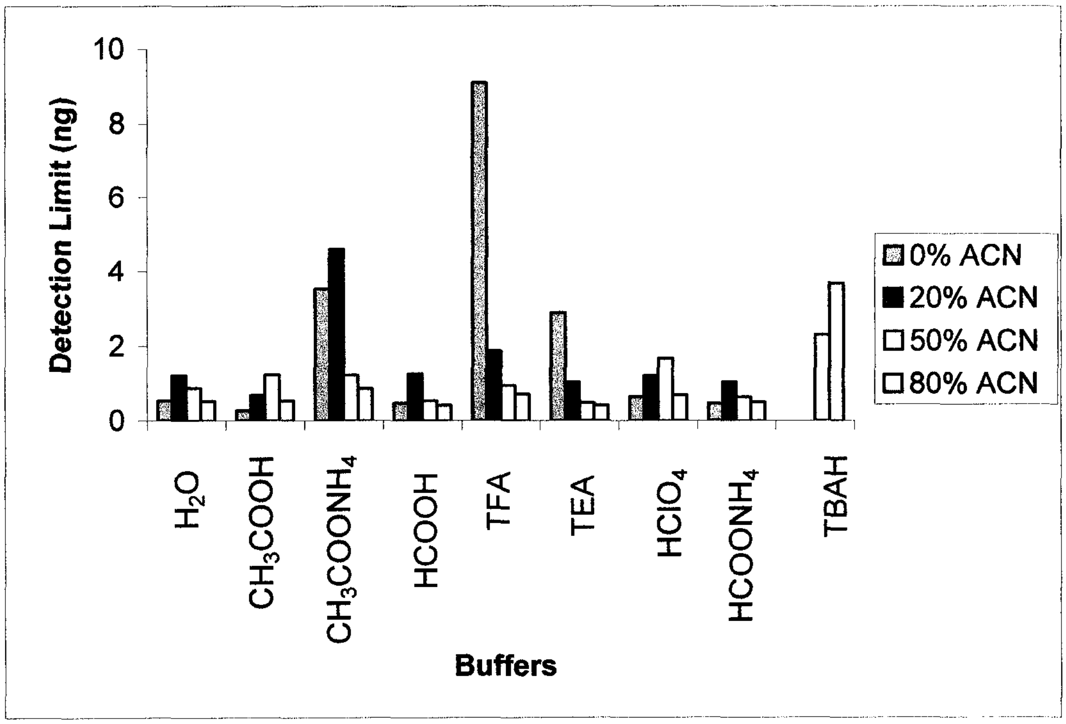

Figure 26. ICP-MS phosphorus detection limits as a function of acetonitrile concentration with various buffers. The detection limit for phosphorus with tetrabutyl ammonium hydroxide in 0% acetonitrile is excluded because of the large value. With the same buffer and 20% acetonitrile, phosphorus was not detectable.

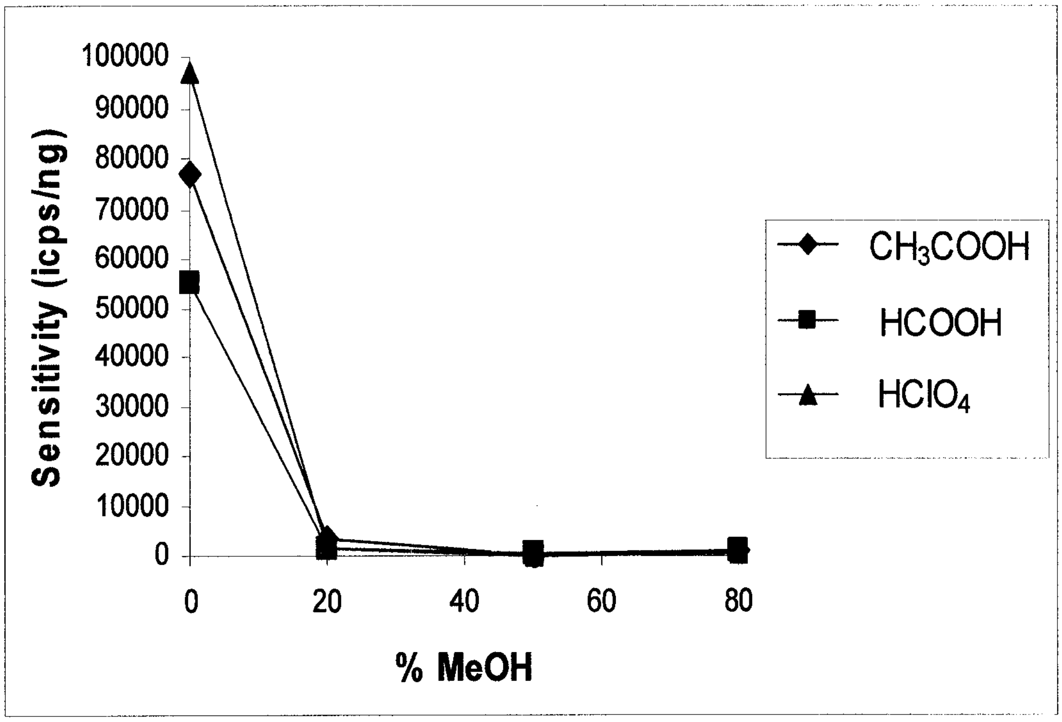

Figure 27. ICP-MS phosphorus sensitivity as a function of methanol concentration for selected buffers.

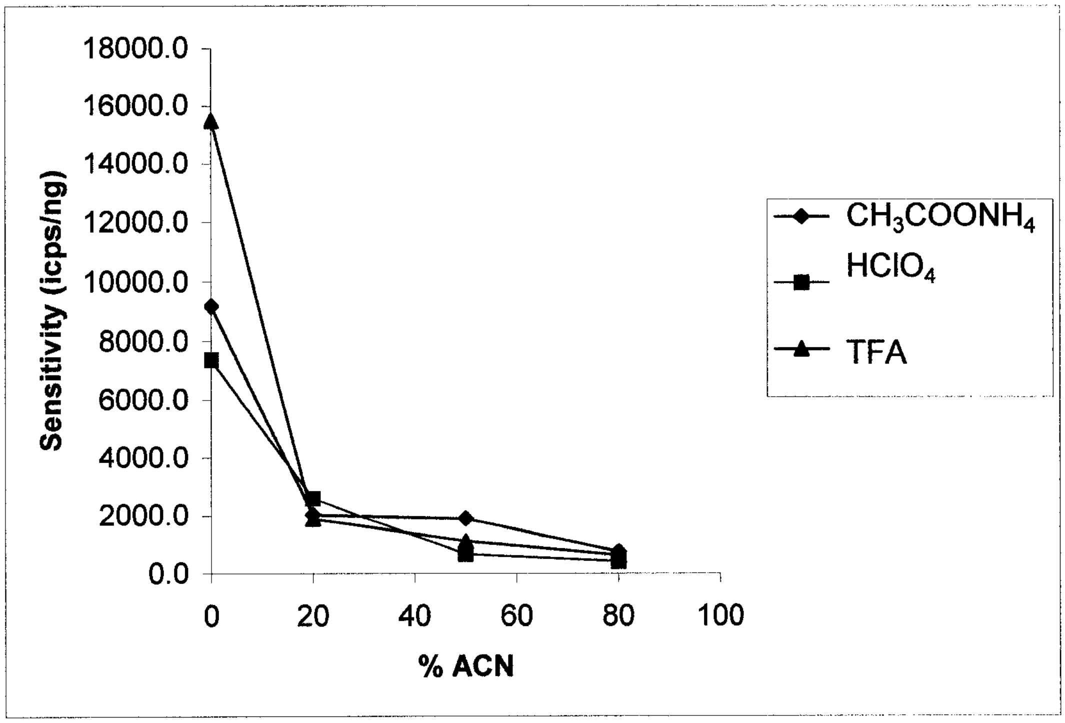

Figure 28. ICP-MS phosphorus sensitivity as a function of acetonitrile concentration for selected buffers.

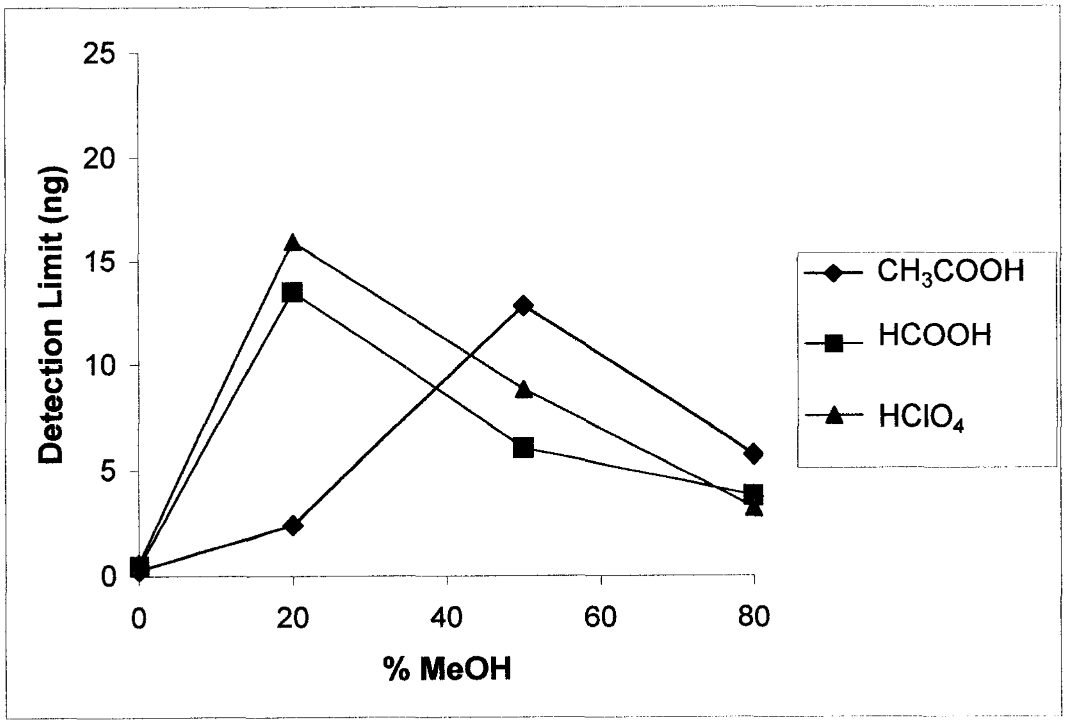

Figure 29. ICP-MS phosphorus detection limits as a function of methanol concentration for selected buffers.

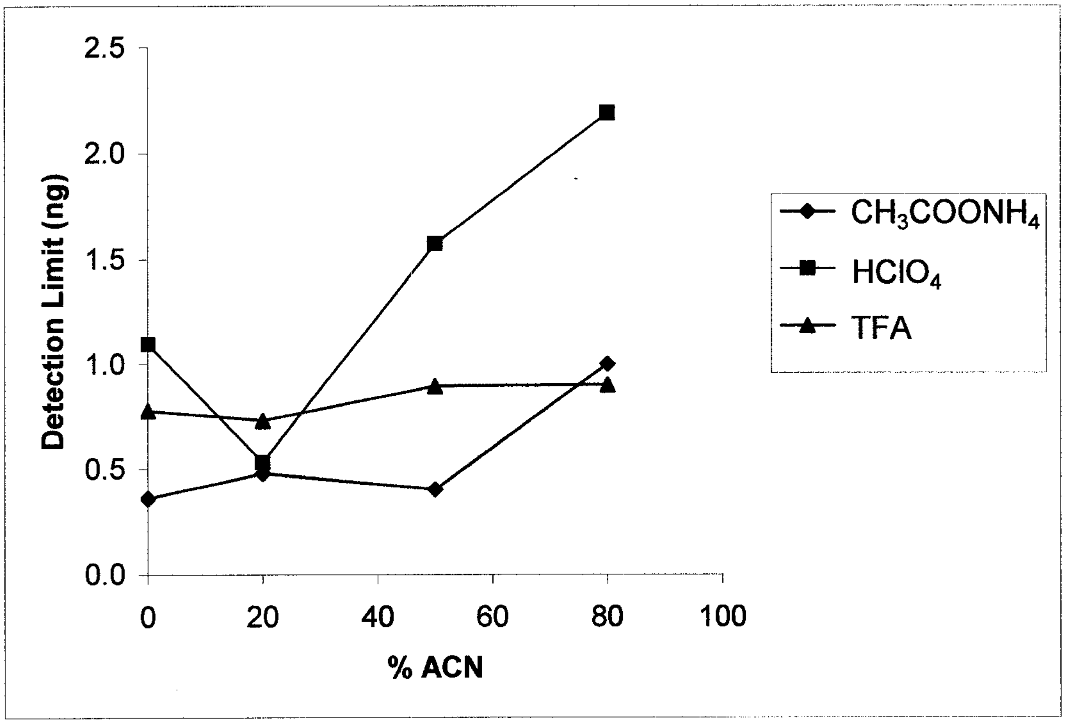

Figure 30. ICP-MS phosphorus detection limits as a function of acetonitrile concentration for selected buffers.

phase compositions include ammonium formate, TFAA, TEA and TBAH. The buffers that least affected detection limits were acetic acid, formic acid, perchloric acid and ammonium formate. Absolute detection limits with each of these buffers remained below 20 ng for all mobile phase compositions. Figure 27 demonstrates the large drop in sensitivity upon addition of methanol. While signal suppression was associated with an increase in detection limits, the increase is not nearly as significant as might be expected by the sensitivity drop as seen in Figure 27. Figure 29 indicates detection limits for a set of buffers for the methanol:water concentration gradient. It is clear that solvent programming will not be possible with methanol:water mobile phase compositions. Isocratic separations can still yield sensitive determinations, although careful matrix matching is necessary, as background and analytical sensitivity vary greatly from one mobile phase combination to another.

While there is some loss in sensitivity upon addition of acetonitrile to the aqueous mobile phase solutions, the drop is much less when compared to the methanol mobile phases. Table 12 shows the absolute detection limits and sensitivity for the acetonitrile mobile phase compositions. Values are in the range of single nanograms or less for a majority of the mobile phase compositions. Figure 26 indicates that TFA, TBAH, TEA and ammonium acetate are the buffers that most negatively affect detection limits. The detection limit for aqueous phosphorus with the TBAH buffer was excluded because it is large in comparison to the other buffer mobile phases. Also, the phosphorus in the 20% acetonitrile:TBAH buffer solution was not detectable using the nebulized concentration. This is most likely due to decreased nebulization efficiency when 20% acetonitrile solutions were introduced. Also, the higher mass loading with the TBAH buffer may be a contributing factor in the significant detectability loss at other acetonitrile:TBAH buffer compositions as compared to other buffers.

Figure 28 illustrates the drop in sensitivity upon an increase in solvent acetonitrile content. However, Figure 30 demonstrates that detection limits for acetonitrile:buffer mixtures are less affected as the acetonitrile content increases as compared to methanol mobile phase compositions. A potential drawback to using acetonitrile-containing mobile phases is the formation of carbon deposits on the sample and skimmer cones. This became more substantial as the acetonitrile content was increased. These deposits were more pronounced with acetonitrile-containing mobile phases as compared to methanol-containing mobile phases and required more frequent maintenance. This observation indicates that 100% desolvation of the aerosol stream is not achieved. The slower buildup of carbon with methanol-containing mobile phases is likely due to the more oxidizing plasma environment produced by methanol.

Comparison of ICP-AES and ICP-MS Results

With detection limits in the single ppb range, ICP-MS is much more sensitive than AES for phosphorus detection. While this has obvious benefits, the technique is also more susceptible to small changes in sample composition. ICP-AES response was relatively independent of the matrix solution. The source of potential interferents for both techniques is substantially different, as discussed previously.

For ICP-MS it is important to identify possible interferences that may be present at the analyte ion mass. When monitoring the $^{31}P^+$ isotope, there may be significant interference contributions from $^{14}N^{16}O^{1}H^+$ and $^{15}N^{16}O^+$. Buffer/solvent combinations containing these atoms may have a deleterious effect on the background signal and stability. This is especially true for buffers that are relatively non-volatile, as an increased percentage will survive to the ICP and potentially contribute to matrix-induced interferences. While several of the buffers in this study contain nitrogen, only TBAH produced a significant increase in the background ion count. Other nitrogen-containing buffers such as ammonium acetate, ammonium formate and TEA did not produce a substantial increase in the background ion signal. A possible explanation for differences as compared to TBAH may be due to the increased mass fraction of the buffer in solution and the lower volatility and, hence, increased transport through the desolvator to the plasma.

The USN nebulization efficiency visibly decreased upon increases in the fraction of either methanol and acetonitrile. These effects may be caused by viscosity and surface tension changes as a function of liquid composition. Any variations in sample nebulization will affect the analytical signal intensity. The nebulization efficiency changes may help explain the loss in sensitivity upon addition of organic solvent. These effects will vary not only with the percent of organic solvent in the solution, but also with the nature of the organic solvent. Additionally, differences in the physical properties of acetonitrile- and methanol-based solvents such as volatility, surface tension, density, thermal conductivity, etc., will alter USN and MD desolvation behavior. For example, the boiling point of methanol is 65.5 °C while that of acetonitrile is 81.6 °C.

Lastly, it is possible that the transport efficiency of a semi-volatile analyte such as the phosphomycin used in this study may be influenced by the volatility of the buffer. For example, if the dry analyte-containing particulate traverses the desolvation system in the presence of a low volatility buffer, transport efficiency may be affected positively. If, on the other hand, the buffer is of high volatility, it may be volatilized and transported through the desolvator to waste, leaving behind less "protected" and more surface evaporable analyte. This has been noted in previous work conducted in this laboratory[54] and deserves additional study. A possible experiment to test this would include a low volatility buffer and a high volatility buffer that do not significantly contribute to the background ion count and analyte compounds of low and high volatility. Obtaining relative response factors for combination of low and high volatility buffer and analyte may help deduce the relative effect the sample introduction system has on low and high volatility analytes and how well buffers can "protect" them from desolvation.

Conclusion

The focus of this study has been to characterize detection behavior as a function of various solvent compositions and buffer combinations that may be utilized in liquid chromatography. The model system of this study examined phosphorus as phosphomycin. Depending on the solvent–buffer combinations, detection limits in the range of single parts per billion were obtained with ICP-MS. Detection limits were approximately 2 orders of magnitude higher with ICP-AES.

Responses changed minimally as the solvent composition was varied in ICP-AES experiments. It appears that within reasonable accuracy constraints, HPLC solvent programming can be performed with methanol solvents without instrument response recalibration. Sensitivities varied a bit more with water:acetonitrile mixtures, but still remained within 20% of that of the pure aqueous solvent.

With ICP-MS, sensitivities decreased significantly as the methanol or acetonitrile content was increased. This behavior may indicate that increased organic solvent may affect phosphorus ionization more significantly than phosphorus atom excitation. As compared to solutions without buffers added utilizing AES, most buffers only minimally affected signals and detection limits. Exceptions were seen with TEA, TBAH and HEPS. At this point, it is not completely clear why these buffers cause significantly more problems. However, the deleterious effects with TBAH and HEPS may possibly be due to higher mass loadings with the concentrations utilized for the chromatography conditions simulated.

Buffer effects are clearly more significant with ICP-MS. Whether in pure aqueous solutions or aqueous–organic mixtures, results were scattered. A number of the buffers produced sensitivity enhancements, but a number produced suppression. It is clear that response calibration is closely related to the nature of the solvent–buffer system and that any calibration standards must be closely matched in composition. Further studies are needed to determine the fundamental reasons for these behaviors.

As the organic mobile phase concentrations are increased, the phosphorus ion signal decreases. These effects are more pronounced with the methanol-based solvents than with the acetonitrile-based solvents. Nebulization efficiency may play a role in the signal reduction at higher organic phase concentrations; however, because the signal reduction is less significant, it is more likely that ionization suppression effects caused by higher organic solvent concentrations are the cause.

Carbon deposition was more significant with acetonitrile-containing mobile phases as opposed to methanol. As noted previously, this may be attenuated by bleeding a steady flow of O_2 into the nebulizer gas. It is typically suggested that O_2 be continuously bled into the system to minimize damage to the cones and decrease the frequency of cleaning. A comprehensive study on the effect of bleeding O_2 into the nebulizer gas flow needs to be performed to ascertain if this significantly affects the sensitivity of the instrument toward heteroatom detection.

In summary, isocratic elution is suggested for HPLC methods involving USN-MD-ICP-MS. Gradient elution with ICP-AES is possible with minimal sensitivity effects. Several buffers led to sensitive nonmetal determinations for both ICP-AES and ICP-MS. Additional studies are required to investigate specific reasons for the large fluctuation in sensitivity in ICP-MS analyses. Additionally, the buffer study presented here was for phosphorus. It is believed that this is a representative model to predict favorable buffer:solvent compositions for other hard to ionize heteroatoms (S, Cl, and F). From the scattered results, it is suggested other studies be performed for the specific element of interest. It is apparent that the analytical signal and any interferences are specific to the element of interest and would need to be characterized for individual atom:buffer:mobile phase combinations.

CHAPTER 3

EFFECT OF SUPPLEMENTAL NEBULIZER GAS ON ANALYTICAL FIGURES OF MERIT FOR USN-MD-ICP-MS DETECTION OF VARIOUS HETEROATOM-CONTAINING PHARMACEUTICAL COMPOUNDS

Introduction to Nebulizer Gas Doping Experiments

Argon ICPs have been shown to be effective in supplying a large pool of excited state atoms and ions for many elements. However, alternatives to a pure argon ICP, such as mixed gas plasmas, have been investigated for several reasons, including: increased tolerance to organic solvent in the matrix[58-62], sensitivity enhancements for harder to excite or ionize atoms[68,63-76], improvements in precision[65], reduction of matrix effects[58,77], and minimization of spectral interferences[58,61,68]. ICPs derive their bulk physical properties from the carrier gas flows that form and sustain the plasma. Argon plasmas will have different properties than helium plasmas. The introduction of molecular and atomic gas species into the cool, auxiliary, or nebulizer gas flows of an argon plasma has been investigated by numerous groups as a means to improve the analytical capabilities of the ICP. The most common bleed gases introduced into the argon gas flows are oxygen, nitrogen, helium, hydrogen and xenon. The effects of oxygen, nitrogen, and helium gas addition to the nebulizer gas flow are detailed in this chapter.

Results from the detection limit, solvent composition and buffer study, described previously in this dissertation, provided a basis for additional experiments utilizing mixed gas plasmas. Principally, although detection limits for several heteroatoms were among the best reported in the literature, any means to lower detection limits should be investigated. Secondly, organic solvent loading for acetonitrile-containing mobile phases became problematic in ICP-MS experiments. Significant carbon deposition on the sample and skimmer cones required increased maintenance. The solvent loading on the plasma and increased carbon deposition may have also negatively impacted the analytical figures of merit for phosphorus detection with organic mobile phase compositions. Finally, the large deviations in sensitivity across mobile phase compositions for heteroatom ICP-MS detection indicate that HPLC gradient programming is currently not feasible with solvents such as acetonitrile. Although it is recognized that other pure or mixed gas excitation and ionization sources such as helium MIPs and helium/nitrogen ICPs may be a viable route to resolving these issues, the discussion presented here will detail efforts to improve sensitivity and organic solvent tolerance utilizing mixed gas argon ICPs.

It was decided that additional experiments investigating nonmetal detection would principally involve ICP-MS. ICP-MS detection displayed greater sensitivity, has simultaneous multi-element detection capability, and allowed the determination of several nonmetal atoms. ICP-MS had detection limits for phosphorus one order of magnitude lower than ICP-AES. The monochromator and PMT detector system allowed only for single-element detection. Finally, sulfur-, chlorine-, and fluorine-containing analytes can not be easily detected with UV-VIS ICP-AES instruments, as the most intense atomic line emissions for these elements occur in the wavelength region of the spectrum below 190 nm, a region where atmospheric oxygen absorbs radiation. Monitoring these emission lines requires a specialized optical path filled with nitrogen or argon, or evacuated.

Oxygen Addition to the Nebulizer Gas

Oxygen addition to an argon plasma is customarily performed when organic solvents are being nebulized[58-62]. The presence of oxygen increases the oxidative environment of the plasma, allowing for more complete combustion of organic solvents. Oxygen-doped plasmas are more resistant to organic solvent loading, leading to increased stability of the discharge. Carbon deposition is greatly reduced on the sample and skimmer cones in ICP-MS analyses. Oxygen is generally added in small quantities, typically 2-10%, to the auxiliary or nebulizer gas flows[58]. A larger fraction of oxygen may be used; however, care must be taken, as high oxygen content may cause deterioration of the nickel sample cone. For high oxygen flow rates, platinum sample cones may be substituted for the stock nickel cones.

Several groups have studied the effect of adding oxygen to the nebulizer gas flow. Goessler and co-workers[59] added a 20:80 oxygen:argon mixture to the argon nebulizer gas flow for the analysis of phospholipids. They tested several nebulizer and supplemental oxygen:argon gas flow rates. It was determined that the signal-to-background ratio was not improved with oxygen addition. The additional oxygen flow rate decreased the residence time of the aerosol in the spray chamber, reducing desolvation. Thus, oxygen addition was not beneficial with this sample introduction technique and optimization procedure.

Björn and Frech[60] introduced 50 mL/min of oxygen into the auxiliary gas flow when analyzing solutions containing ethanol and hexane for mercury (m/z = 202), tin (m/z = 120), and lead (m/z = 208). This group attempted to add oxygen to the nebulizer gas flow but noticed a significant decrease in plasma stability. Alternatively, oxygen was added to the auxiliary gas flow. Brenner and co-workers[61] characterized a USN-MD sample introduction system for the detection of several metal dithiocarbamates in chloroform. The effect of a 30 mL/min of oxygen addition to the auxiliary gas on $^{40}Ar^{12}C^+$ and $^{40}Ar^{12}C^1H^+$ polyatomic interferences of $^{52}Cr^+$ and $^{53}Cr^+$ was characterized. They found a significant decrease in these ion counts. Carbon deposition on the sample cones was greatly reduced as well.

Cai et al.[62] performed computer simulations on the effect of added oxygen to the outer and nebulizer gas flows. These simulations predicted an increase in the central channel temperature of an argon-oxygen plasma as compared to a pure argon plasma. The predicted increase in temperature suggests additional benefits in the use of oxygen as a supplemental gas, namely the reduction of spectral and matrix interferences as the formation of polyatomic interferences is inhibited in a hot plasma.

Nitrogen Addition to the Nebulizer Gas

Nitrogen addition to argon plasmas has been investigated as a means to increase sensitivity and decrease spectral and matrix interferences for several atomic species. Wang, Evans, and Caruso[68] added 3% nitrogen to the nebulizer gas flow rate and noted the elimination of $^{40}Ar^{35}Cl^+$ and reduction of $^{35}Cl^{16}O^+$, $^{40}Ar^{37}Cl^+$, and $^{39}Ar_2^+$ polyatomic ions. These cause spectral interferences when determining $^{75}As^+$, $^{51}V^+$, $^{77}Se^+$, and $^{78}Se^+$, respectively. A decrease in analyte sensitivities was also noted.

Pröfrock and co-workers[69] added nitrogen (0-50 mL/min) to the nebulizer gas in an attempt to enhance ionization of phosphorus, sulfur, chlorine, bromine, and iodine-containing compounds. A slight increase in sensitivity was shown for several analytes, although a large increase in the background for phosphorus had a deleterious effect on its detection limit. Addition of greater than 20 mL of nitrogen caused a dramatic reduction in ion signals for all species. Enhancement of phosphorus signal was also noted by Vonderheide, Meija, Montes-Bayón, and Caruso[63]. The increase in sensitivity was offset by an increase in background ions, principally from $^{15}N^{16}O^+$ and $^{14}N^{16}O^1H^+$.

Beauchemin and Craig[64] added from 0 to 10% nitrogen to the outer gas flow and monitored the effect on the analytical signal for several analytes. Also, the effect of nitrogen on alleviating ionization suppression from a mobile phase containing sodium was studied. Easily ionized elements such as sodium and potassium present in the matrix may cause suppression of ionization for other analytes. It was found that the addition of 10% nitrogen to the outer gas flow alleviated suppressions of 12% and 82% for 0.01M and 0.1M sodium-containing solutions, respectively. Sensitivity towards other analytes decreased slightly, although the signal-to-background ratio improved for iron and selenium, a result of the reduction of spectral interferences. A separate study by Holliday and Beauchemin[65] also demonstrated a reduction in matrix effects upon nitrogen addition to the outer plasma gas. There was, however, a concurrent drop in analyte sensitivity.

Other groups have added nitrogen to the auxiliary or coolant gas flows with varied results[70,71]. Discrepancies in results can be attributed to differences in instrumental conditions and optimization procedures. Some groups performed exhaustive optimization studies. Others groups optimized the system prior to supplementary gas addition and minimally altered instrumental settings as the flow of nitrogen is increased.

Fundamental studies of nitrogen supplemented argon plasmas indicate that nitrogen has a dramatic effect on the bulk properties of the plasma. Sesi et al.[72] noted a visible widening of the central channel when nitrogen was added to the nebulizer gas flow. Measured electron density decreased markedly compared to oxygen and helium bleed gases, while decreases in electron and gas-kinetic temperatures were also noted. Computer simulations by Mingxiang Cai et al. [62] support these experimental findings.

Helium Addition to the Nebulizer Gas

Supplemental helium addition to argon ICPs has received only modest attention, in large part due to the benefits of constructing a pure helium ICP-MS[73-77]. Supplementation or complete replacement of argon as a plasma gas in favor of helium is accomplished to increase ionization of harder to ionize elements and contain higher energy moieties due to the high ionization energy of helium (24.6 eV) as compared to argon (15.8 eV). Helium discharges have been shown to increase the intensity of nonmetal ion line emissions [7,78].

Pröfrock and co-workers[69] found sensitivity enhancements for several nonmetal-containing pesticides with the addition of 30 mL/min helium to the nebulizer gas flow. Caruso and co-workers[79] observed an increase in sensitivity with 5% helium added to the nebulizer gas flow for a bromine-containing compound. Fundamental studies, performed by Sesi et al.[62], on the effect of added helium to the nebulizer gas flow of argon ICPs indicated a decrease in the electron number density in the central region of the plasma. The addition of helium did not significantly alter the appearance, shape or density of the plasma, in contrast to the addition of nitrogen. The electron temperature did not increase when helium was added to the nebulizer or auxiliary gas flows; however, it was found that the gas kinetic temperature increased 1500 K with the addition of 16.7% helium to either gas flow.

Considerations for Nebulizer Gas Doping Experiments With USN-MD-ICP-MS

The addition of oxygen, nitrogen, and helium has not been thoroughly characterized for the detection of heteroatoms utilizing an USN-MD sample introduction system. Since oxygen is commonly added as a supplementary gas when organic matrices are analyzed, a comprehensive examination of the background and analytical signal response to increasing amounts of oxygen was performed for phosphorus-, sulfur-, chlorine-, and fluorine-containing analytes. Nitrogen and helium supplemental nebulizer gas addition is less prevalent as a standard technique in ICP-MS analysis. The effect on the background and analytical signal response for sulfur- and phosphorus-containing analytes was characterized for nitrogen addition. The effect of helium supplementary gas addition was performed for sulfur-containing analytes.

Experimental procedures and methods to optimize instrumental settings and conditions when supplemental gases are introduced to the argon flow rates is non-uniform in the literature. Protocols for oxygen addition supplied with our instrument suggest increasing the oxygen flow rate, while nebulizing the organic solvent, until the green emission from C_2 is not present in the plasma. However, the amount of oxygen necessary to significantly reduce the carbon emission will be different depending on the type of organic solvent and the composition of the matrix. Also, changing the oxygen gas flow rate without adjusting the nebulizer gas flow rate will alter the nebulization and transport efficiency, affecting the amount of solvent load on the plasma. This could significantly alter the analytical properties of the USN-MD-ICP-MS system.

For systematic studies of the effect of supplemental nebulizer gas flows, it was decided to maintain the nebulization and transport efficiency. Oxygen experiments utilized an oxygen inlet port on the instrument using a calibrated mass flow controller. This allowed direct mixing of the oxygen and argon nebulizer gas prior to the USN-MD sample introduction system. The combined flow of oxygen and argon was maintained at 1.00 L/min to maintain nebulization and transport efficiency.

Nitrogen and helium experiments utilized post USN-MD addition of gas via a glass T-junction pictured in Figure 31. The T-junction was connected to the quartz torch. The nebulizer gas flow was maintained at 1.00 L/min and helium or nitrogen was bled in via a calibrated mass flow controller. This allowed nebulizer and transport efficiency to be maintained. However, the total gas flow rate into the plasma was altered as the amount of supplementary gas varied. This could have an effect on the density of the plasma in the central channel and will change the residence time of the analyte and solvent in the plasma. This may change the analytical zone of the plasma where the locus of ions is sampled. Several groups re-optimize the position of the torch relative to the sample cone, termed the sampling depth, after adjusting any plasma gas flows. The adjustment of sampling depth is not easily reproducible on our instrument and was kept constant as supplemental gas flow rates were varied. However, nitrogen and helium studies were carried out over a range of forward power levels. Altering the forward power changes the plasma's density and will compensate for reduced residence times by imparting a greater

Figure 31. Glass T-junction utilized for nitrogen and helium supplementary gas studies. Dimensions are 7.0 x 4.0 cm.

amount of energy to the analyte molecules and solvent. This effectively changes the position of the analytical zone of the plasma, hence a comprehensive study of analytical and background signals over a range of forward powers will help deduce the ability of supplemental gases to enhance the analytical sensitivity of ICP-MS to heteroatom-containing compounds.

One final consideration needs to be mentioned concerning the instrumentation utilized in this study. Studies conducted prior to the supplementary gas experiments used the original r.f. generator and forward powers were typically 800-1400 W for all analytes monitored. A refurbished r.f. generator was purchased and installed after the original showed signs of failure. A power study was performed utilizing the new r.f. generator to determine the background and signal response and optimum forward power for the analysis of phosphorus as phosphomycin in aqueous solution. Figures 32 and 33 illustrate phosphorus signal to background ratios and signal and background counts as a function of applied forward power, respectively. Optimum forward powers changed significantly to lower power levels than required previously for sensitive nonmetal analysis. Above 600 W, there is little or no ion transmission; both the phosphorus ion and background signals tend towards zero. The trend is observed with other analytes as well. Figure 34 is a mass spectrum obtained at 350 W for a nebulized solution of 10 ppb strontium (m/z = 87). Figure 35 shows a mass scan obtained at 750 W with the same solution being nebulized. No discernible mass peaks are present on the same scale as the 350 W mass scan. Visually, at lower power levels the plasma is smaller and less dense. When nebulized solvent is directed into the plasma, a clear central channel can be distinguished between the

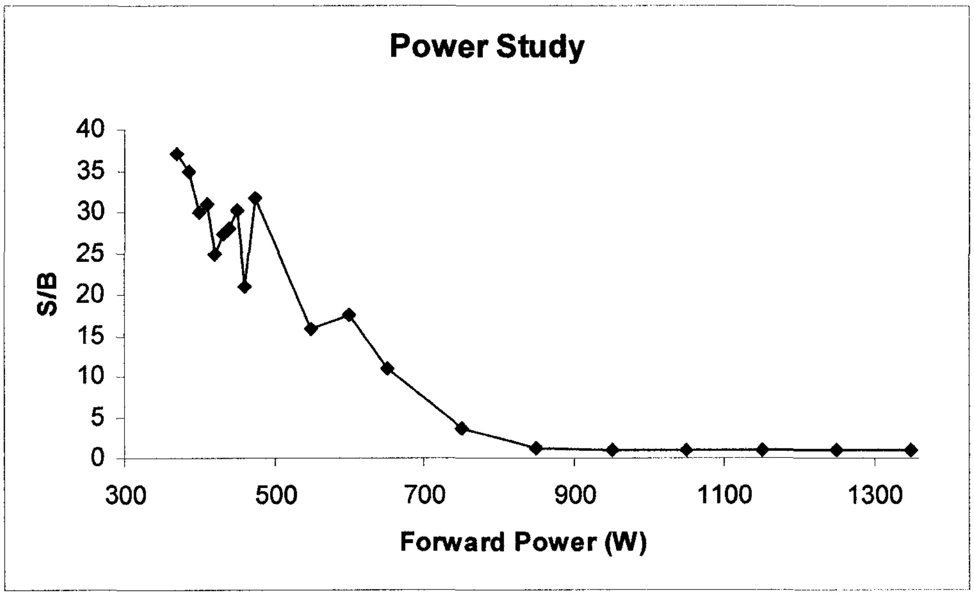

Figure 32. Graph of signal to background ratio vs. applied forward power for a 100 ppb solution of phosphorus as phosphomycin.

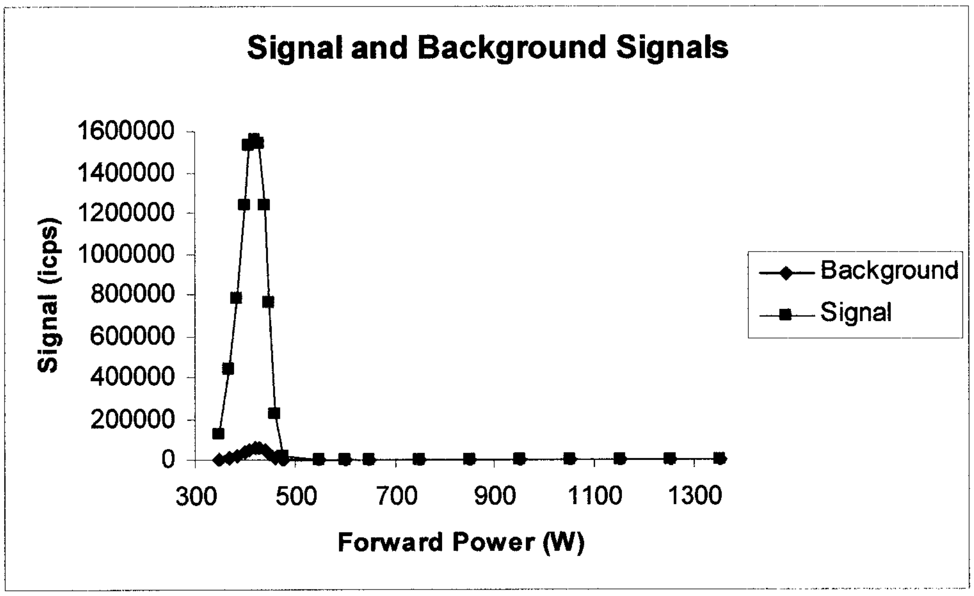

Figure 33. Graph of raw signal and background counts vs. applied forward power for a 100 ppb solution of phosphorus as phosphomycin.

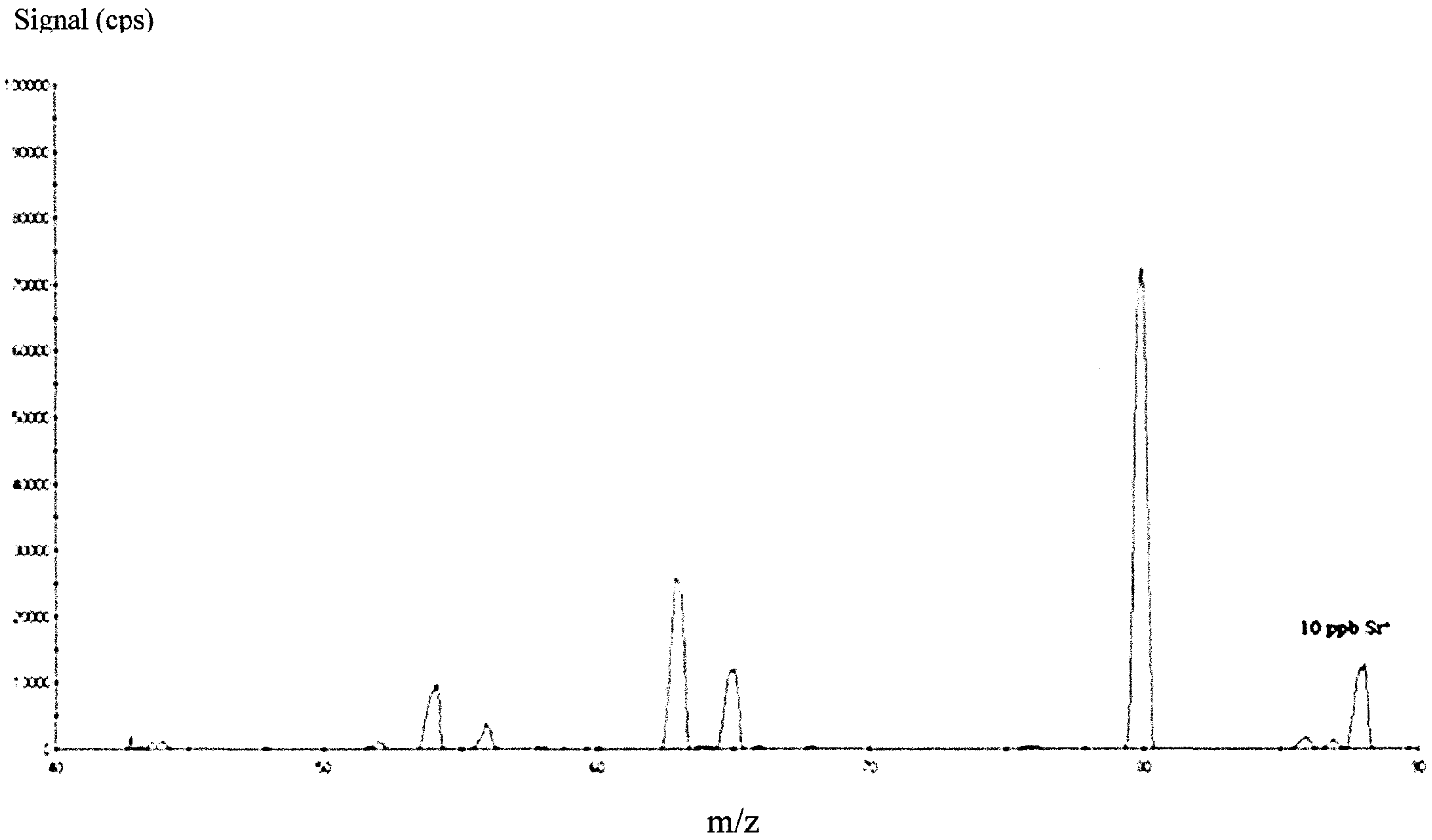

Figure 34. Mass spectrum of a 10 ppb Sr aqueous solution at a forward power of 350 watts.

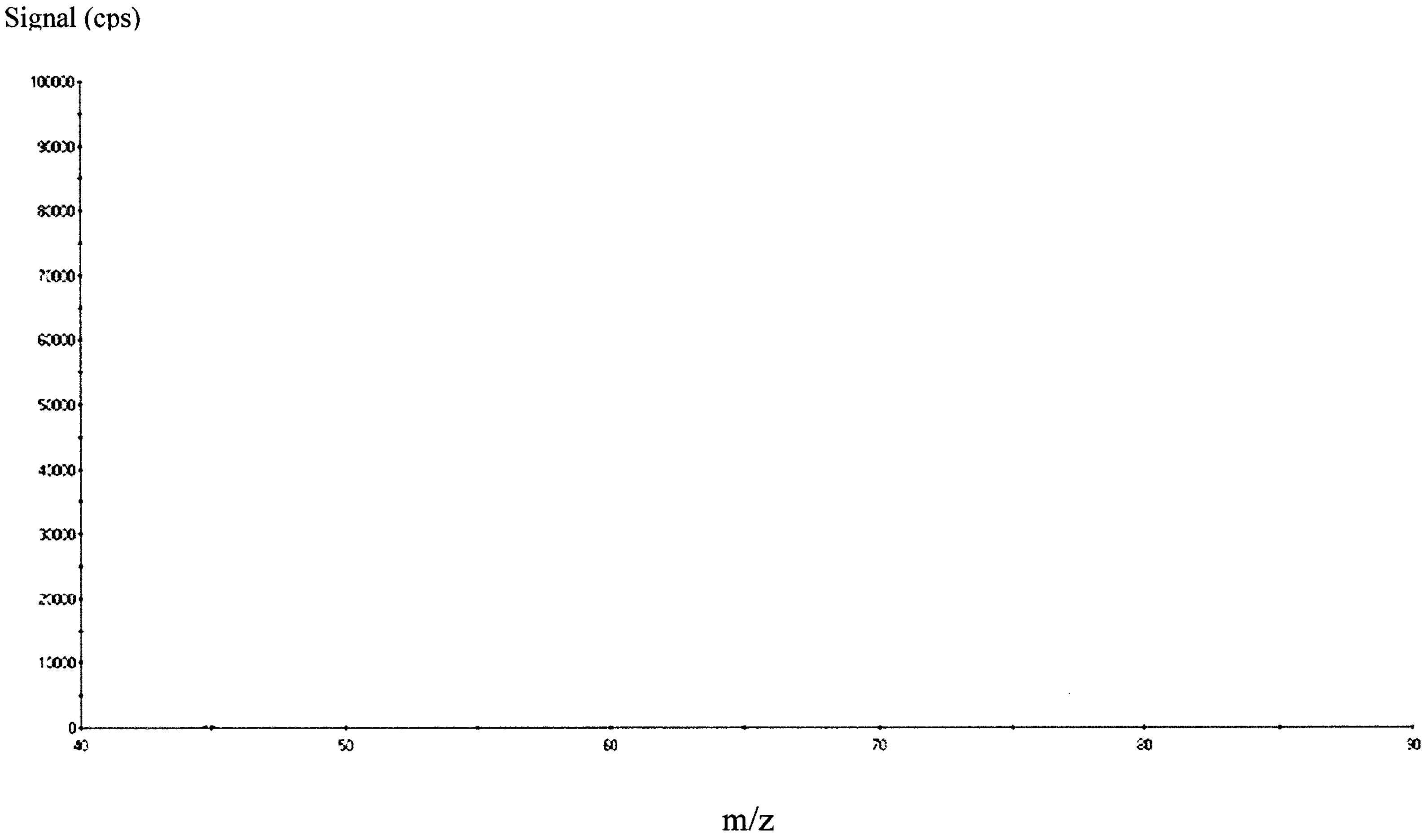

Figure 35. Mass spectrum of a 10 ppb Sr aqueous solution at a forward power of 750 watts

nebulizer gas injector tip and the front of the sample cone. As the power level is increased, this central channel diminishes and eventually disappears. These power levels are not attainable with standard nebulizers or an USN. The reflected power will become too high and the plasma will extinguish. MD is required when operating at power levels below 600 W on our instrument.

A thorough review of published literature found no other articles describing the utilization of these low power levels in ICP-MS. It is generally accepted that lower forward powers produce a plasma that is lower in temperature, less stable, has poorer ionization efficiency, and does not tolerate high solvent load. In the context of supplemental gas addition, it is important to note that additional gas flows may have quite a different effect on the plasma properties at low power levels as compared to high power levels typically discussed in literature.

Experimental

ICP-MS Instrumentation

A Fisons (Thermo Electron) Instruments PlasmaQuad II 27 MHz ICP-MS was used. Ion signals from a Burle (Sturbridge, MA) Channeltron 4870V were acquired utilizing Thermo Electron PlasmaLab software (Version 1.06.007, Ionflight, Boston, MA). The nebulizer gas flow rate was maintained at 1.00 L/min. Supplemental oxygen was bled in to form a nebulizer gas composed of 2, 4, 6, 8 and 10% oxygen.

Helium and nitrogen gases were added as described previously in flow rates of 0-80 mL/min. The isotopes monitored for the oxygen doping experiments were $^{35}Cl^+$, $^{31}P^+$, $^{34}S^+$, and $^{19}F^+$. During the nitrogen addition experiments $^{31}P^+$ and $^{34}S^+$ were monitored. In the supplemental helium addition experiments, $^{34}S^+$ was monitored. A weekly routine calibration of the instrument was performed by continuously nebulizing a peristaltically pumped 10 ppb solution of Li, Mg, Co, In, Pb, Ce, and U in 1% (v/v) nitric acid at a forward power of 1350 W. Tables 13-15 summarize the operational parameters used for the oxygen, nitrogen, and helium supplemental gas studies.

Reagents and Sample Preparation

An 80 ppm phosphorus-containing stock solution was prepared by dissolving an appropriate mass of phosphomycin calcium salt (Sigma-Aldrich, Milwaukee, WI) into deionized water. A 50 ppm sulfur-containing stock solution was prepared by dissolving an appropriate mass of amoxicillin (Sigma-Aldrich, Milwaukee, WI) in an aqueous 0.2% HNO_3 solution. A 60 ppm chlorine-containing stock solution was prepared by dissolving an appropriate mass of chlorpropamide (Sigma-Alrich, Milwaukee, WI) in an aqueous 0.02 M KOH solution. A 500 ppm fluorine-containing stock solution was prepared by dissolving ofloxacin (Sigma-Aldrich, Milwaukee, WI) in a 4% NH_3 solution. The stock solutions were used to prepare diluted solutions with appropriate solvents for analyses. HPLC grade methanol and acetonitrile (Sigma-Aldrich, Milwaukee, WI) and 18 MΩ•cm deionized water were used for

Table 13. Operating parameters for oxygen addition experiments.

Sample introduction system	
Peristaltic pump flow rate, mL/min	1.0
Nebulizer gas flow rate, L/min	1.0
Oxygen gas flow rate, mL/min	20-100
Nebulizer heater temperature, °C	140
Nebulizer condenser temperature, °C	3
Membrane desolvator temperature, °C	160
Membrane desolvator countercurrent flow rate, L/min	1.5
ICP-MS system	
Optimal RF power, W	490 (P, S); 510 (Cl, F);
Detector	Burle Channeltron 4870V
Outer gas flow rate, L/min	14.0
Intermediate gas flow rate, L/min	0.8
Data acquisition parameters	
Scan mode	Single ion monitor
Dwell time, ms	250
Isotopes monitored	^{31}P, ^{34}S, ^{35}Cl, ^{19}F

Table 14. Operating parameters for nitrogen addition experiments.

Sample introduction system	
Peristaltic pump flow rate, mL/min	1.0
Nebulizer gas flow rate, L/min	1.0
Nitrogen gas flow rate, mL/min	10-70
Nebulizer heater temperature, °C	140
Nebulizer condenser temperature, °C	3
Membrane desolvator temperature, °C	160
Membrane desolvator countercurrent flow rate, L/min	1.5
ICP-MS system	
Optimal RF power, W	450-1350 (P, S)
Detector	Burle Channeltron 4870V
Outer gas flow rate, L/min	14.0
Intermediate gas flow rate, L/min	0.8
Data acquisition parameters	
Scan mode	Single ion monitor
Dwell time, ms	250
Isotopes monitored	^{31}P, ^{34}S

Table 15. Operating parameters for helium addition experiments.

Sample introduction system	
Peristaltic pump flow rate, mL/min	1.0
Nebulizer gas flow rate, L/min	1.0
Helium gas flow rate, mL/min	10-80
Nebulizer heater temperature, °C	140
Nebulizer condenser temperature, °C	3
Membrane desolvator temperature, °C	160
Membrane desolvator countercurrent flow rate, L/min	2.2
ICP-MS system	
Optimal RF power, W	450-590
Detector	Burle Channeltron 4870V
Outer gas flow rate, L/min	14.0
Intermediate gas flow rate, L/min	0.8
Data acquisition parameters	
Scan mode	Single ion monitor
Dwell time, ms	250
Isotope monitored	^{34}S

sample preparation. The structures of analytes used in this study can be found in Figure 10.

Results and Discussion for Oxygen Addition

Data for Oxygen Addition

The effects of oxygen addition were observed for pure aqueous, 50:50 methanol:aqueous (MeOH:aqueous), and 50:50 acetonitrile:aqueous (ACN:aqueous) solvent compositions. Tables 16-19 contain the results of oxygen addition for sulfur-, phosphorus-, chlorine-, and fluorine-containing analytes. Figures 36-47 contain plots of effects of oxygen addition on sensitivities, background signal intensities, and detection limits for all analytes.

Physical Characteristics of an Oxygen Doped ICP

The addition of oxygen had a visibly noticeable effect on the size, shape, and density of plasma. The central channel appeared to constrict with addition of oxygen to the nebulizer gas. The density of the plasma slightly increased near the sample cone and slightly decreased near the nebulizer injector tube from the torch. These changes may indicate a shift of the analytical zone of the plasma. Fluctuations in analytical and background signals may be due to such a shift. When operating at

Table 16. Analytical figures of merit for sulfur as amoxicillin.

<table>
<tr><th colspan="5">100% H_2O</th></tr>
<tr><th>% O_2</th><th>Analyte Conc. (ppb)</th><th>Avg Bkgd (icps/10^2)</th><th>Avg Analytical Signal (icps/10^2)</th><th>Avg DL (ppb)</th></tr>
<tr><td>0</td><td>1000</td><td>3.5</td><td>77</td><td>21</td></tr>
<tr><td>2</td><td>1000</td><td>5.3</td><td>78</td><td>22</td></tr>
<tr><td>4</td><td>1000</td><td>5.1</td><td>100</td><td>15</td></tr>
<tr><td>6</td><td>1000</td><td>5.3</td><td>120</td><td>18</td></tr>
<tr><td>8</td><td>1000</td><td>8.2</td><td>150</td><td>23</td></tr>
<tr><td>10</td><td>1000</td><td>9.3</td><td>170</td><td>19</td></tr>
<tr><th colspan="5">50% MeOH
50% H_2O</th></tr>
<tr><th>% O_2</th><th>Analyte Conc. (ppb)</th><th>Avg Bkgd (icps/10^2)</th><th>Avg Analytical Signal (icps/10^2)</th><th>Avg DL (ppb)</th></tr>
<tr><td>0</td><td>1000</td><td>1.7</td><td>110</td><td>11</td></tr>
<tr><td>2</td><td>1000</td><td>1.9</td><td>100</td><td>13</td></tr>
<tr><td>4</td><td>1000</td><td>1.7</td><td>83</td><td>14</td></tr>
<tr><td>6</td><td>1000</td><td>1.3</td><td>70</td><td>14</td></tr>
<tr><td>8</td><td>1000</td><td>1.0</td><td>62</td><td>14</td></tr>
<tr><td>10</td><td>1000</td><td>0.8</td><td>45</td><td>15</td></tr>
<tr><th colspan="5">50% ACN
50% H_2O</th></tr>
<tr><th>% O_2</th><th>Analyte Conc. (ppb)</th><th>Avg Bkgd (icps/10^2)</th><th>Avg Analytical Signal (icps/10^2)</th><th>Avg DL (ppb)</th></tr>
<tr><td>0</td><td>1000</td><td>2.2</td><td>120</td><td>12</td></tr>
<tr><td>2</td><td>1000</td><td>3.3</td><td>110</td><td>15</td></tr>
<tr><td>4</td><td>1000</td><td>3.0</td><td>85</td><td>21</td></tr>
<tr><td>6</td><td>1000</td><td>2.1</td><td>86</td><td>18</td></tr>
<tr><td>8</td><td>1000</td><td>1.7</td><td>72</td><td>15</td></tr>
<tr><td>10</td><td>1000</td><td>1.1</td><td>50</td><td>17</td></tr>
</table>

Table 17. Analytical figures of merit for phosphorus as phosphomycin.

100% H_2O

% O_2	Analyte Conc. (ppb)	Avg Bkgd (icps/10^3)	Avg Analytical Signal (icps/10^3)	Avg DL (ppb)
0	40	0.1	7.2	2.4
2	40	3.4	5.5	11
4	40	2.8	7.2	6.1
6	40	2.9	8.5	5.3
8	40	2.1	11	3.8
10	40	2.9	12	5.8

50% MeOH
50% H_2O

% O_2	Analyte Conc. (ppb)	Avg Bkgd (icps/10^3)	Avg Analytical Signal (icps/10^3)	Avg DL (ppb)
0	40	0.5	3.4	4.3
2	40	0.6	3.4	4.7
4	40	0.7	1.7	6.9
6	40	0.6	2.1	6.5
8	40	0.6	1.9	5.7
10	40	0.5	1.2	7.4

50% ACN
50% H_2O

% O_2	Analyte Conc. (ppb)	Avg Bkgd (icps/10^3)	Avg Analytical Signal (icps/10^3)	Avg DL (ppb)
0	4000	3.1	680	4.3
2	4000	2.1	860	2.4
4	4000	3.9	820	5.3
6	4000	3.3	750	4.5
8	4000	2.9	680	4.9
10	4000	1.3	570	2.8

Table 18. Analytical figures of merit for chlorine as chlorpropamide.

100% H_2O				
% O_2	Analyte Conc. (ppb)	Avg Bkgd (icps/10^3)	Avg Analytical Signal (icps/10^3)	Avg DL (ppb)
0	1200	0.3	34	9.3
2	1200	0.3	31	9.1
4	1200	0.6	28	18
6	1200	1.0	25	28
8	1200	1.4	25	32
10	1200	2.1	26	33

50% MeOH 50% H_2O				
% O_2	Analyte Conc. (ppb)	Avg Bkgd (icps/10^3)	Avg Analytical Signal (icps/10^3)	Avg DL (ppb)
0	6000	1.5	250	6.2
2	6000	1.5	170	8.8
4	6000	1.5	210	7.5
6	6000	1.5	180	11
8	6000	1.5	160	14
10	6000	2.0	150	13

50% ACN 50% H_2O				
% O_2	Analyte Conc. (ppb)	Avg Bkgd (icps/10^3)	Avg Analytical Signal (icps/10^3)	Avg DL (ppb)
0	1200	3.2	4.2	19
2	1200	7.2	3.6	30
4	1200	7.0	2.8	28
6	1200	6.2	2.6	23
8	1200	7.8	1.6	25
10	1200	8.8	ND	27

Table 19. Analytical figures of merit for fluorine as olfoxacin.

100% H_2O				
% O_2	Analyte Conc. (ppm)	Avg Bkgd (icps/10^3)	Avg Analytical Signal (icps/10^3)	Avg DL (ppm)
0	20	1.2	4.2	2.1
2	20	1.1	3.6	2.0
4	20	1.5	2.8	3.1
6	20	1.9	2.6	4.4
8	20	2.6	1.6	11
10	20	3.6	ND	ND
50% MeOH 50% H_2O				
% O_2	Analyte Conc. (ppm)	Avg Bkgd (icps/10^3)	Avg Analytical Signal (icps/10^3)	Avg DL (ppm)
0	20	4.4	3.5	5.5
2	20	4.8	2.9	4.6
4	20	6.2	3.6	4.3
6	20	6.6	4.6	3.7
8	20	7.7	3.5	5.7
10	20	10.1	3.6	7.7
50% ACN 50% H_2O				
% O_2	Analyte Conc. (ppm)	Avg Bkgd (icps/10^3)	Avg Analytical Signal (icps/10^3)	Avg DL (ppm)
0	100	4.9	2.7	18
2	100	4.9	2.6	19
4	100	4.9	4.1	12
6	100	6.2	3.3	16
8	100	7.8	2.8	23
10	100	8.8	3.6	21

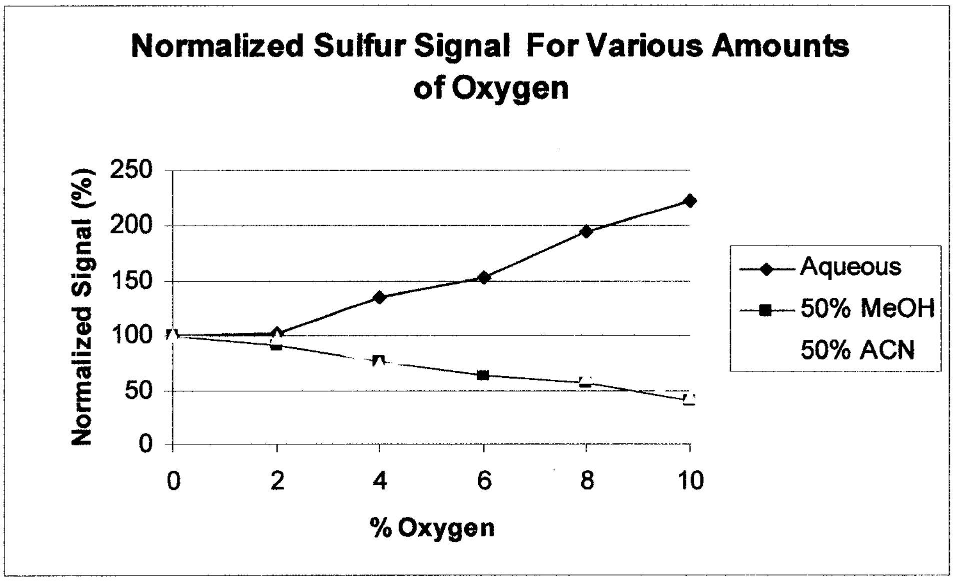

Figure 36. Analytical signal trends for sulfur as a function of oxygen nebulizer gas composition. Signal has been normalized to a value of 100 with respect to the signal seen with 0% added.

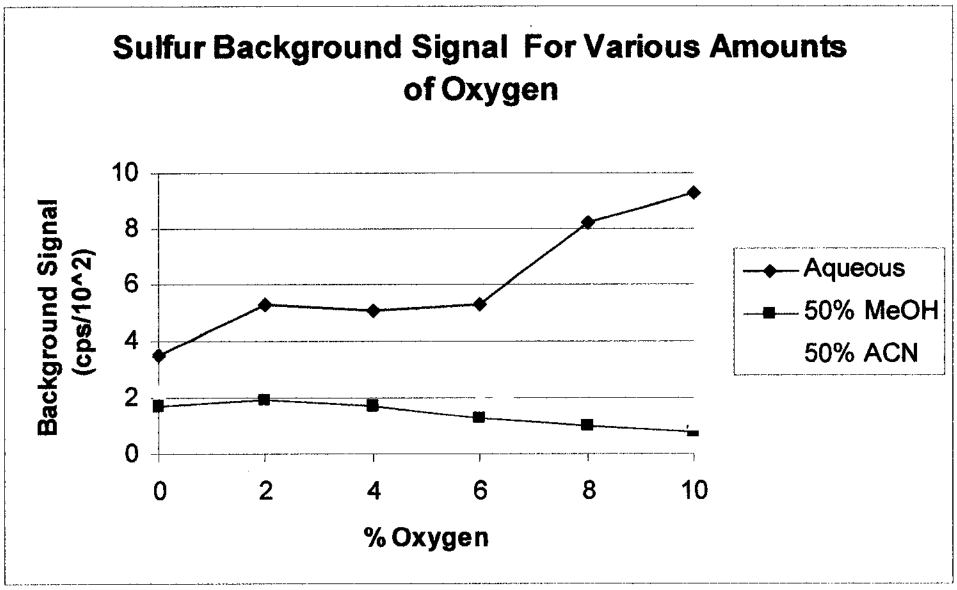

Figure 37. Background signal intensity for sulfur as a function of oxygen nebulizer gas composition.

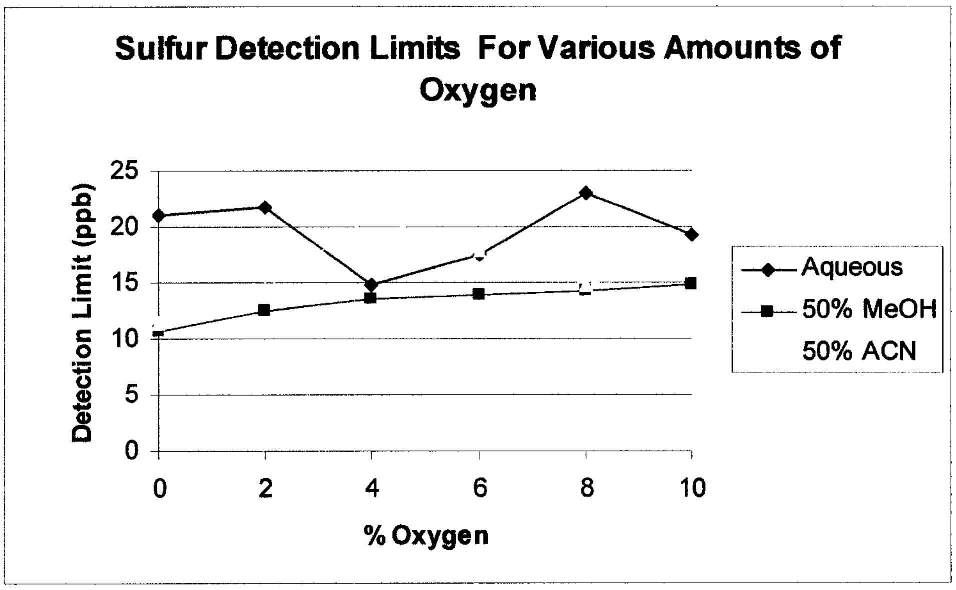

Figure 38. Detection limits for sulfur as a function of oxygen nebulizer gas composition.

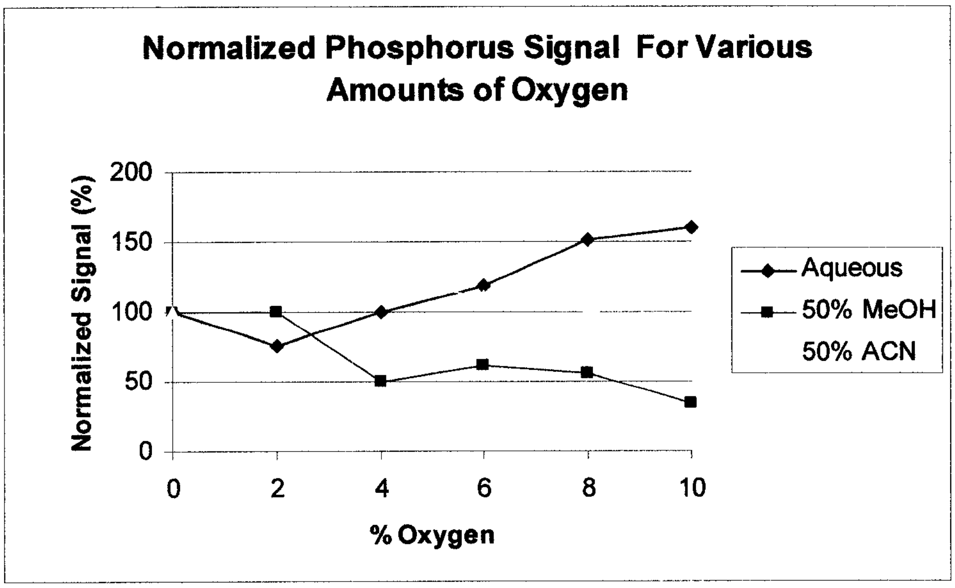

Figure 39. Analytical signal trends for phosphorus as a function of oxygen nebulizer gas composition. Signal has been normalized to a value of 100 with respect to the signal seen with 0% added.

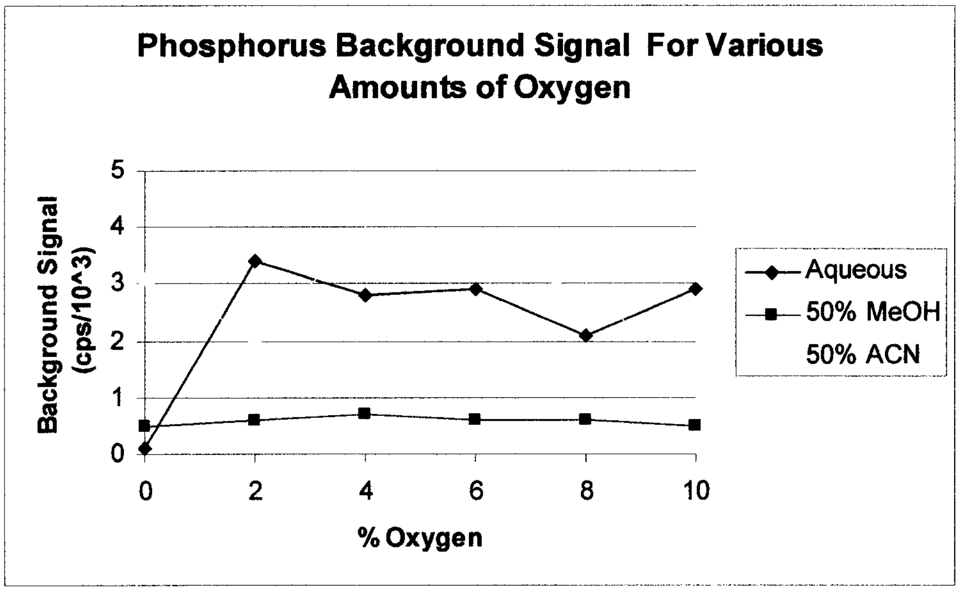

Figure 40. Background signal intensity for phosphorus as a function of oxygen nebulizer gas composition.

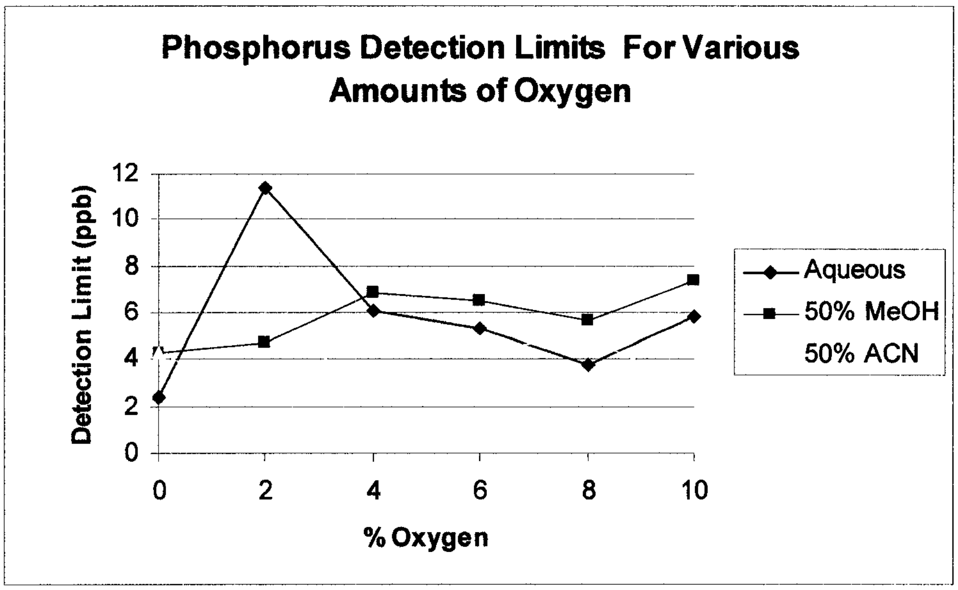

Figure 41. Detection limits for phosphorus as a function of oxygen nebulizer gas composition.

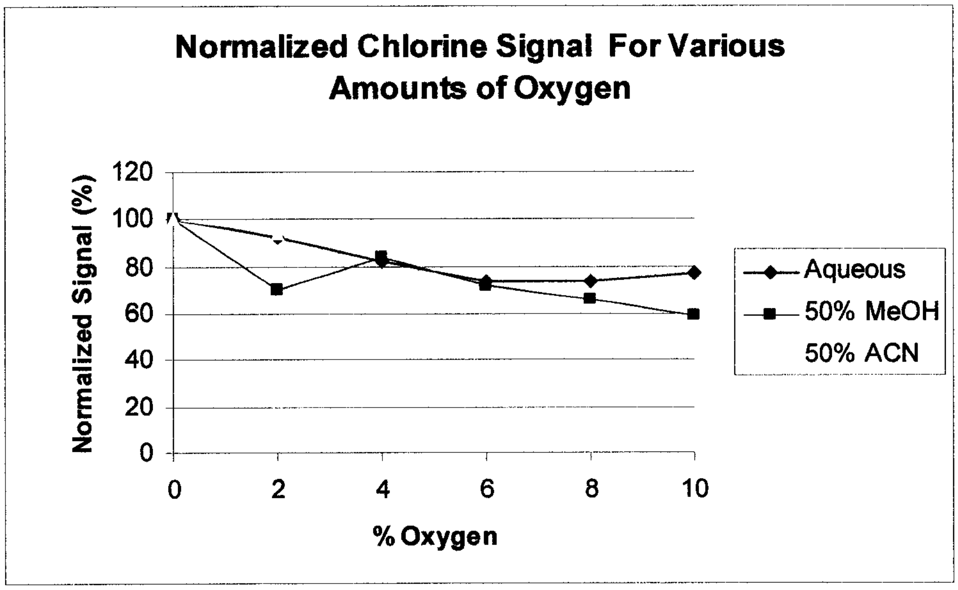

Figure 42. Analytical signal trends for chlorine as a function of oxygen nebulizer gas composition. Signal has been normalized to a value of 100 with respect to the signal seen with 0% added.

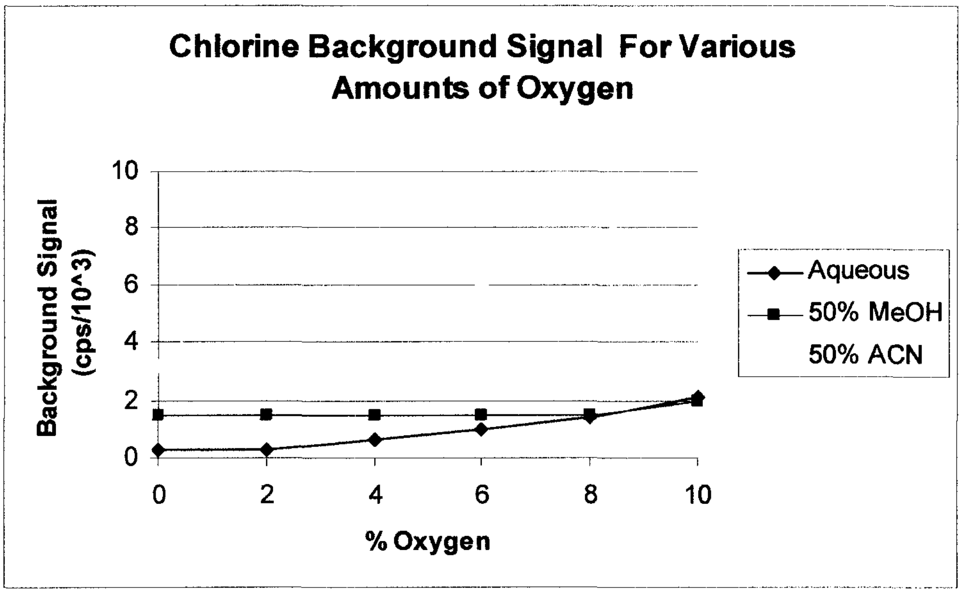

Figure 43. Background signal intensity for chlorine as a function of oxygen nebulizer gas composition.

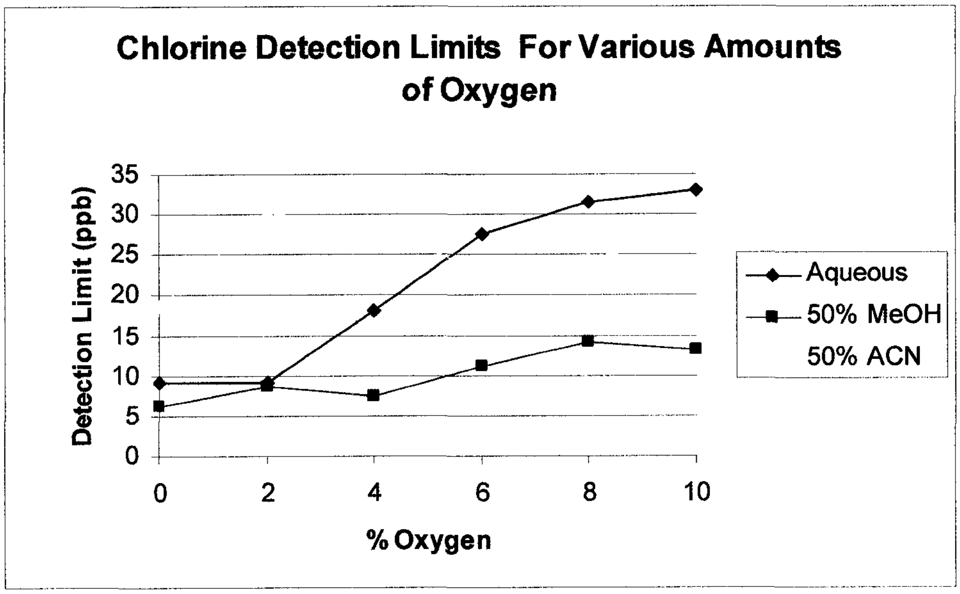

Figure 44. Detection limits for chlorine as a function of oxygen nebulizer gas composition.

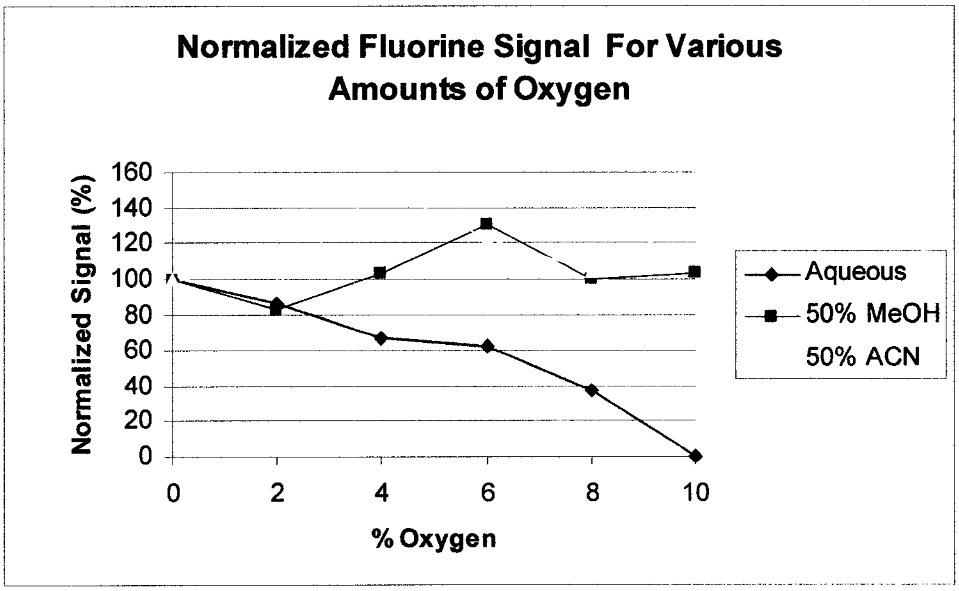

Figure 45. Analytical signal trends for fluorine as a function of oxygen nebulizer gas composition. Signal has been normalized to a value of 100 with respect to the signal seen with 0% added.

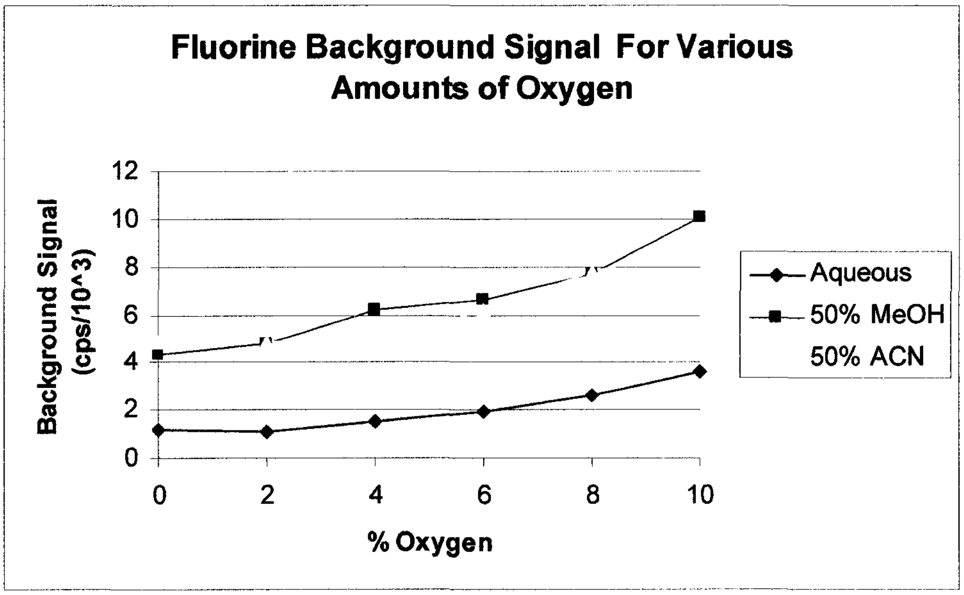

Figure 46. Background signal intensity for fluorine as a function of oxygen nebulizer gas composition.

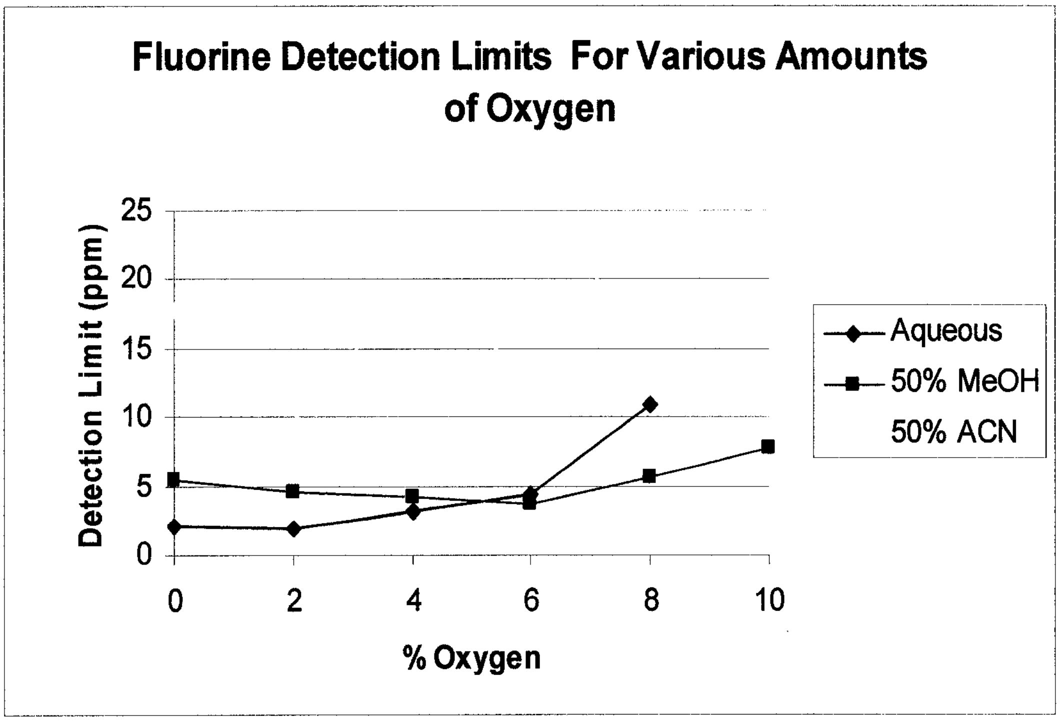

Figure 47. Detection limits for fluorine as a function of oxygen nebulizer gas composition.

standard ICP forward powers (greater than 1 kW), the addition of oxygen gas does not yield noticeable changes in the plasma. Consequently, several groups do not optimize any instrumental parameters when oxygen is bled into the nebulizer gas flow. As noted previously, optimization procedures vary for bleed gas experiments. Optimization procedures performed in this experiment involved maximizing the S/B ratio for aqueous solutions. All other conditions were kept the same as oxygen was added.

The introduction of organic solvent produced a light green C_2 emission signaling solvent load on the plasma. This was more pronounced with the ACN:H_2O solution. Membrane desolvation allowed the plasma to maintain its stability. Green emission was not observed in the buffer study where the plasma forward powers were higher than in this study. Membrane desolvator countercurrent flow rates were increased and nebulizer flow rates were decreased in an attempt to alleviate the solvent load. Changing these parameters lessened the intensity of the emission, but had a negative impact on the background and analyte signal. It was decided to maintain optimal settings for the aqueous solution.

Minimum Oxygen Flow Rate for Effective Carbon Removal

Using increasing amounts of oxygen may decrease the amount of system maintenance, but may cause performance sacrifices to be necessary. With no oxygen, a 50% acetonitrile solution was nebulized until some carbon deposition was noted on the sample cone. Oxygen was then introduced into the nebulizer gas in increasing volume flow rates until the carbon on the cone was removed. This established a lower limit of 6% oxygen required to remove carbon building up on the sample cone faster than it was being deposited.

Interferences in Oxygen Addition Experiments

Table 20 lists the potential atomic and polyatomic interferences present at the nominal m/z values of the analytes monitored in this study. The table differentiates between interferences that are most problematic and ones less likely to be present in appreciable amounts. For example, due to the low natural abundances of ^{18}O and ^{13}C, interferences at m/z = 31 from $^{13}C^{18}O^+$ are expected to be much less than interferences from $^{15}N^{16}O^+$. For this study, it would be expected that an analyte with an oxygen-, carbon-, or argon-containing interferent would have a greater likelihood of producing an interference.

Another interference effect arises from the possibility of the formation of molecular analyte species. For instance, oxides of the analyte may be formed. Mass spectral scans were obtained for all solvent compositions with different percentages of oxygen added. Special attention was paid to potential oxides of sulfur, phosphorus and chlorine. An example mass spectral scan of $^{32}S^{16}O^+$ at m/z 48 is shown in Figure 48. A peak appeared after nebulization of a 1000 ppb sulfur solution. Figure 49 is a mass spectral scan taken with an aqueous background solution and a 100 ppb solution of phosphorus. The appearance of a peak at m/z 48 indicates the formation of

Table 20. Common interferents for elements of interest.

Element	Isotope	Abundance	More Likely Interferences	Less Likely Interferences
Phosphorus	^{31}P	100%	$^{15}N^{16}O$, $^{14}N^{16}O^{1}H$	$^{13}C^{18}O$, $^{12}C^{18}O^{1}H$, $^{15}N_2{}^{1}H$
Sulfur	^{32}S	95.02%	$^{16}O^{16}O$	$^{15}N^{16}O^{1}H$, $^{14}N^{18}O$
	^{34}S	4.67%	none	$^{33}S^{1}H$, $^{15}N^{18}O^{1}H$
	^{36}S	0.02%	^{36}Ar	
Chlorine	^{35}Cl	75.77%	none	$^{16}O^{18}O^{1}H$, $^{34}S^{1}H$
	^{37}Cl	24.23%	$^{36}Ar\,^{1}H$, $^{36}S^{1}H$	
Fluorine	^{19}F	100%	$^{16}O^{1}H_3$, $^{38}Ar^{2+}$	$^{18}O^{1}H$

Main Interfering Atomic Solvent and Atmospheric Species

Element	Isotope	Abundance
Nitrogen	^{14}N	99.63%
	^{15}N	0.37%
Oxygen	^{16}O	99.757%
	^{17}O	0.038%
	^{18}O	0.205%
Carbon	^{12}C	98.93%
	^{13}C	1.07%
Hydrogen	^{1}H	99.9885%
	^{2}H	0.0115%
Argon	^{36}Ar	0.34%
	^{38}Ar	0.06%
	^{40}Ar	99.60%

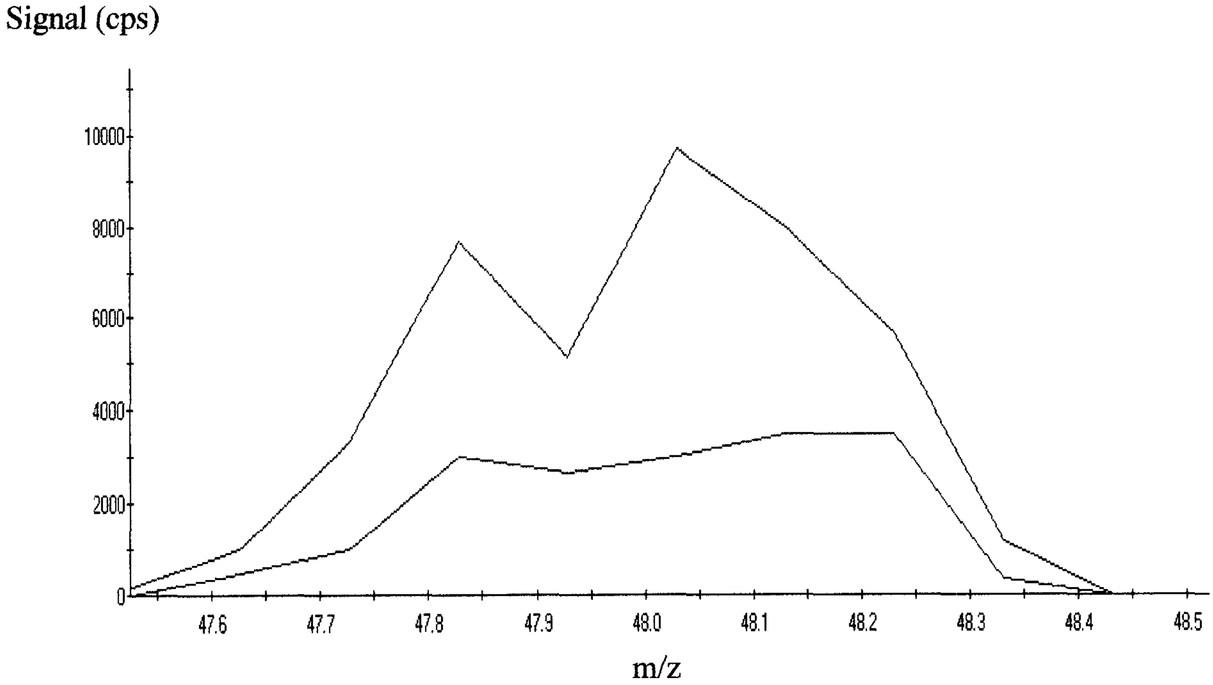

Figure 48. Mass spectrum of the m/z = 48 ion for a 1000 ppb sulfur solution of 50:50 (ACN:Aqueous): 10% oxygen (blue) and 4% oxygen (black). Background counts with no sulfur analyte were negligible.

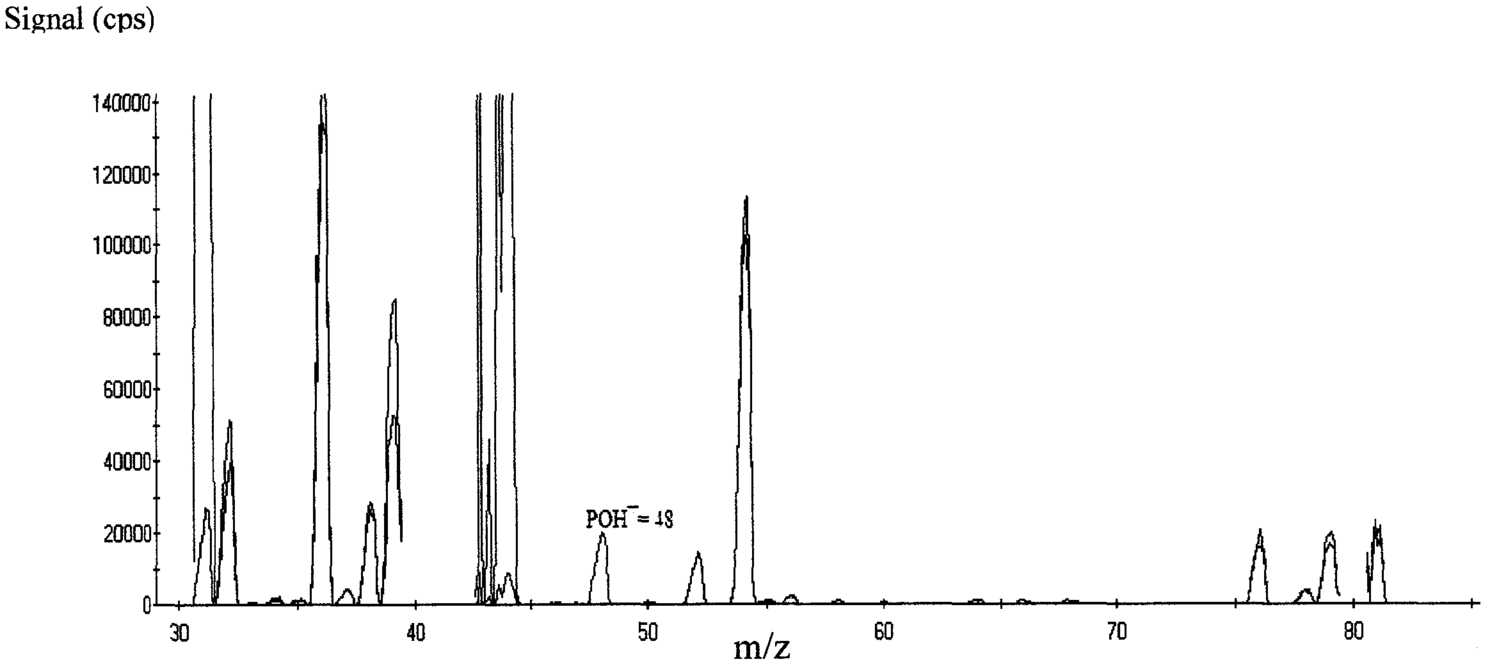

Figure 49. Mass spectrum of aqueous background (black) and a 100 ppb solution of phosphorus as phosphomycin (blue). Note the peak at m/z 48.

$^{31}P^{16}O^{1}H^{+}$. Subsequent mass scans were performed with various oxygen addition amounts to attempt to elucidate whether oxide interferences were enhanced or mitigated with oxygen addition. Signal intensity at the oxide masses displayed variable changes with the addition of oxygen and were of low intensity, making determination of the formation of oxide species difficult. It is probable that oxide species are formed for sulfur- and phosphorus-containing analytes in limited quantities with small additions of oxygen to the nebulizer gas. No oxide species were noted for chlorine- or fluorine-containing analytes.

Oxygen Addition: Sulfur Results

Sulfur was monitored as the $^{34}S^{+}$ isotope in preference to the $^{32}S^{+}$ isotope, which has a significant $^{16}O_2^{+}$ interference (Table 20). Observing the average analytical signal for methanol and acetonitrile in Table 16 and Figure 36, it is shown that there is a decrease in sensitivity as the amount of oxygen in the nebulizer gas is increased. Analytical signals for both methanol and acetonitrile solutions were suppressed by greater than 50% with 10% added oxygen. The analytical signal response in the pure aqueous solution for sulfur was markedly different than in the organic solutions. Instead of a signal decrease with increasing flow of oxygen, the analytical signal was enhanced. With 10% added oxygen, the analytical signal was enhanced by over a factor of 2.

Figure 37 and Table 16 illustrate the effect oxygen addition had on the background signal intensity for all solutions. Interestingly, trends are similar to those observed for the analytical sensitivities. The background signal intensity for both organic solvent compositions decreased with increasing amounts of oxygen added. The background intensity dropped by a factor of 2 with 10% oxygen added. The aqueous solvent background signal increased with increasing percentages of oxygen added to the nebulizer gas flow. With 10% added oxygen, the background signal was increased by over a factor of 2.

Figure 38 and Table 16 show the detection limit trends for all solvent compositions. All three solvent compositions display variability in detection limits across the oxygen flow rate range. Neither large improvements nor degradations in detection limits were observed. For the organic solvent compositions, detection limits deteriorated marginally ($\leq$ 50%) from initial conditions with no oxygen added to 10% oxygen in the nebulizer gas flow. For the aqueous solution, there was not a statistically significant change in the detection limit.

The analytical and background signal trends observed with sulfur analytes are likely due to subtle shifts in the analytical zone with respect to the ion sampling cone as oxygen gas is added to the nebulizer gas flow. While the total gas flow rate is held constant, the oxygen gas added will affect the macroscopic properties of the argon plasma. The graphs illustrating sensitivity and background signal trends as a function of oxygen in the nebulizer gas are similar. This indicates a loss or increase of both analyte and background ions with increasing oxygen content for solvent compositions. There was an increase in both the analytical signal and background for the pure aqueous solvent.

The S/B for all the solvent compositions were relatively stable. For the pure aqueous solution, the average S/B for all flow rates was approximately 19 with a relative standard deviation of 14%. MeOH:H_2O had an average S/B of 56 with a relative standard deviation of 10%. Finally, the ACN:H_2O solvent had an average S/B of 40 with a relative standard deviation of 20%. It is apparent from these results that there is neither significant ionization enhancement nor depression for sulfur with oxygen addition. Furthermore, there is not a large increase in background from polyatomic interferences. The main interferents for $^{34}S^+$ (Table 20) contain low natural abundance oxygen atoms. Addition of oxygen or the nebulization of organic solvent would not be expected to appreciably increase the background ion counts at $^{34}S^+$.

Oxygen Addition: Phosphorus Results

Phosphorus was monitored as the $^{31}P^+$ isotope. Table 17 and Figure 39 illustrate a loss in analytical signal and sensitivity with increasing amounts of oxygen for both MeOH:H_2O and ACN:H_2O solvents. The analytical signal increased for the pure aqueous solvent exhibiting behavior similar to the sulfur analyte.

Figure 40 and Table 17 display the background signal trend at m/z = 31 for all solvent compositions. There are several points to note. First, the background increased dramatically when oxygen was introduced for the aqueous solutions. Second, background ion counts for the MeOH:H_2O solution are not significantly affected by the presence of oxygen in the nebulizer gas. Finally, the addition of oxygen yielded a variable response of the background ion count for the ACN:H_2O solvent.

Figure 41 shows the detection limit trends for phosphorus as a function of added oxygen for each solvent composition. With the exception of a repeatable spike in the detection limit at 2% oxygen, detection limits remained low for all solvent compositions and oxygen flow rates. The best detection limits for the pure aqueous and MeOH:H_2O solution occur with no oxygen added to the nebulizer gas flow. The detection limit as a function of oxygen flow rate was variable for the ACN:H_2O solution. The best detection limit was obtained at 2% added oxygen.

Similar to sulfur, responses in the analytical and background signal for phosphorus as a function of added oxygen are likely affected by shifts in the analytical zone of the plasma. However, the data also indicates significantly different behavior with respect to the S/B ratio for the pure aqueous solvent. With no oxygen added, the S/B ratio is found to be 72. Introducing 2% oxygen lowered this ratio to 1.6. The background signal rose by over a factor of 34 without a corresponding elevation in the analytical signal. This likely indicates that additional interfering ions such as $^{14}N^{16}O^{1}H^{+}$ (Table 20) are being formed and/or sampled when oxygen is entrained in the nebulizer gas. The analytical signal decreases when 2% oxygen is added to the nebulizer gas flow. This suggests either that the production of $^{31}P^{+}$ is being suppressed or the analytical zone is shifted so that a region of the central channel with a lower ion number density is being sampled. A further possibility is that phosphorus oxide species are being formed in small quantities, reducing the production of $^{31}P^{+}$. As noted previously, mass spectral scans were obtained at various oxygen flow rates. These scans indicated the presence of ions at the $^{31}P^{16}O^{1}H^{+}$. Deducing whether added oxygen mitigates or enhances the formation of this ion is difficult. This is due to its low intensity and the variability in ion signals as the analytical zone of the plasma shifts with increasing amounts of added oxygen.

With aqueous solutions, as the amount of added oxygen is increased, the analytical signal recovers and is slightly enhanced with 8% or greater oxygen added. The S/B ratio is variable from 1.6 to a maximum of 5.2 with 8% oxygen added. From the data, it is unclear what is causing the enhancement of ionization. It is possible that the higher thermal temperatures predicted with oxygen addition may enhance the ionization of phosphorus atoms. The higher thermal energy may mitigate the formation of polyatomic phosphorus species. It may also be that the analytical zone shifts with increasing amounts of oxygen so that the relative number of phosphorus ions sampled is larger than the number of background ions.

For the MeOH:H_2O solution, the background ion signal is relatively constant as the amount of added oxygen is increased. Added oxygen may be consumed to an extent where it is not causing large increases in the background ion count as in aqueous solvents. The analytical signal generally decreases as the amount of oxygen added increases, indicating either ionization suppression or that fewer phosphorus ions are being sampled due to slight shifts in the analytical zone.

For ACN:H_2O solutions, a consistent trend in background or analyte signal was not apparent. S/B ratios fluctuated considerably as well. Due to its lower volatility and increased carbon content relative to methanol, ACN will have a larger effect on the plasma. It will not be as easily oxidized as methanol and will require larger flow rates of oxygen to mitigate its deleterious effects on the plasma. In addition, background interferences from nitrogen-containing species may be more problematic (Table 20) ACN. The fluctuations in signal for both the background and analytical signal are likely due to these factors as well as subtle shifts in the analytical zone of the plasma.

Oxygen Addition: Chlorine Results

As it is the most abundant isotope and relatively free from interferences, chlorine was monitored as the $^{35}Cl^{+}$ isotope. For all solvent compositions, Table 18 and Figure 42 show trends of decreasing analytical signals with increasing oxygen flow rates. The depression was greatest for the MeOH:H_2O solution. Signal loss was least with the ACN:H_2O solution.

Figure 43 and Table 18 present the background signal trends as a function of added oxygen. The background ion intensity for ACN:H_2O and pure aqueous solutions increases the most. The background ion intensity for the MeOH:H_2O remained essentially constant for all oxygen flow rates up to 8%. With 10% oxygen the background intensity also increased.

Figure 44 and Table 18 show the detection limit trends as a function of added oxygen. The best detection limits for all solvent compositions were obtained when no oxygen was added to the nebulizer gas flow. Deterioration in the detection limits was noted for all three solvent compositions. The pure aqueous solvent displayed the most dramatic rise in detection limits, increasing by over a factor of 3 when going from 0% oxygen to 10% added oxygen.

The S/B ratio decreases for all three solvent compositions. The increase in background intensity for the pure aqueous and the ACN:aqueous solvents is likely due to the formation of $^{16}O^{18}O^{1}H^{+}$ polyatomic ions and a shifting of the analytical zone of the plasma so that an increased number of background ions are sampled. The MeOH:H_2O background intensity did not increase proportionally, suggesting that the spatial distribution of background ions in the plasma is different than both the aqueous and ACN:H_2O solvents.

Analytical signal trends are consistent for all three solvent compositions. Signal decreases are likely due to a combination of three factors. The analytical zone is shifting, potentially reducing the number of ionized chlorine atoms sampled by the mass spectrometer. Chlorine oxides may be forming, although there is no direct mass spectral data that indicates this. Finally, as described previously, the plasma becomes less dense in the central channel and is shifted away from the injector tube. Hence the residence times of analyte atoms may not be as long. This would cause a decrease in analytical signal, especially for harder-to-ionize elements. The analytical signal for chlorine in the pure aqueous solvent is depressed as the flow rate of oxygen is increased. This breaks a trend established from sulfur and phosphorus results. Both phosphorus and sulfur displayed an increase in analytical signal with increased oxygen addition. It should be noted that the ionization energy for chlorine (13.01 eV) is greater than that of either sulfur (10.98 eV) or phosphorus (10.48 eV). The effect of the ionizing power of the ICP with added oxygen may play a role in more greatly affecting chlorine ionization.

Oxygen Addition: Fluorine Results

Monoisotopic fluorine was monitored at m/z = 19. Table 19 and Figure 45 display the analytical signal trends for fluorine as a function of oxygen added to the nebulizer gas flow. With the pure aqueous solution there is a significant decrease in the fluorine analytical signal as the amount of oxygen is increased. At 10% oxygen, the fluorine ion signal is not visible above the background noise. In contrast, the analytical signals for the organic solutions fluctuate and are enhanced at some oxygen flow rates.

Table 19 and Figure 46 show the background signal trends for fluorine. All three solvent compositions exhibited a rise in the background ion signal with increasing amounts of added oxygen. The rise in background signal is likely due to the highly interfering oxygen-containing polyatomic ions (Table 20) formed in greater quantities as increasing amounts of oxygen are added.

Detection limits trends are displayed in Figure 47 and Table 19. For each solvent composition, detection limits became worse as the amount of added oxygen was increased. At 10% oxygen, the detection limit for fluorine in the aqueous solution could not be calculated. Detection limits for the ACN:H_2O solution were scattered and also greater than with the MeOH:H_2O and pure aqueous solutions.

As stated previously, the rise in background signal for all solutions is likely due to an increased amount of $^{16}O^{1}H_3^+$ polyatomic ions interfering at m/z=19. For the pure aqueous solvent, the decrease in analytical signal may be due to poorer high energy ionization characteristics of the plasma. For the organic solvent compositions, the analytical signal did not decrease as it had for most other analytes. One possible explanation is that the other analytes are forming polyatomic oxide ions with the entrained oxygen while fluorine is not. Fluorine is much less likely to form bonds with oxygen than sulfur, phosphorus, and chlorine. Further experimentation is necessary to draw any conclusions from these results.

Oxygen Study Conclusions

The analytical and background responses for four nonmetal-containing analytes in aqueous, MeOH:H_2O, and ACN:H_2O solutions with addition of oxygen has been demonstrated across the working range of oxygen flow rates. In general, degradations in sulfur, phosphorus, and chlorine analytical signals are observed as the percentage of oxygen bled into the nebulizer gas is increased. As the percentage of oxygen is increased, the fluorine signal displayed signal intensity scatter in the organic solutions. With pure aqueous solutions, sulfur and phosphorus analytes display an increase in sensitivity with increasing plasma oxygen content. Chlorine- and fluorine-containing analytes display a decrease in aqueous solutions as the oxygen content is increased. Signal degradation may be due to ionization interference effects and subtle shifts of the analytical zone of the plasma. Further studies and simulations are necessary to deduce any differences between plasma behavior and temperature in this system (<500W) as compared to previous studies (>800W). These results indicate that moderate amounts of oxygen may be added to the nebulizer gas without a large overall increase in detection limits while obtaining the benefit of carbon removal and sample cone lifetime.

Additional experiments to further understand the observed plasma behavior would include performing oxygen addition after the sample stream passed through the membrane desolvator. Power levels would be varied to ascertain the best conditions for both organic solvent pyrolysis and sensitive nonmetal determinations. Supplemental oxygen gas flows to the auxiliary or cool gas flows could be investigated as well. Finally, a second set of optimization procedures, such as maximizing the analytical signal after each oxygen addition by changing the plasma forward power or the torch sampling depth, would aid in defining the optimal oxygen addition conditions.

Results and Discussion for Nitrogen Addition

Introduction

Nitrogen addition to the nebulizer gas flow was investigated in an effort to improve nonmetal detection limits. As previously discussed, sensitivity enhancements have been noted for a number of metal and nonmetal-containing analytes. However, the literature contains conflicting results. The mechanism for sensitivity enhancement is not well understood. Previous research indicates a reduction of polyatomic interferences yielding lower backgrounds and higher analytical signals. It has also been found that nitrogen addition to the outer gas of an argon plasma boosts plasma temperatures resulting in more efficient ionization. The addition of nitrogen to the nebulizer gas, however, is expected to lower the temperature in the central channel of the plasma[69]. The effects of nitrogen upon nonmetal determinations with USN-MD sample introduction has not been investigated thoroughly.

The study presented in this dissertation is intended to examine trends for nonmetal analytical response for small additions of nitrogen to the nebulizer gas flow. Phosphorus and sulfur were the nonmetal elements studied in these experiments. Nebulization and transport efficiencies were held constant with a fixed nebulizer gas flow of 1.00 L/min. Nitrogen gas was added following sample introduction, immediately before the quartz torch by attachment of the previously described glass T-junction (Figure 31). Nitrogen was bled in at flow rates ranging from 0-70 mL/min. System optimization was performed by maximizing the analytical signal for an aqueous solution containing phosphorus or sulfur analytes. Sampling was held constant and flow rates were tested at forward powers between 450-1350 W in increments of 100 W. Mass spectral scans were obtained for background and analyte-containing solutions.

Physical Properties of a Nitrogen Doped ICP

Similar to the addition of oxygen, nitrogen addition had a noticeable effect on the size, shape, and density of plasma. However, these effects were more pronounced and affected the stability of the plasma. At the lower forward powers, the ICP could not tolerate high nitrogen flow rates due to high reflected power levels. The r.f. generator has an interlock that automatically extinguishes the plasma at high reflected powers. Table 21 lists the attainable nitrogen volume flow rates at the power levels studied in these experiments. Visible effects of added nitrogen on the plasma were different and more significant than in oxygen addition experiments. The central channel widened and appeared less intense from the torch injector to the sample cone. The plasma shifted away from the torch injector and shrank considerably. In contrast to oxygen addition, noticeable changes in the plasma remained when operating at standard forward powers (greater than 1 kW), although they diminished with increasing forward powers. The analytical zone of the plasma shifts with nitrogen addition and is expected to cause larger fluctuations in the analytical and background signals.

Interferences in Nitrogen Addition Experiments

Table 20 lists the interferences expected for phosphorus and sulfur. Strong nitrogen-containing interferences ($^{15}N^{16}O^+$, $^{14}N^{16}O^1H^+$) are present at the phosphorus ion mass. The mass = 34 ion, $^{34}S^+$, also contains a nitrogen-based interferent

Table 21. Tolerable nitrogen flow rates at forward powers utilized.

Forward Power (W)	Nitrogen Flow Rate (mL/min)
450	0-30
550	0-40
650	0-50
750	0-50
850	Full Range (0-70)
950	Full Range (0-70)
1050	Full Range (0-70)
1150	Full Range (0-70)
1250	Full Range (0-70)
1350	Full Range (0-70)

($^{15}N^{18}O^{1}H^{+}$). This interferent is expected to be less problematic due to the low natural abundances of ^{18}O and ^{15}N (Table 20). Additionally, experimental results[79] and computer simulations[69] predict a decrease in the temperature of the plasma when nitrogen is added to the nebulizer gas flow. This may contribute to increased background ion counts, as reduced plasma temperatures allow the formation of polyatomic interferences in an argon ICP.

Similar to the oxygen doping experiments, phosphorus and sulfur have the potential to form oxides, leading to monoatomic analyte ion reductions. As noted previously, Figures 48 and 49 indicate the formation of sulfur and phosphorus oxides. Subsequent mass spectral scans, obtained with increasing flow rates of nitrogen, cause these ion peak intensities to diminish. However, it is unclear whether nitrogen is eliminating oxide formation or there is a reduction in the number of ions sampled by the mass spectrometer. Other ion signal intensities, including those of the analyte, also decreased.

Nitrogen Addition: Phosphorus Results

Phosphorus was monitored at $^{31}P^{+}$. Figures 50-59 exhibit the analytical and background signals as a function of nitrogen flow rate for all powers tested. Although the absolute intensity for the signal and background is not directly comparable between forward powers because they were run on different days, the y-axis range was held constant to give a relative indication of which power levels yielded higher ion counts. Results are not reported for some nitrogen flow rates due

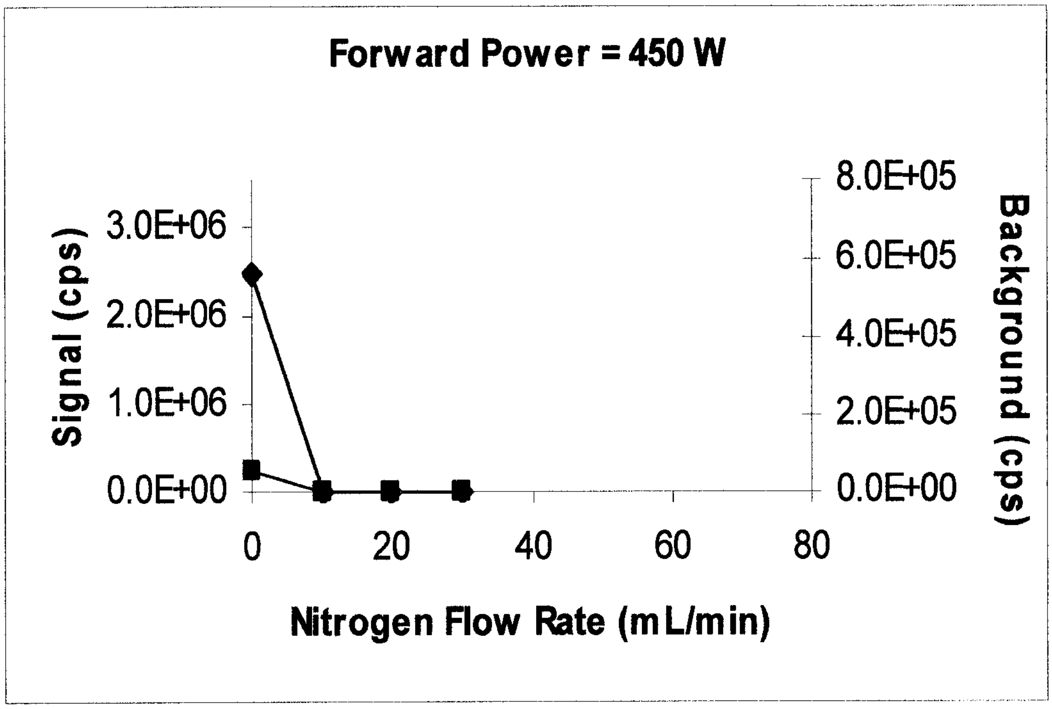

Figure 50. Plot of analytical (♦) and background (■) signals for phosphorus at an applied forward power of 450 watts.

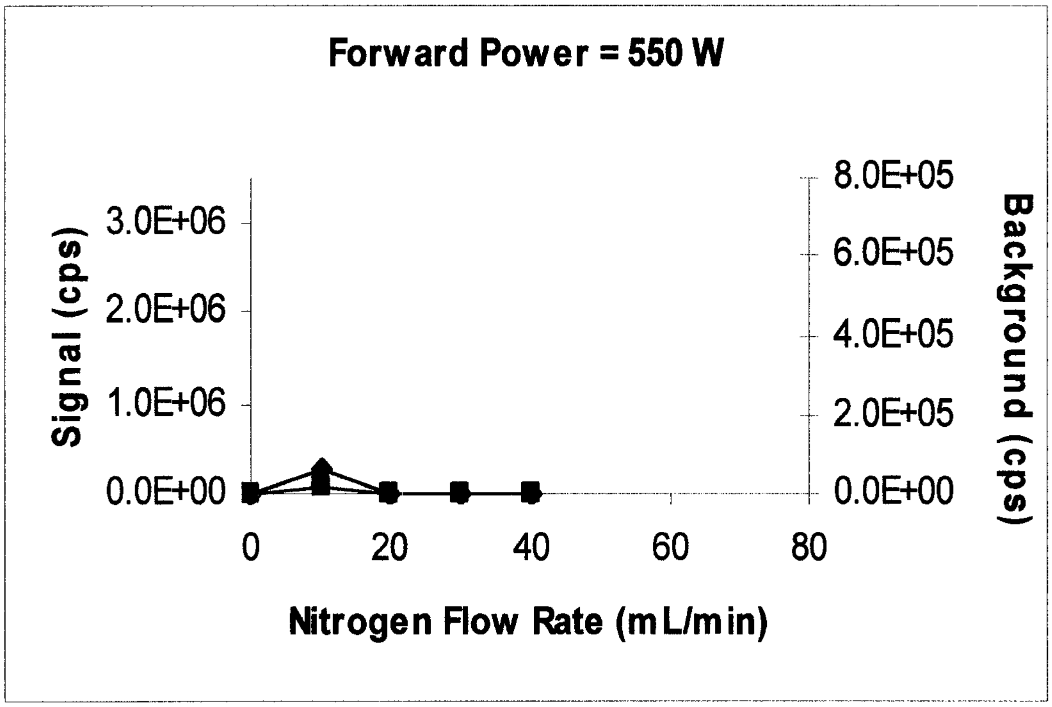

Figure 51. Plot of analytical (♦) and background (■) signals for phosphorus at an applied forward power of 550 watts.

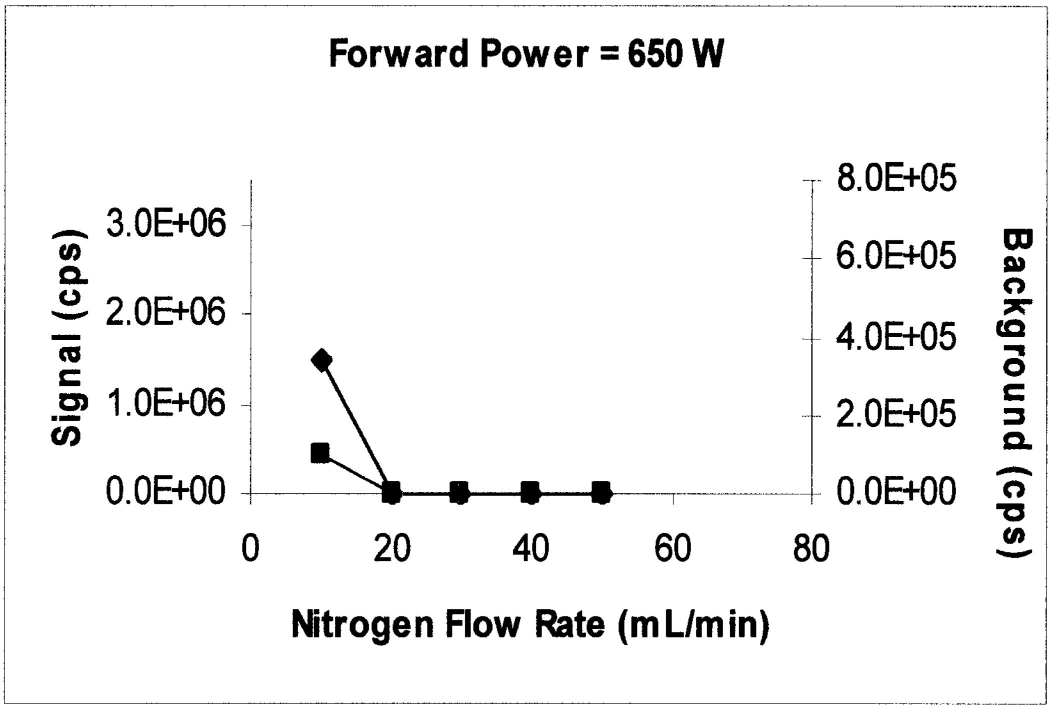

Figure 52. Plot of analytical (♦) and background (■) signals for phosphorus at an applied forward power of 650 watts.

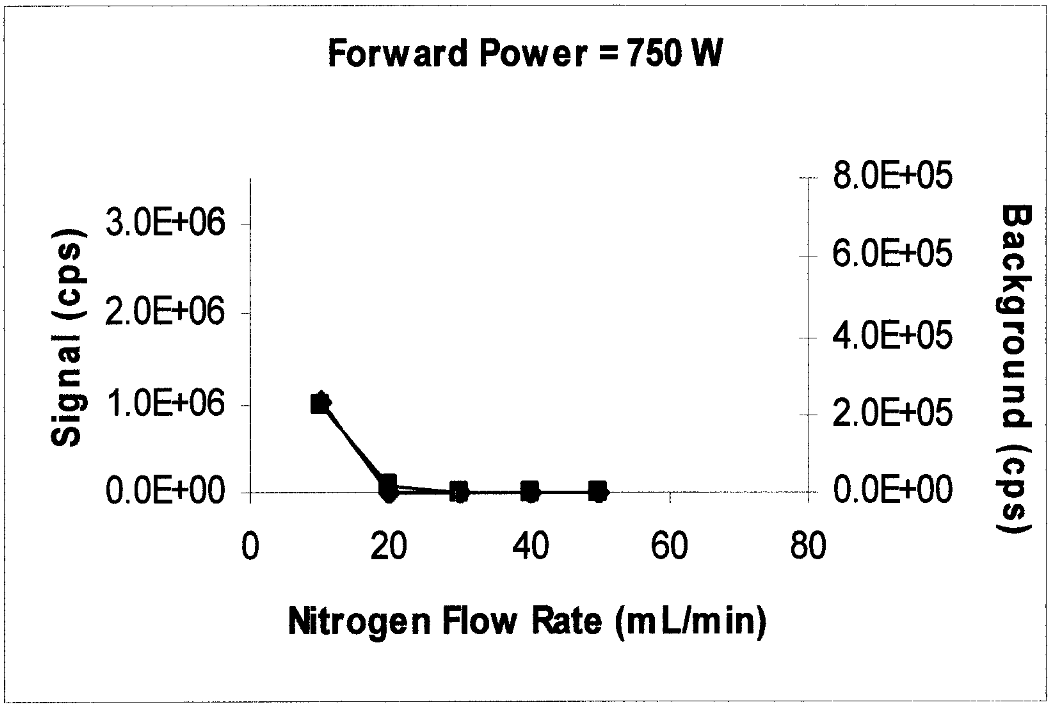

Figure 53. Plot of analytical (♦) and background (■) signals for phosphorus at an applied forward power of 750 watts.

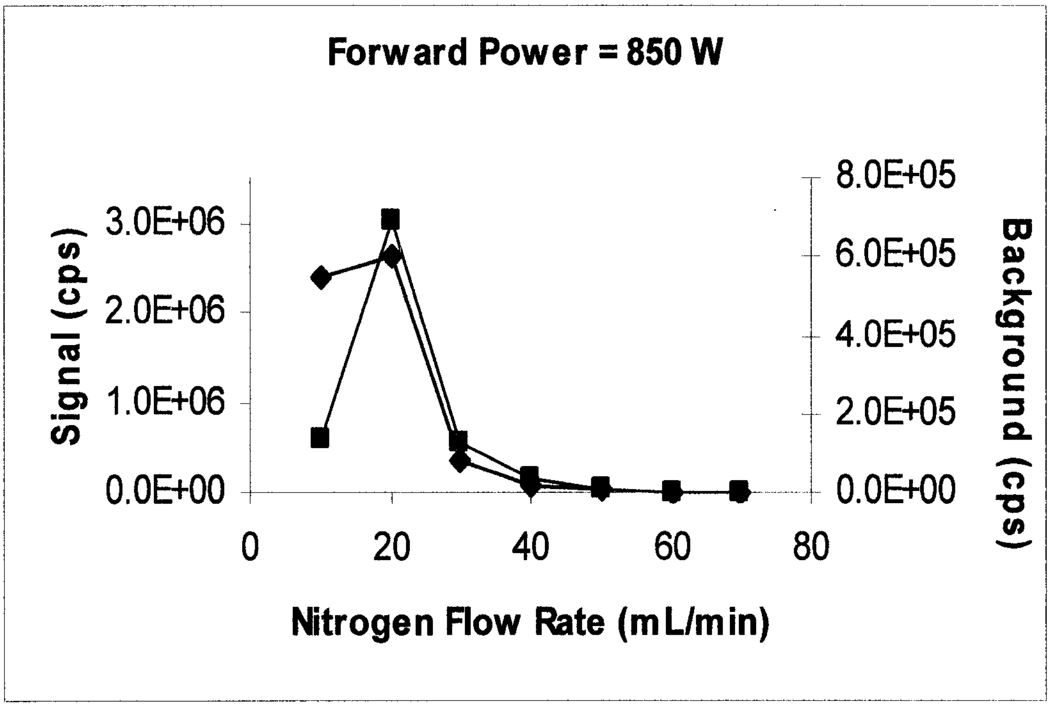

Figure 54. Plot of analytical (♦) and background (■) signals for phosphorus at an applied forward power of 850 watts.

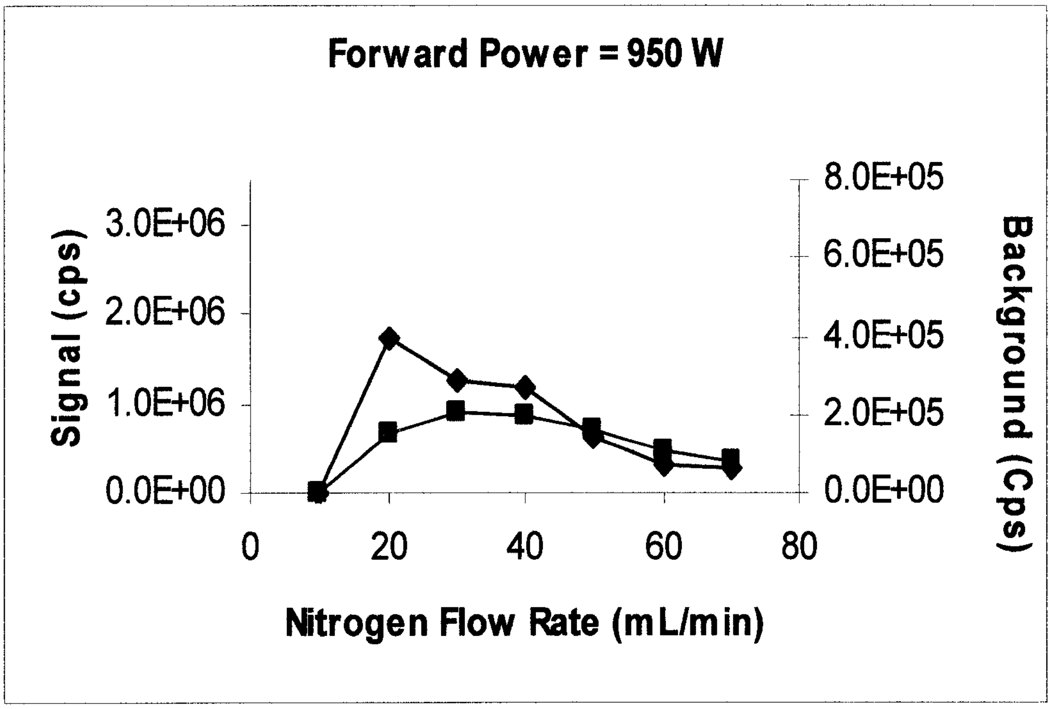

Figure 55. Plot of analytical (♦) and background (■) signals for phosphorus at an applied forward power of 950 watts.

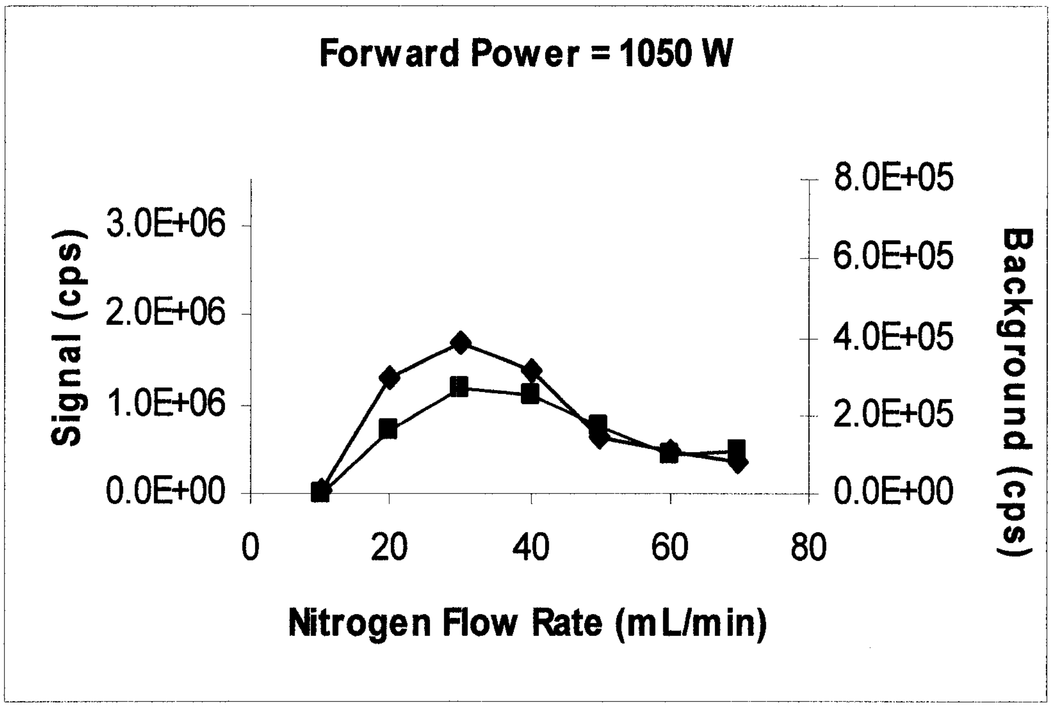

Figure 56. Plot of analytical (♦) and background (■) signals for phosphorus at an applied forward power of 1050 watts.

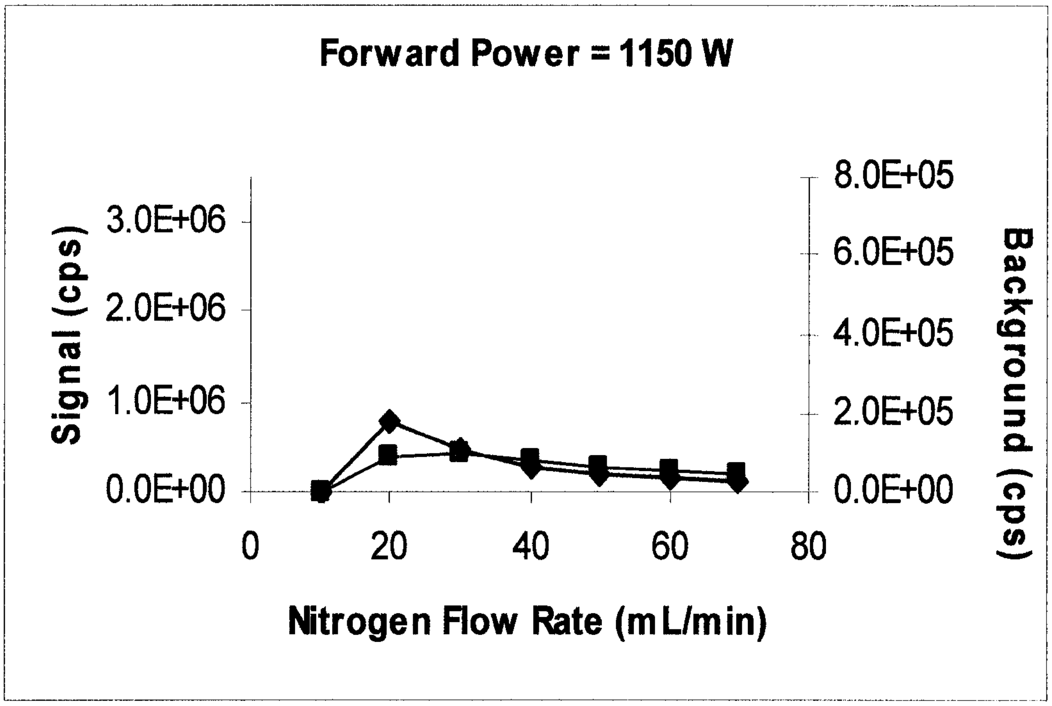

Figure 57. Plot of analytical (♦) and background (■) signals for phosphorus at an applied forward power of 1150 watts.

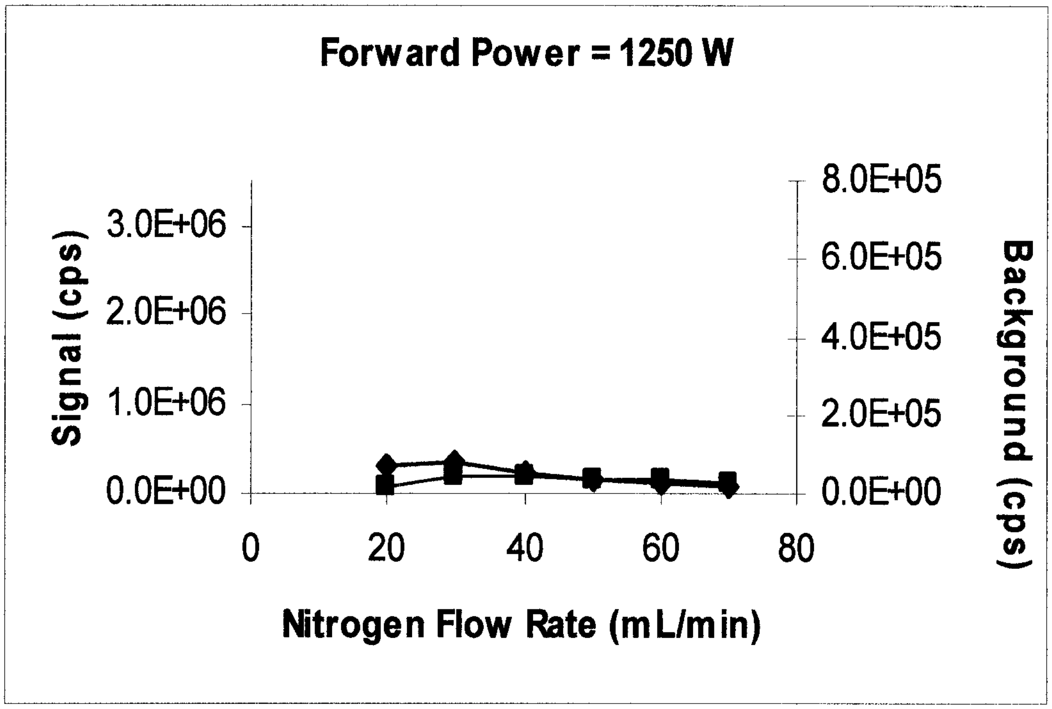

Figure 58. Plot of analytical (♦) and background (■) signals for phosphorus at an applied forward power of 1250 watts.

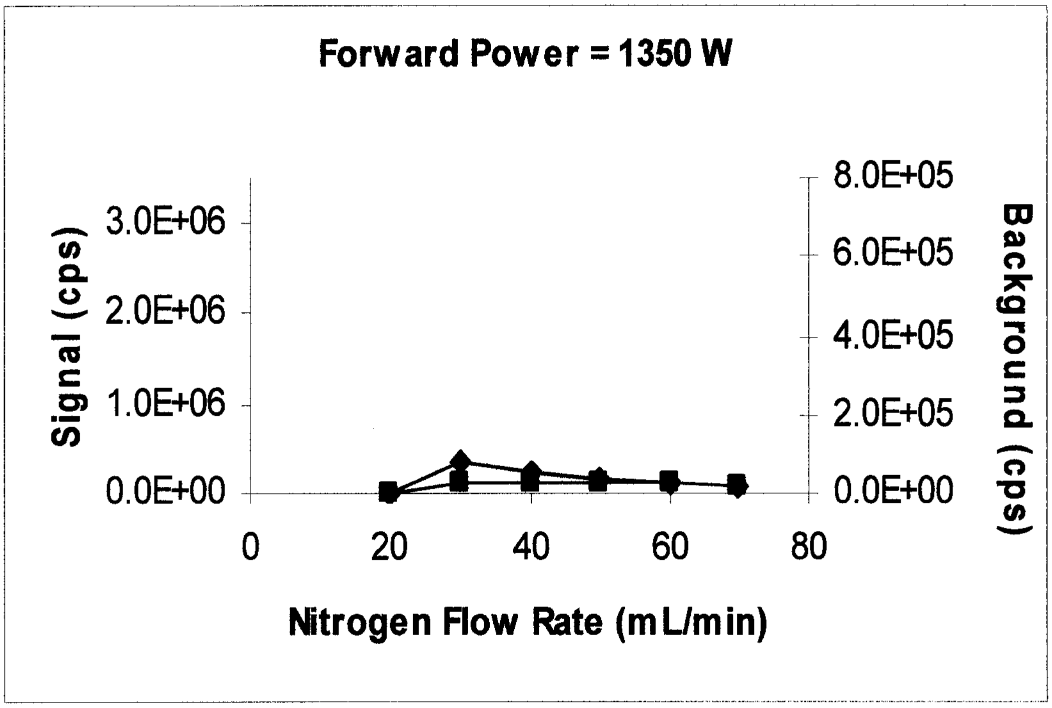

Figure 59. Plot of analytical (♦) and background (■) signals for phosphorus at an applied forward power of 1350 watts.

to low count rates or plasma extinguishment due to high reflected powers. For example, Figure 53 displays no data for 0, 60, and 70 mL/min of nitrogen added. Count rates for the background and analyte signals were nearly identical and low (<20 cps) with no added nitrogen. The high reflected forward power made the plasma system inoperable with 60 mL/min or more of added nitrogen.

Figures 50-59 show that there is a narrow range of nitrogen flow rates that yields a sensitive analytical signal. At low forward powers, there are maxima in the analytical signals at discrete nitrogen flow rates. These maxima appear at 10 (650 and 750 W) and 20 mL/min (850 W) of added nitrogen. All other nitrogen flow rates yield extremely low analytical signals. As the forward power levels are increased to the range of 1000 W (Figures 55 and 56), a wider window of nitrogen flow rates yield a measurable analytical signal. The largest signals occurred under the initial starting conditions (450 W and no added nitrogen) and with 20 mL/min of nitrogen at 850 W.

Figure 60 illustrates a plot of the flow rate of nitrogen that yields the largest analytical signal at each power. The graph clearly indicates that increasing flow rates of nitrogen are necessary to obtain the highest analytical signals as the forward power increases. In Figure 61 the maximum analytical signal obtained is plotted as a function of forward power. The graph indicates a depression in analytical signal as the forward power is increased from 450 to 550 W. At higher powers (650 to 1350 W), the signal exhibits a maximum at 850 W.

The right y-axes correspond to background signal intensities in Figures 50-59. The background signals display trends similar to those of the analytical signals. At

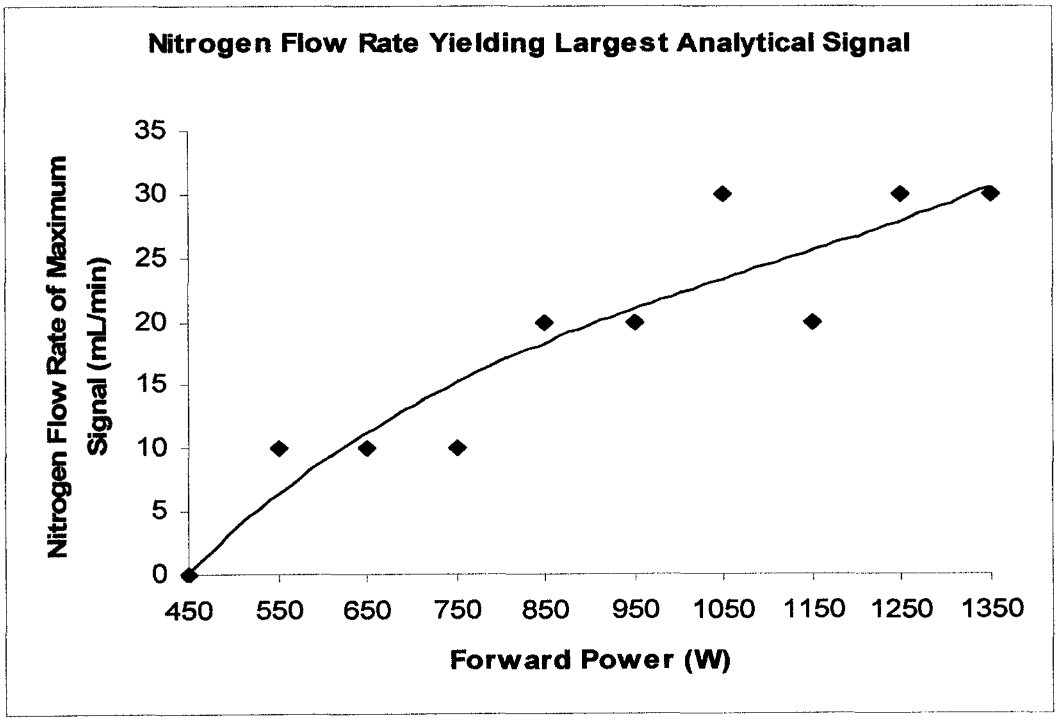

Figure 60. Plot of nitrogen flow rate that yields the largest analytical signal at all forward powers.

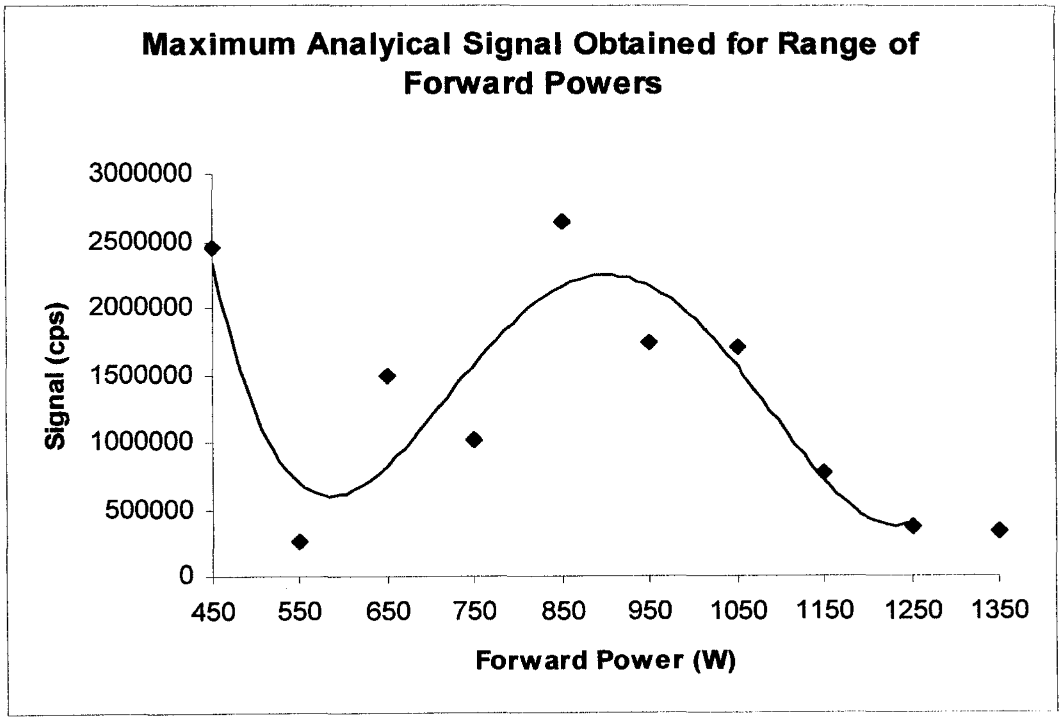

Figure 61. Plot of maximum analytical signal observed for all forward powers.

lower forward powers, 450 to 850 W, the background signals reach a maximum at one nitrogen flow rate relative to other flow rates (Figures 50-54). The flow rate range of the signal enhancement is small. At higher forward powers, 950 to 1150 W, a wider range of nitrogen flow rates produces a noticeable increase in the background signals (Figures 55-57). At the highest forward powers, 1250 and 1350 W, both background and analytical signals are depressed (Figures 58 and 59). A wide range of nitrogen flow rates yielded similar background signals. The largest background signal occurred at a forward power of 850 W with 20 mL/min of nitrogen added to the nebulizer gas flow. In all cases, it is likely that polyatomic species such as ${}^{14}N^{16}O^{1}H^{+}$ and ${}^{15}N^{16}O^{+}$ (Table 20) are contributing to the increase in the background signal.

Figure 62 depicts the flow rate of nitrogen that yields the highest background signal as a function of applied power. In general, the background increases as the forward power is increased. This may indicate that higher forward powers facilitate background ion formation due to the increased thermal energy of the plasma. Increasing the amount of nitrogen may lower the central channel temperature, allowing more favorable reaction conditions for polyatomic ion formation. Figure 63 shows the maximum background signal as a function of applied forward power. The highest background signal is obtained at a nitrogen flow rate of 20 mL/min at a forward power of 850 W. At this point, conditions favor a combination of background ion formation and sampling.

Figure 64 displays the S/B ratios for all forward power levels and nitrogen flow rates tested. The highest S/B ratio is found at 450 W with no added nitrogen.

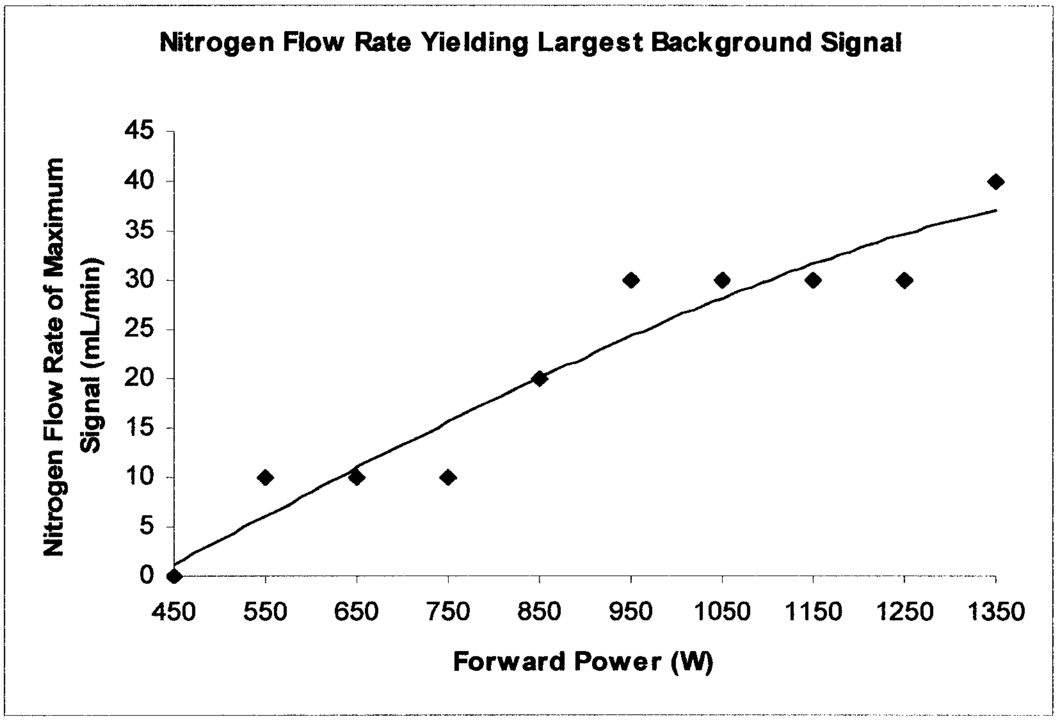

Figure 62. Plot of nitrogen flow rate that yields the largest background signal at all forward powers.

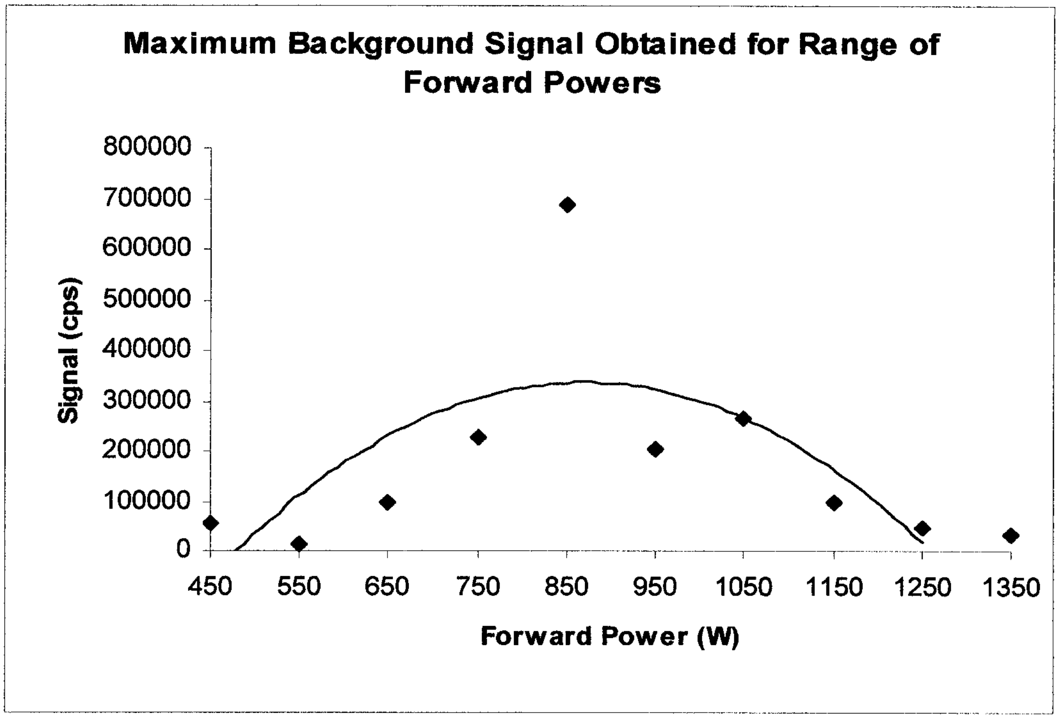

Figure 63. Plot of maximum background signal observed for all forward powers.

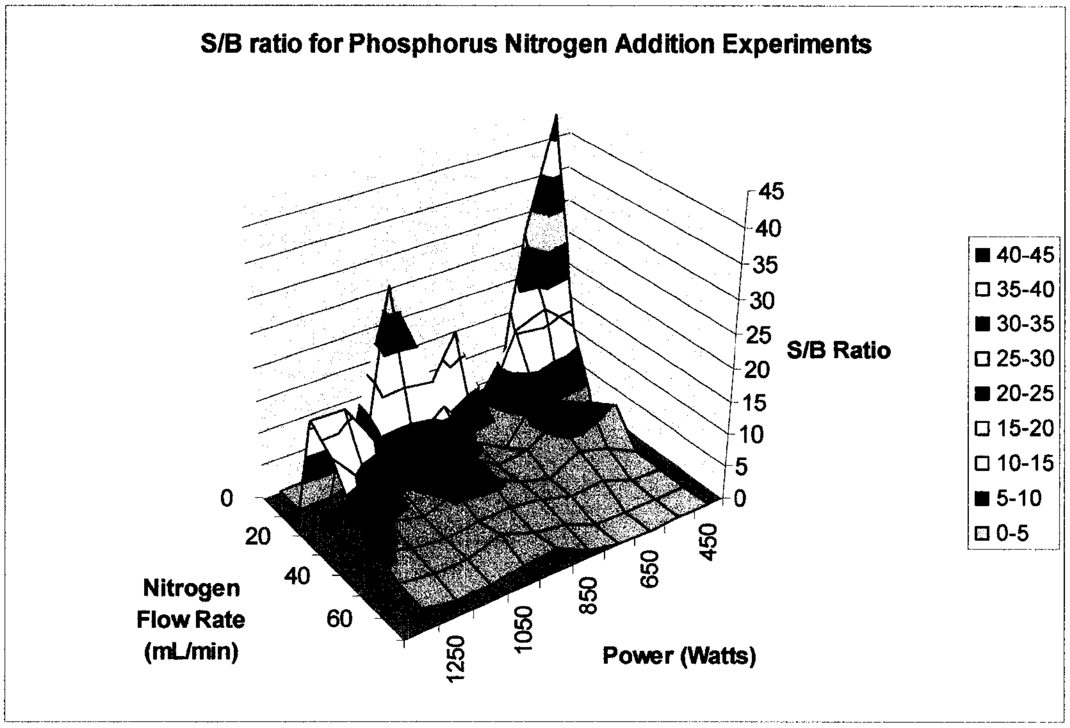

Figure 64. Surface contour displaying S/B trends for phosphorus against applied power and nitrogen flow rate added to the nebulizer gas.

With nitrogen addition, the highest S/B ratio is at 1050 W with 10 mL/min of nitrogen added. In general, the S/B ratio was depressed with increasing flow rates of nitrogen.

Table 22 lists the nitrogen flow rate that yielded the lowest detection limit for every forward power. Detection limits, with few exceptions, did not demonstrate significant enhancement or deterioration from nitrogen addition. The lowest detection limit achieved was 3 ppb P. This value was attained at 450 W with no addition of nitrogen and at 850 W with 10 mL/min of nitrogen added. A number of the conditions tested had detection limits for phosphorus in the single ppb range.

Some conclusions may be drawn from the results and observations noted in these studies. It appears that there is a reduction in ionization and/or an increase in background intensity leading to a reduction in the S/B ratio for $^{31}P^+$ when nitrogen is added to the nebulizer gas flow. At 450 W and no nitrogen added, the S/B ratio is greatest with a value of 43. All other instrumental conditions yielded S/B levels reduced by greater than 50%. Comparing the analytical and background signals at low and high power, there appears to be a greater number of analyte and background ions within the plasma at higher forward powers. The addition of nitrogen will shift the analytical zone of the plasma, causing a change in both the background and analytical signal. Also, the net background signal is greater with the addition of nitrogen. The results indicate increased reaction chemistry within the plasma that leads to higher levels of nitrogen-containing polyatomic ions. At low power levels, the small flow rate range of the enhancement in background and analytical signals indicates that the optimum sampling region is critically sensitive to changes in plasma

Table 22. Table of nitrogen flow rates yielding the lowest detection limit for phosphorus at each forward power utilized.

Forward Power (W)	Detection Limit (ppb)	S/B Ratio	Nitrogen Flow Rate (mL/min)
450	3	43	0
550	10	17	10
650	6	15	10
750	22	3	30
850	3	18	10
950	4	11	20
1050	6	8	20
1150	7	9	20
1250	6	8	30
1350	5	8	40

conditions. That this flow rate range becomes larger at higher power levels indicates an increase in the size of the useful analytical sampling zone.

Nitrogen Addition: Sulfur Results

Sulfur was monitored at $^{34}S^{+}$. Figures 65-70 illustrate the analytical and background signals as a function of nitrogen flow rate for forward powers of 450 to 1350 W. At lower forward powers (Figures 65 and 66), 450 to 550 W, there are narrow ranges of nitrogen flow rates at which significant analytical signals are seen. As the forward powers are increased above 750 W, a greater range of nitrogen flow rates yields measurable analytical signals (Figures 67 and 68). This behavior parallels trends seen in the phosphorus experiments. However, at the highest forward power levels, at 1250 and 1350 W (Figures 69 and 70), there is a trend of small nitrogen flow rate ranges yielding large analytical signals.

Figure 71 depicts the nitrogen flow rate that yields the greatest analytical signal for all forward powers. Similar to the phosphorus experiments, there is a general trend of increasing nitrogen flow rate for maximum signal with increasing forward power. However, at 1150 W and above 1250 W, there is a notable decrease in the nitrogen flow rate yielding the maximum analytical signal.

In Figure 72, the maximum analytical signal obtained at each power level is plotted. The maximum signal is seen at 450 W. There is a substantial decrease in the analytical signal as the plasma power is increased. At 450 W, the addition of nitrogen appears to either quench the formation of sulfur ions or shift the analytical zone of the

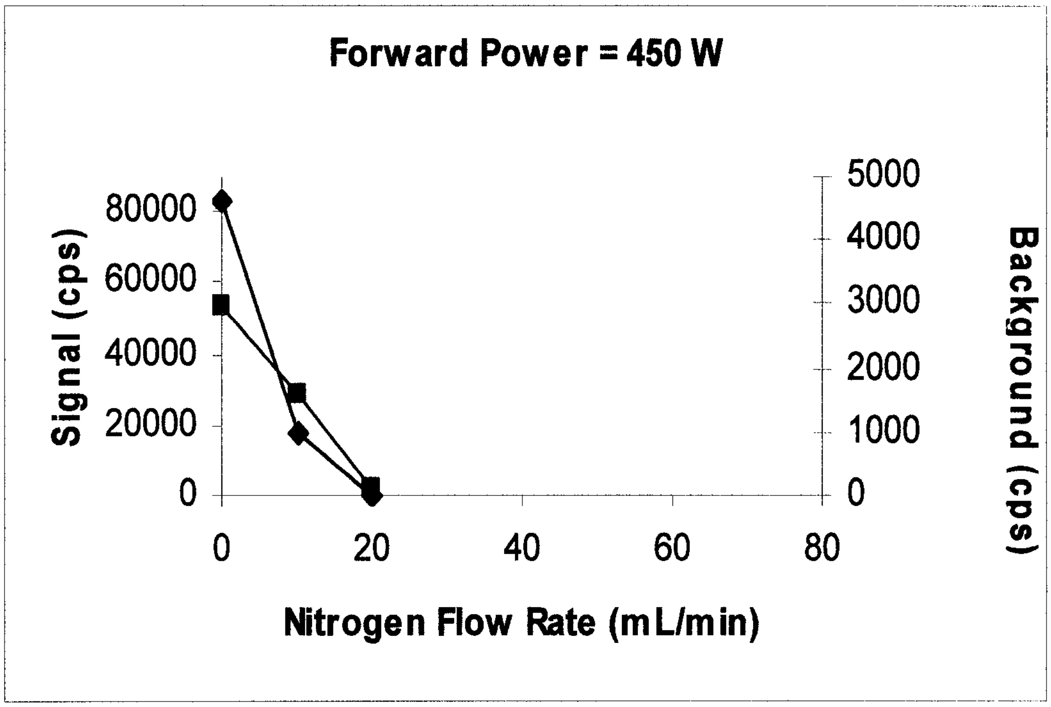

Figure 65. Plot of analytical (♦) and background (■) signals at an applied forward power of 450 watts.

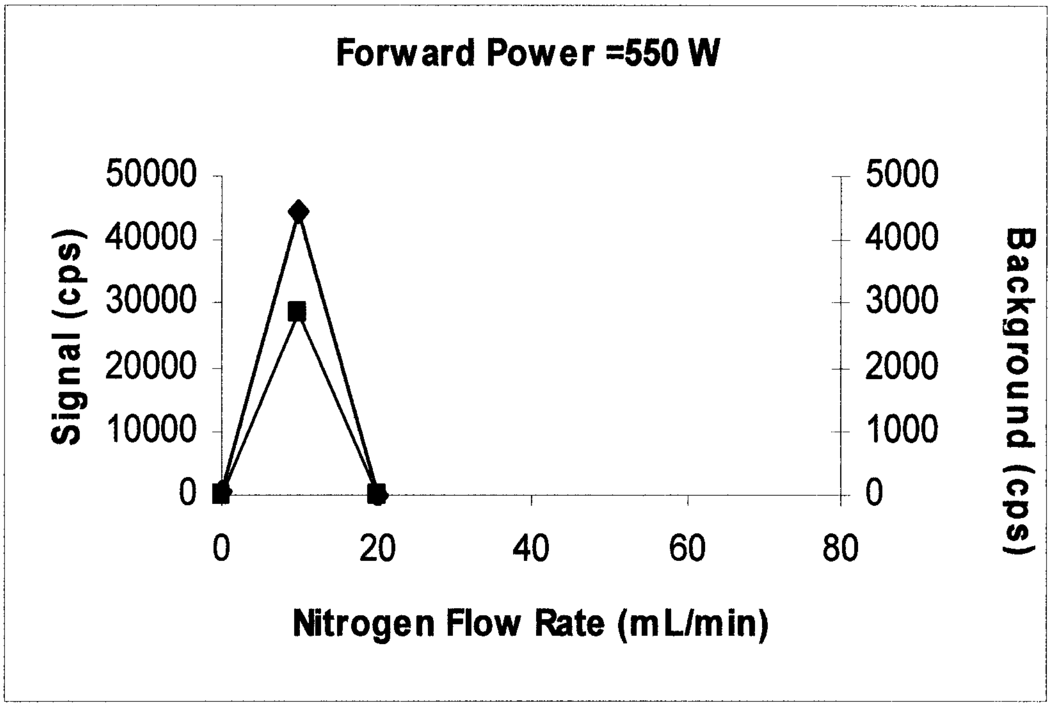

Figure 66. Plot of analytical (♦) and background (■) signals at an applied forward power of 550 watts.

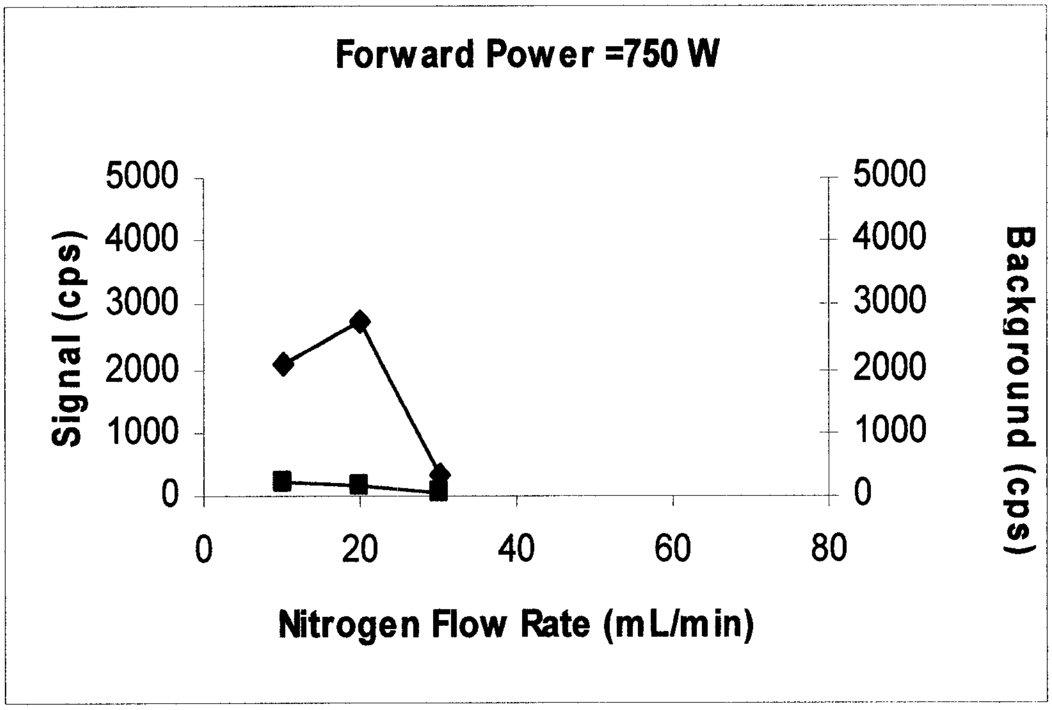

Figure 67. Plot of analytical (♦) and background (■) signals at an applied forward power of 750 watts.

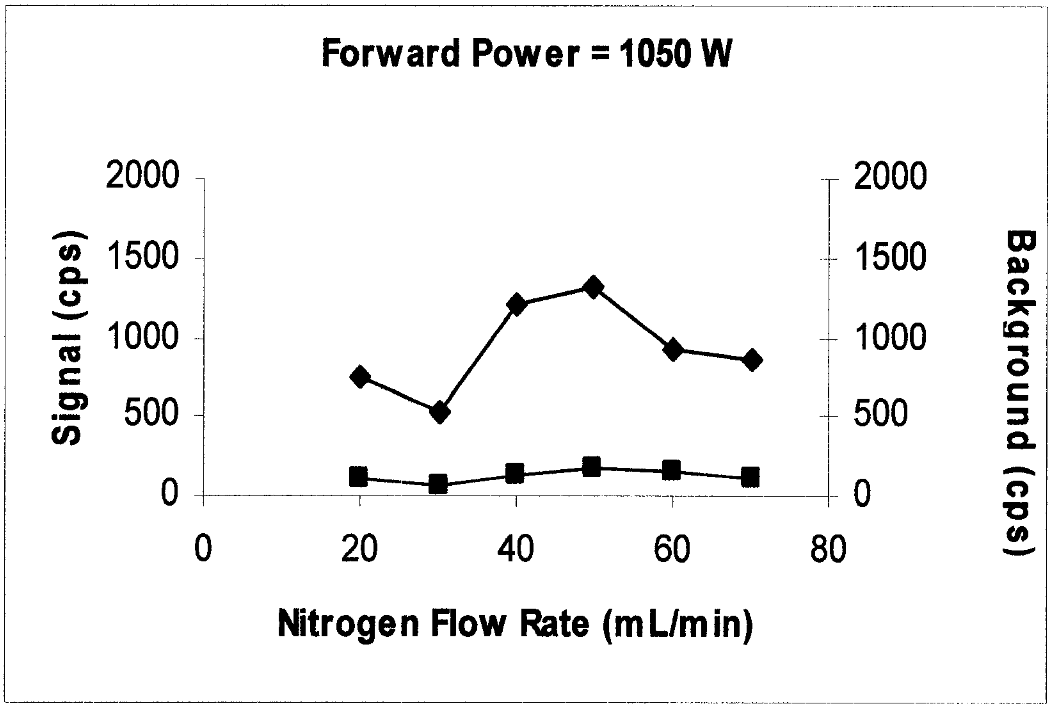

Figure 68. Plot of analytical (♦) and background (■) signals at an applied forward power of 1050 watts.

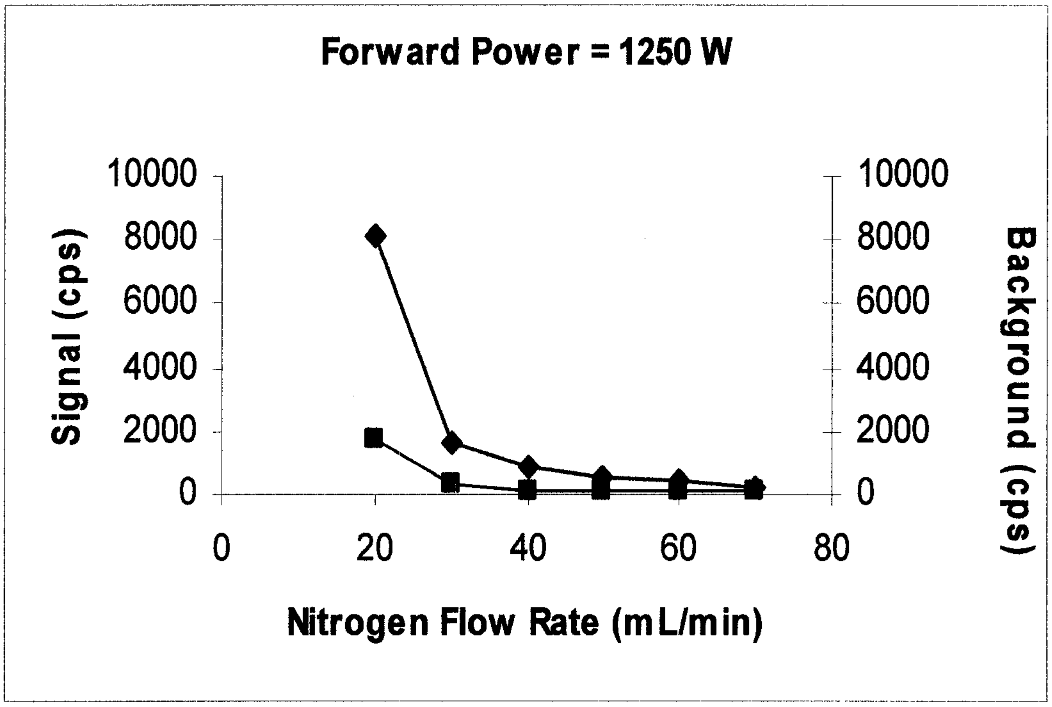

Figure 69. Plot of analytical (♦) and background (■) signals at an applied forward power of 1250 watts.

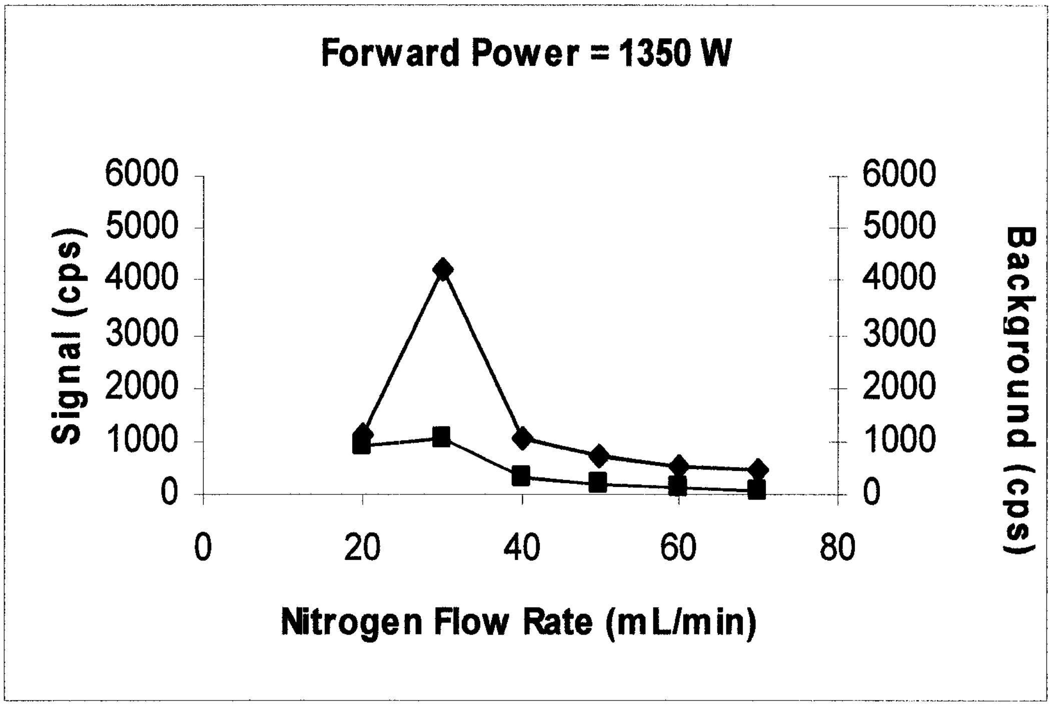

Figure 70. Plot of analytical (♦) and background (■) signals at an applied forward power of 1350 watts.

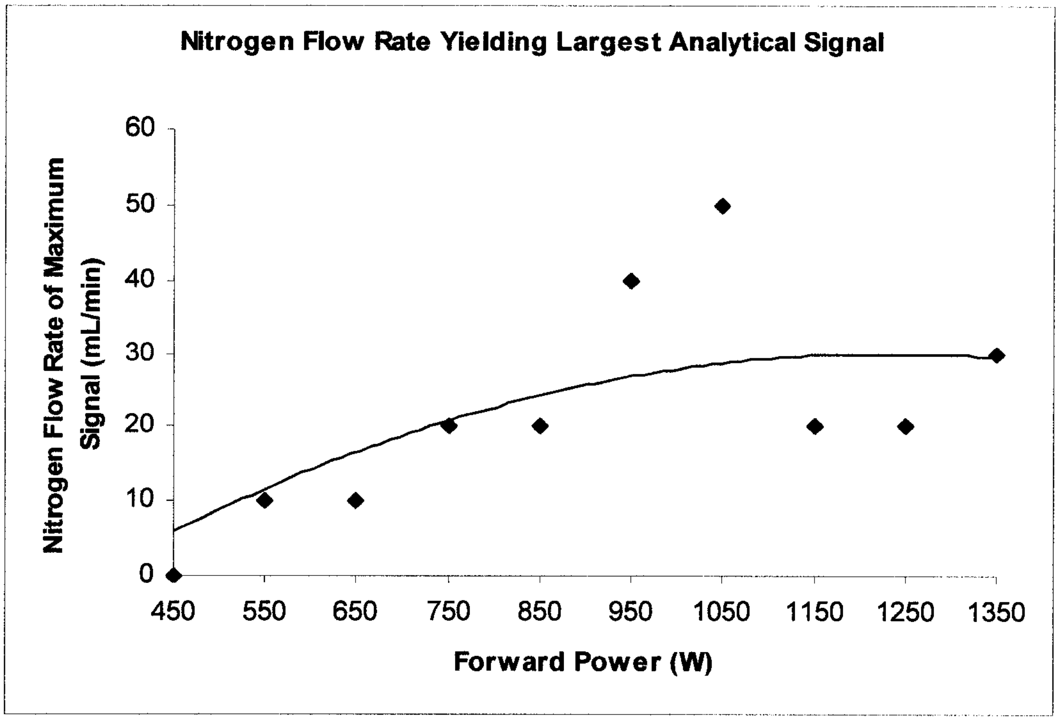

Figure 71. Plot of nitrogen flow rate that yields the largest analytical signal at all forward powers.

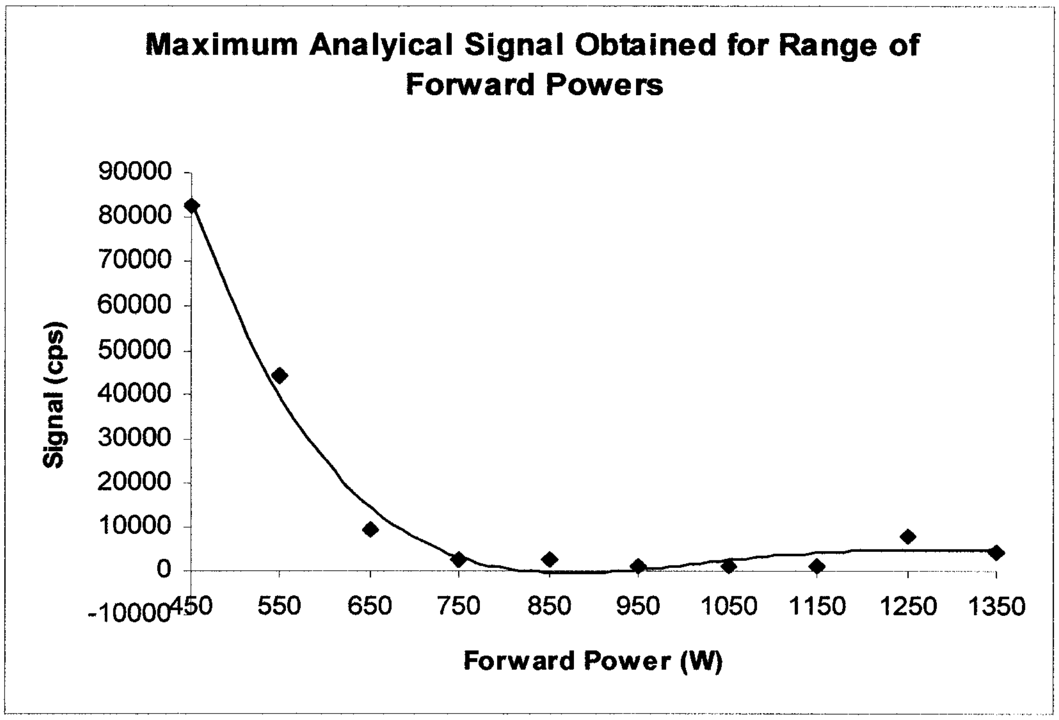

Figure 72. Plot of maximum analytical signal observed for all forward powers.

plasma so that regions of the plasma sampled by the mass spectrometer contain low concentrations of sulfur ions.

Figure 73 shows a plot of the nitrogen flow rates yielding the maximum background signal for all forward powers tested. A trend of increasing nitrogen flow rate with increasing forward power is noted in the range of 450 to 1050 W. Above that power, signals decrease. Figure 74 depicts background signal maxima as a function of applied forward power. Similar to the analytical signal trends of Figure 72, there is a decrease in the background signal with increasing forward powers. As in the $^{31}P^{+}$ study, conditions giving rise to an increase in the analytical signal corresponded to increases in background signals. This indicates that nitrogen addition is shifting the analytical ionization zone of the plasma relative to the sample cone. In contrast to the phosphorus experiments, the highest absolute background signal is found at 450 W with no nitrogen added. This indicates that the addition of nitrogen did not result in an absolute increase in the formation of polyatomic interferences. Table 20 indicates $^{15}N^{18}O^{1}H$ as a weakly interfering species, so a significant increase in the background was not expected.

Figure 75 shows a contour plot of the S/B ratio as a function of forward power and nitrogen flow rate. The highest S/B ratios are found at a forward power of 450 W with 0 and 10 mL/min nitrogen added to the nebulizer gas flow. Similar to phosphorus experiments, S/B ratios tend to decrease with increasing forward powers and nitrogen gas flow rates. It is likely that decreases in signal are due to a shifting of the analytical zone of the plasma and ionization quenching, as nitrogen is expected to lower the temperature of the central channel.

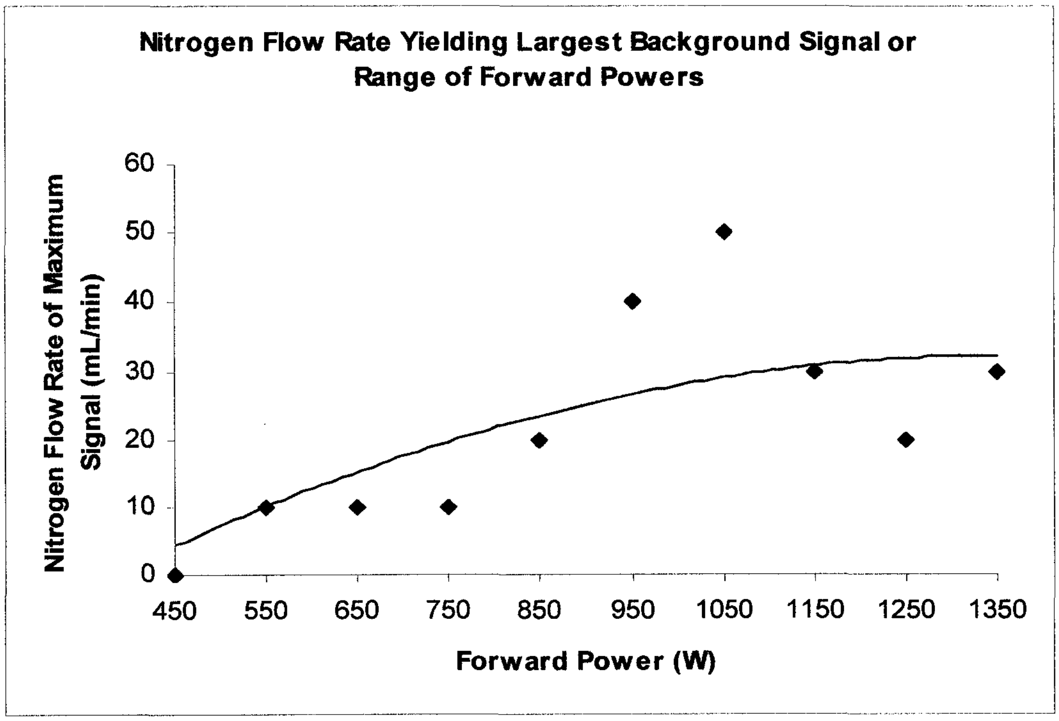

Figure 73. Plot of nitrogen flow rate that yields the largest background signal at all forward powers.

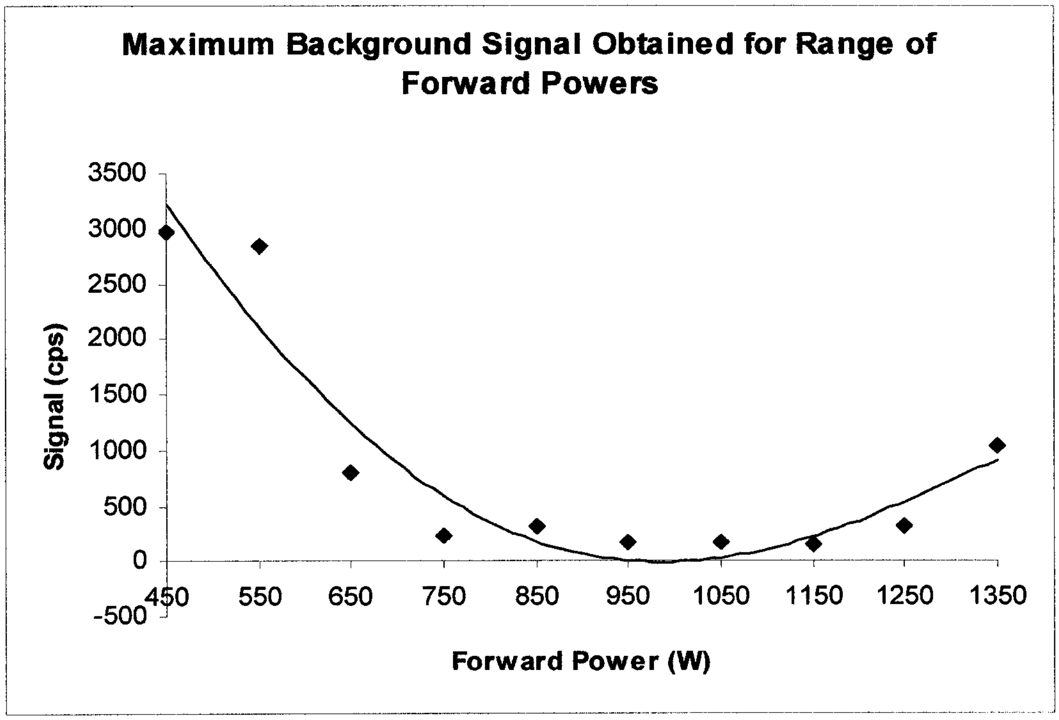

Figure 74. Plot of maximum background signal observed for all forward powers.

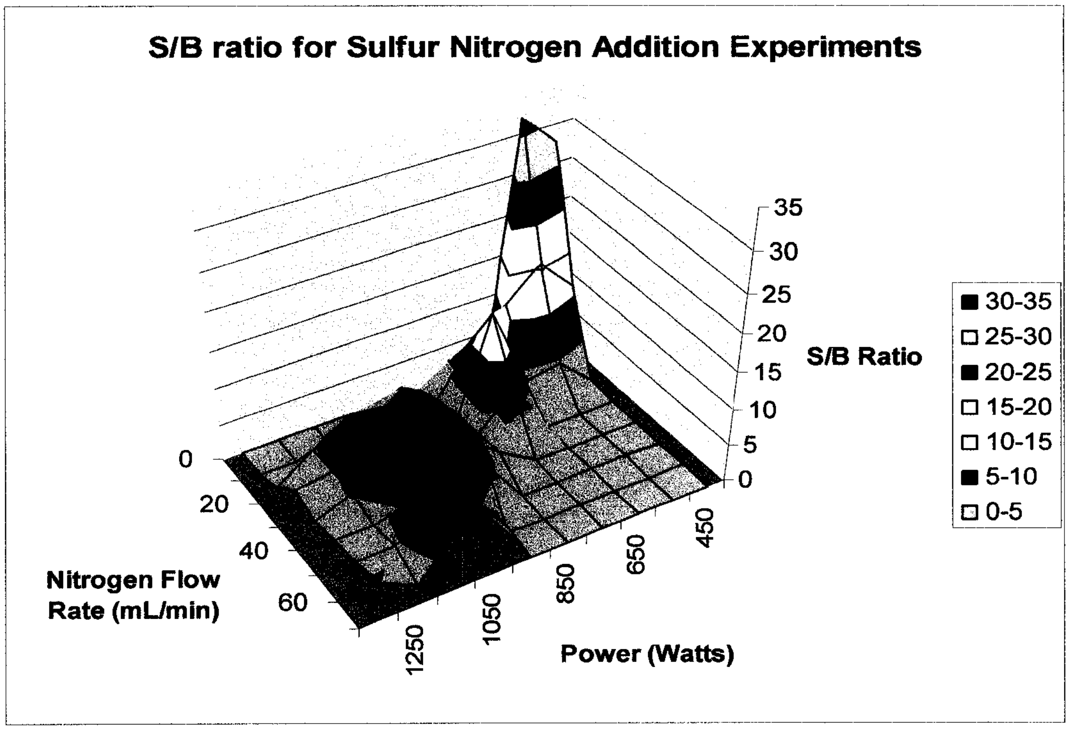

Figure 75. Surface contour displaying S/B trends for sulfur against applied power and nitrogen flow rate added to the nebulizer gas.

Table 23 lists the forward power and nitrogen flow rates that yield the lowest detection limits for sulfur. Detection limits remain in the single ppb range for almost all power levels. The best detection limit is obtained at a forward power of 450 W with no additional nitrogen added to the nebulizer gas flow.

Nitrogen Study Conclusions

At lower power levels, the size and stability of the plasma is reduced with increasing amounts of nitrogen. Higher power levels allow the plasma to tolerate higher flows of nitrogen gas. The plasma does not shrink significantly and the plasma demonstrates increased stability. The central channel, however, appears less dense. This has been observed by other groups utilizing nitrogen addition to the nebulizer gas flow[79]. The darkening of the central channel indicates plasma cooling as thermal energy is absorbed by the strong nitrogen covalent bonds (9.80 eV). Spectroscopic experiments[77] and computer simulations[66] support this. Cooling of the central channel of the plasma would increase the time required to efficiently atomize and ionize nonmetal atoms, negatively affecting sensitivity.

For sulfur at m/z = 34, sensitivity was depressed with the addition of nitrogen. This may be due to plasma cooling and chemistry changes that lead to less efficient sulfur ionization. Significant increases in the background ion count were not observed with supplemental nitrogen gas. Higher powered plasmas were more able to tolerate increasing flows of nitrogen. For phosphorus at m/z = 31, background levels tended to increase with added nitrogen. It is likely that these background

Table 23. Table of nitrogen flow rates yielding the lowest detection limit for sulfur at each forward power utilized.

Forward Power (W)	**Detection Limit (ppb)**	**S/B Ratio**	**Nitrogen Flow Rate (mL/min)**
450	1	28	0
550	3	16	10
650	3	12	10
750	4	15	20
850	10	9	20
950	9	9	30
1050	9	9	40
1150	11	8	20
1250	7	5	20
1350	13	4	30

increases are due to $^{14}N^{16}O^{1}H^{+}$. It is likely that S/B depression with the addition of nitrogen is due to a combination of background interferences, ionization suppression, and shifts in the analytical region of the plasma.

Results and Discussion for Helium Addition

Introduction

There have been few reported studies involving helium addition to the nebulizer gas flow. As noted previously, Pröfrock and co-workers[76] and Caruso and co-workers[73] found sensitivity enhancements for several nonmetal analytes with the addition of 30 mL/min of helium and 5% helium added to the nebulizer gas flow, respectively. Sesi et al.[79] performed fundamental studies of helium gas addition. With the addition of 16.7% helium to the nebulizer gas flow, these workers found a decrease in the electron number density in the central region of the plasma and an increase in the gas kinetic temperature of 1500 K. They also observed that, in contrast to experiments with nitrogen, the addition of helium did not significantly alter the appearance, shape or density of the plasma.

The study presented in this dissertation is intended to examine trends for the analytical response of small additions of helium to the nebulizer gas flow, with the goal of improving the ionization behavior of difficult to ionize elements. Sulfur was the nonmetal element studied in this experiment. Nebulization and transport efficiency was held constant with a fixed nebulizer gas flow of 1.00 L/min. Helium gas was added post-sample-introduction in amounts ranging from 0-80 mL/min. System optimization was performed by maximizing the analytical signal for an aqueous solution of sulfur at a forward power of 450 W. Sampling was held constant and helium gas flow rates were tested at forward powers between 450-590 W in increments of 20 W. Mass spectral scans were obtained for blank and sulfur-containing solutions.

Physical Properties of an Argon ICP with Added Helium

In contrast to oxygen and nitrogen addition experiments, the addition of helium did not have a noticeable effect on the size, shape, and density of the plasma. Reflected power remained below 5 watts at all helium flow rates for all power levels. The lack of a visible effect on the plasma may indicate that helium is not being significantly ionized by the ICP. Small shifts in the analytical zone of the plasma are still expected as the total gas flow rate changes due to the additional helium.

Data for Helium Addition

Initial experiments involving helium gas addition were carried out under conditions identical to those of the nitrogen addition experiments. Forward powers ranged from 450-1350 W with 0-80 mL/min of helium added to the nebulizer gas. At powers of 650 W and greater, the analytical and background signals were not measurable with any helium gas flow rate except those at 70 and 80 mL/min. These signals were very small at 650 W and disappeared entirely when the forward power reached 750 W. It appeared that the signal and background trends are similar to that of an all-argon plasma, shown previously in Figure 33. It is likely that helium is not being ionized and is not affecting the macroscopic properties of the argon ICP.

In an effort to further characterize this behavior, the helium addition experiments were repeated at forward power levels between 450-570 W in increments of 20 W. Figures 76-79 show the background and analytical signals for 450, 490, 550 and 590 W and helium flow rates ranging from 0 to 80 mL/min. Figures 80-82 show the signal and background trends as a function of forward power at 0, 10 and 30 mL/min helium. Figures 83 and 84 show the S/B trend at a forward powers of 450 and 550 W, respectively.

Helium Addition: Sulfur Results

Sulfur was monitored at $^{34}S^+$. The analytical signal is plotted as a function of helium flow rate for selected power levels in Figures 76-79. The graphs show a large variability in trends from one power level to another. At higher powers, 550 and 590 W, the addition of helium increased the analytical signal. At these powers, the analytical signal also exhibited a larger helium flow rate range in which a significant $^{34}S^+$ signal was observed. It is likely that at the lower forward powers, 450 and 490 W, the analytical zone of the plasma, where the concentration of sulfur ions is highest, is in close proximity to the sample cone orifice. At low forward powers, an increase in the helium flow rate results in a decrease in the analytical signal. When

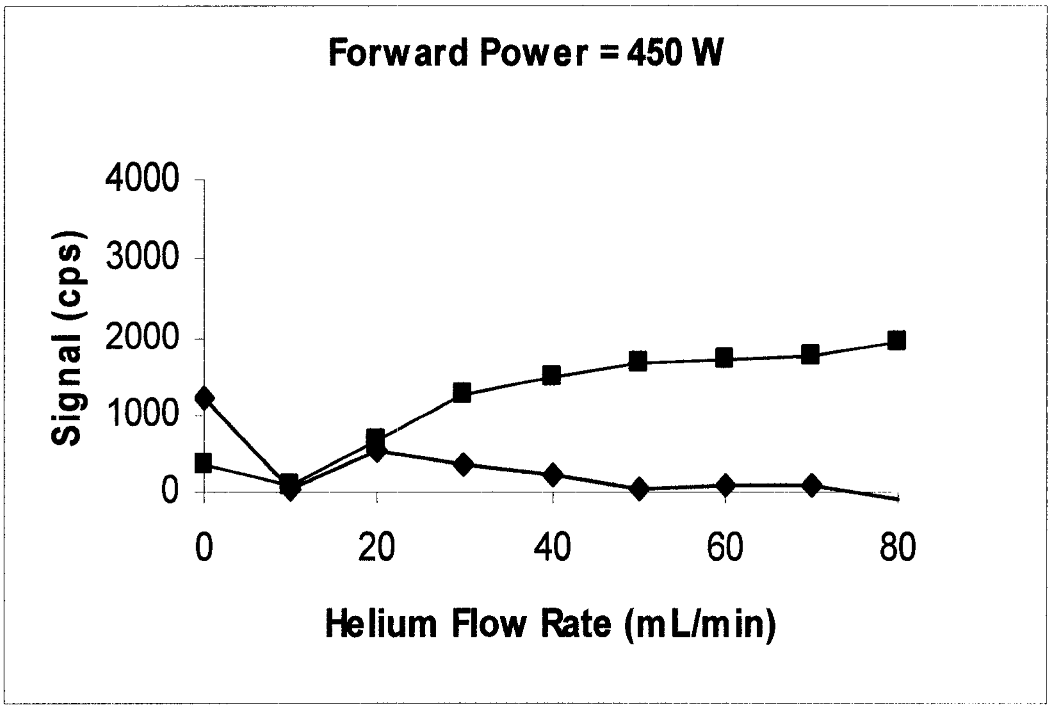

Figure 76. Plot of analytical (♦) and background (■) signals at an applied forward power of 450 watts.

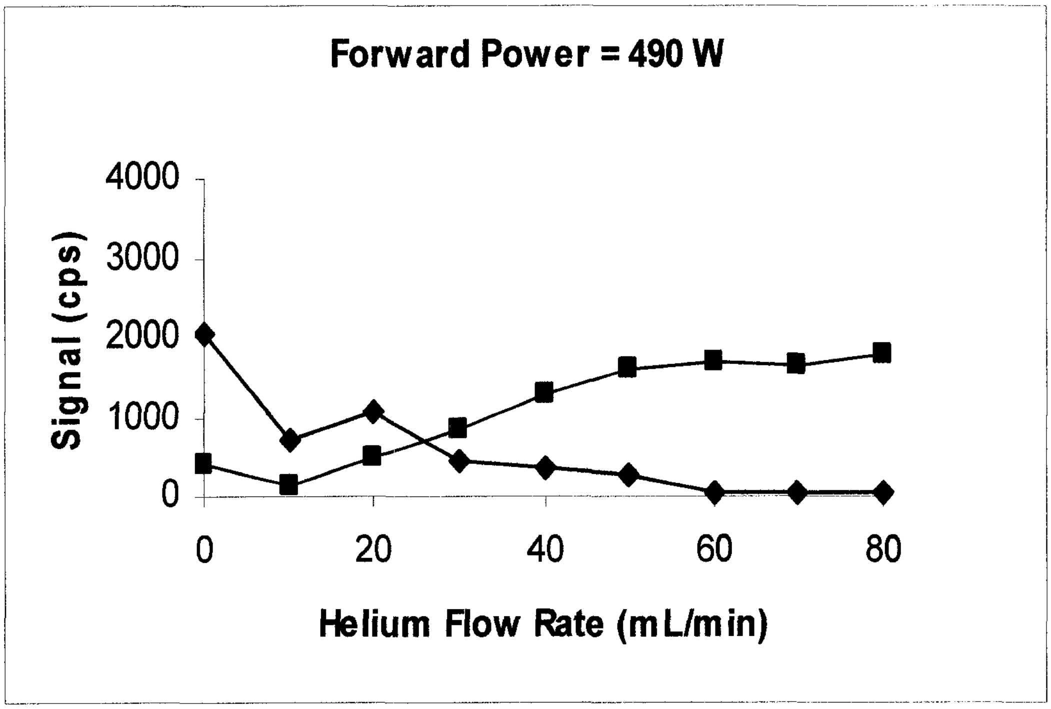

Figure 77. Plot of analytical (♦) and background (■) signals at an applied forward power of 490 watts.

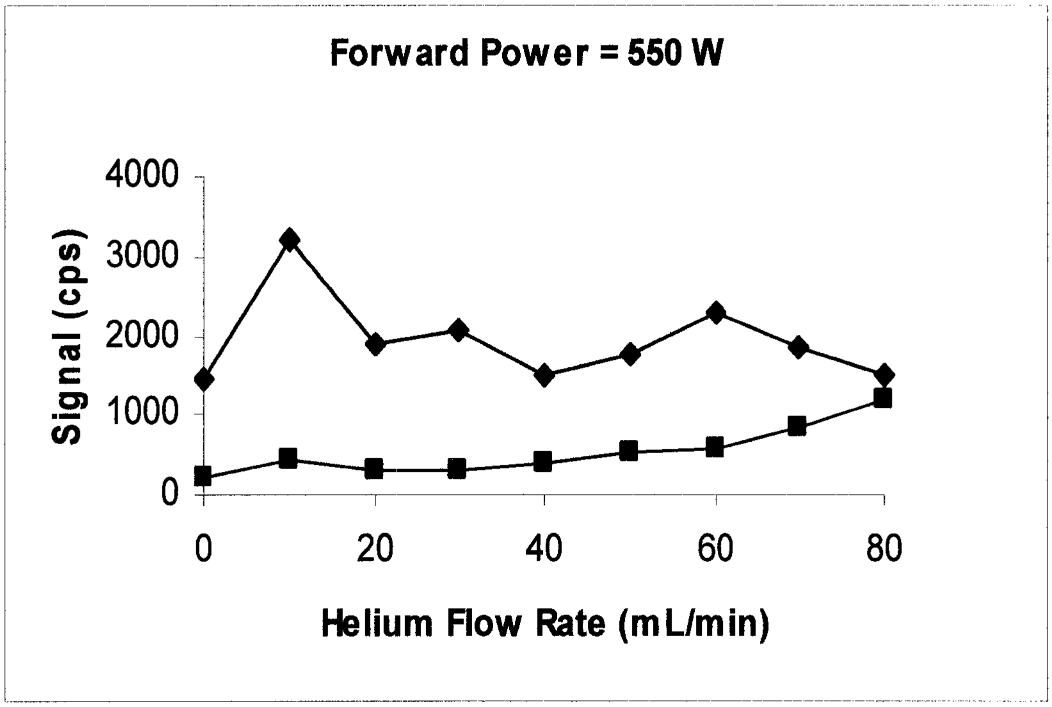

Figure 78. Plot of analytical (♦) and background (■) signals at an applied forward power of 550 watts.

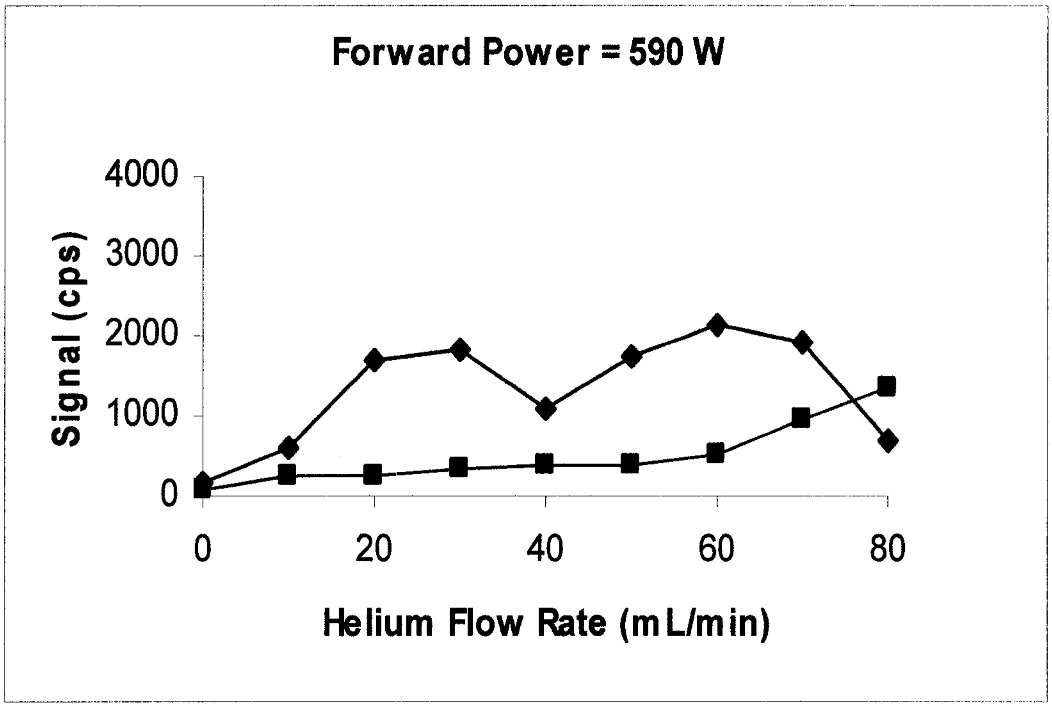

Figure 79. Plot of signal analytical (♦) and background (■) signals at an applied forward power of 590 watts.

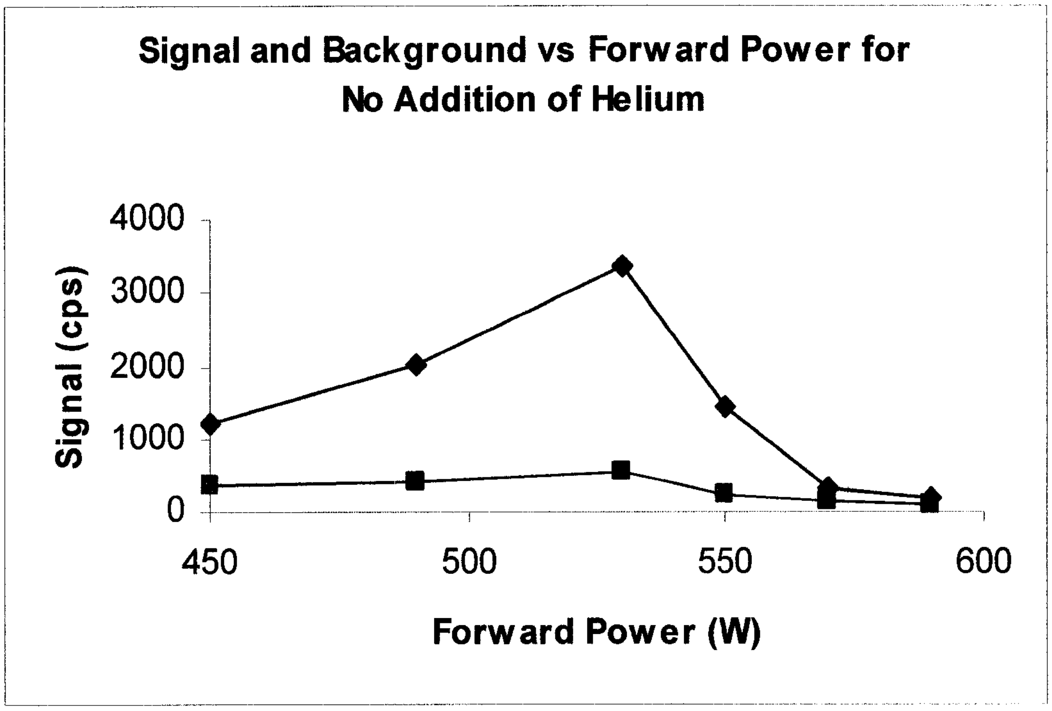

Figure 80. Plot of analytical (♦) and background (■) signals against applied forward power with no helium added to the nebulizer gas flow.

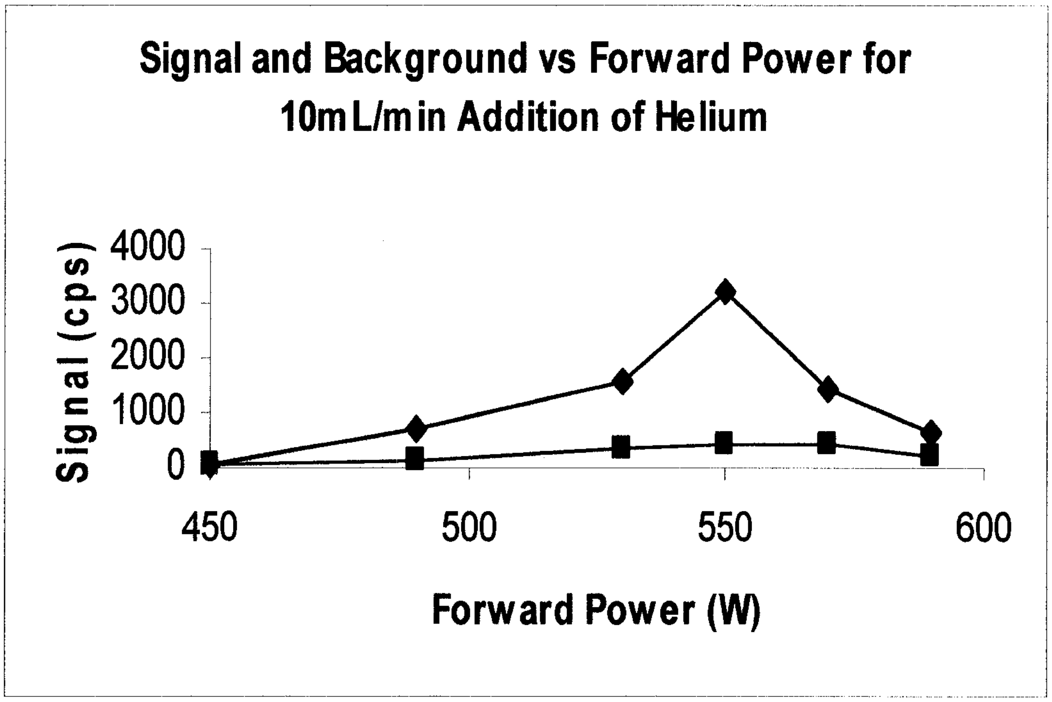

Figure 81. Plot of analytical (♦) and background (■) signals against applied forward power with 10 mL/min of helium added to the nebulizer gas flow.

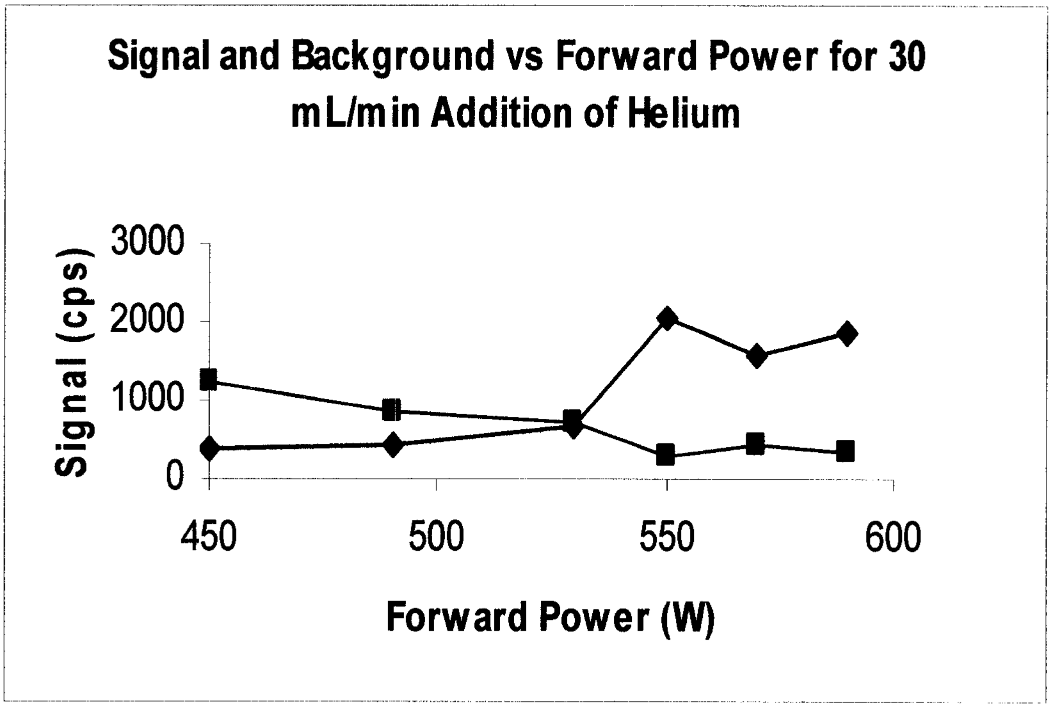

Figure 82. Plot of analytical (♦) and background (■) signals against applied forward power with 30 mL/min of helium added to the nebulizer gas flow.

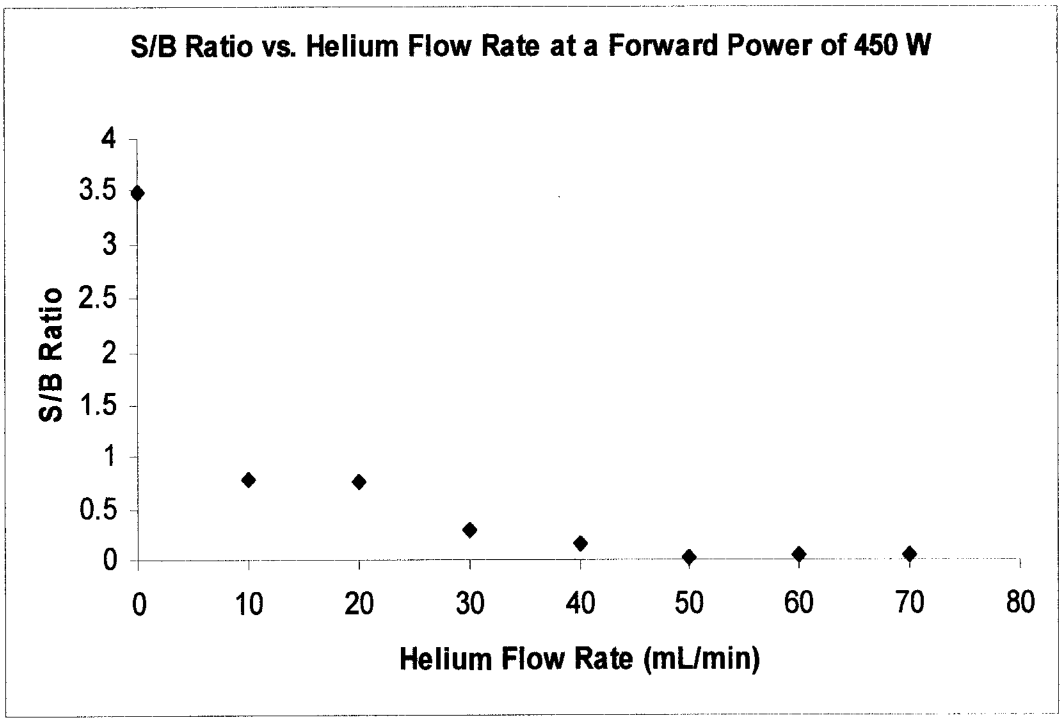

Figure 83. Plot of S/B ratio against helium gas flow rate at an applied forward power of 450 W.

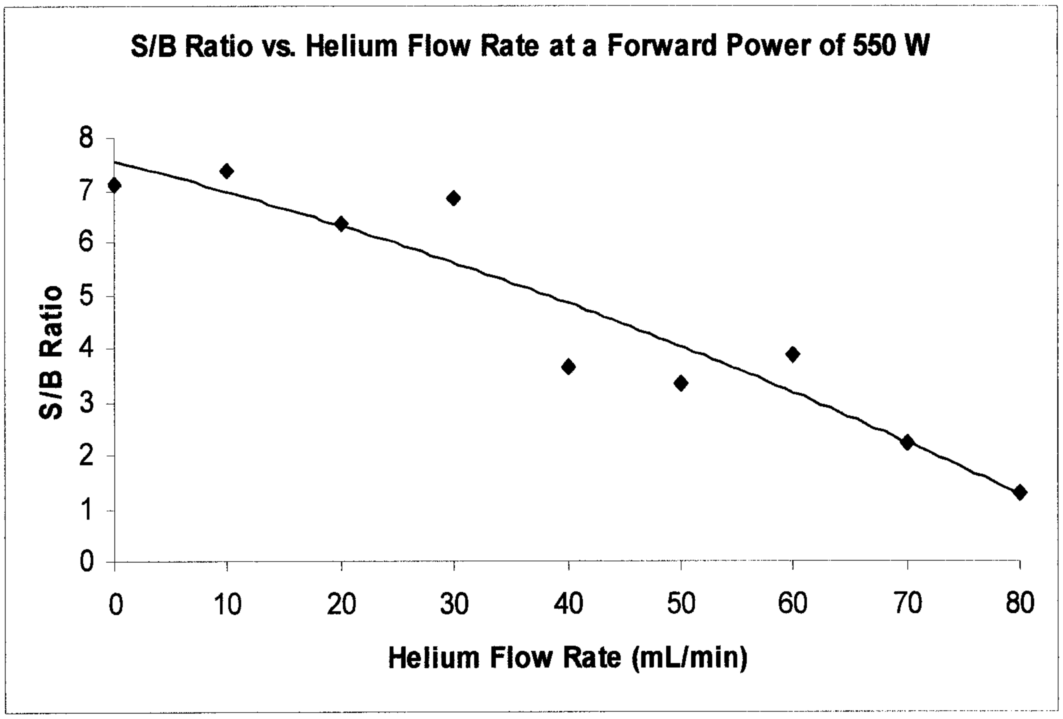

Figure 84. Plot of S/B ratio against helium gas flow rate at an applied forward power of 550 W.

operated at 590 W, the plasma is more dense and the ion channel is less well defined. Ionization likely occurs earlier in the plasma, increasing the size of the analytical zone and shifting the zone of maximum ionization towards the load coil. Hence, at high forward powers, larger flows of helium are required to shift the analytical zone of the plasma towards the sample cone.

Figures 76-79 also show the background signal trends. The background signal intensity increases with increases in helium flows. It is unclear why this occurs. It has been shown that the addition of helium raises the gas kinetic temperature[79] of the plasma. Generally, an increase in temperature yields a robust plasma, with increased resistance to the formation of polyatomic species. It is possible that higher helium flow rates shift the region of the plasma with a high concentration of background ions closer to the sample cone. Another potential explanation is that the plasma is actually "cooled" by the helium and/or the residence times of all species within the plasma is reduced. These conditions might contribute to increases in the molecular ion interferences. Table 20 indicates that the major polyatomic ion that would cause high backgrounds is $^{15}N^{18}O^{1}H^{+}$. Noting that the natural abundance of these elements are low and that helium is not an interferent, the increase in the background signals with increasing helium flow is unexpected. Further experimentation is necessary to deduce the cause for this background level increase.

As qualitatively seen in Figures 76-79, both analytical and background ion signals decrease significantly at higher forward powers (>600 W). These trends are similar to signal reductions shown for an all-argon plasma (Figure 33). This trend can be visualized with the helium doped argon plasma by plotting the signal and background as a function of applied forward power at various helium flow rates. Figures 80-82 show such plots at 0, 10, and 30 mL/min helium. This data clearly shows a profile similar to that of Figure 33. Results indicate an optimal plasma power, and perhaps an optimal sampling region, at each helium flow rate. The graphs also indicate the peak signals are obtained at higher forward powers with increasing helium gas flow rates. It is possible that higher helium gas flows cause the volume of the analytical region to increase, allowing for similar ion counts to be obtained at a wider range of forward powers.

Figures 83 and 84 demonstrate the depressive effect helium addition has on the S/B ratio. This is shown for forward powers of 450 and 550 W, although all power levels tested show this trend. The graphs indicate that the rate of change in the S/B ratio is greater at the lower 450 W forward power (Figure 83) as compared to that at 550 W (Figure 84). This is an indication that the analytical zone of the plasma is either shifted less or is larger at higher forward powers.

To conclude, the addition of helium gas to the nebulizer gas flow of an argon ICP did not yield any benefit in the analytical sensitivity of $^{34}S^{+}$. The helium-doped plasma behaved similarly to an all-argon plasma, indicating that helium in these amounts and operating powers is not significantly being ionized or affecting plasma chemistry. Fluctuations in analytical and background signals are likely due to shifts in the analytical zone of the plasma relative to the sample cone.

Conclusion

The addition of supplemental gases to the nebulizer gas flow caused signal depression, in most cases, for all gases and analytes studied. This depression is most likely due to a combination of plasma cooling and a shift in the analytical zone of the plasma away from the sampler and skimmer cones. Oxygen addition mitigated the buildup of carbon deposits on the sampler and skimmer cones. Nitrogen addition depressed S/B ratios for both phosphorus and sulfur analytes, reducing sensitivity and degrading detection limits somewhat. Helium addition had no appreciable effect on either the appearance of the plasma or the analytical or background signals for sulfur. Signal response to changing forward power levels mirrors that of an argon plasma indicating that helium is not being ionized to an extent sufficient to influence analytical signals.

Additional experiments would include performing oxygen addition post MD and varying the power levels to ascertain the best conditions for both organic solvent pyrolysis and sensitive nonmetal determinations. Supplemental gas added to the auxiliary or coolant gas flows should be studied with USN-MD sample introduction and the low powers utilized in our laboratories.

CHAPTER 4

APPLICATION OF ICP-MS AS A DETECTOR FOR HPLC: SELECTED EXAMPLES AND VOLATILITY CONSIDERATIONS

Background

A critical objective of utilizing ICP-MS detection of nonmetals is its successful application to the analysis of molecules that are difficult to detect with standard HPLC detection methods. A starting point in developing additional applications for harder-to-ionize molecules is to select a series of nonmetal-containing analytes that may be speciated by HPLC. A review of what has been accomplished in the literature is also necessary to help guide research initiatives.

Currently a number of industries benefit from the direct coupling of HPLC to ICP-MS. Examples of sensitive metal and semi-metal determinations have been published by a number of groups. Vanhaecke and co-workers[80] speciated Cr(III) and Cr(IV). Pu, Hu, Jiang, and Huang[81] demonstrated the speciation of Fe(II) and Fe(III). Other groups have performed speciation and determination of metal-containing compounds utilizing ICP-MS[82-87].

Determinations of nonmetals by HPLC-ICP-MS have also been accomplished by a number of groups. B'Hymer and Caruso[88] recently published a thorough review of the current and past literature for the speciation and detection of selenium with ICP-MS. Kovačevic and co-workers[89] used LC-ICP-MS to speciate digested cell membrane phospholipids by monitoring phosphorus. Quinones and co-workers[90] utilized ion chromatography to speciate bromate and bromide in blood plasma. They obtained detection limits of 5 ppb utilizing ICP-MS. Caruso and co-workers[91] utilized an octopole collision cell with helium to remove nitrogen oxide interferences at m/z = 31 for $^{31}P^+$. Detection limits in the sub-ppb range were reported for several phosphorus-containing analogues of nerve agents. Marshall et al.[92] quantified with HPLC-ICP-MS the metabolic by-products of brominated bradykinin. Jensen and co-workers[93] presented a paper demonstrating micro-bore HPLC with ICP-MS for the detection of several drug compounds. Compounds detected monitoring chlorine included furosemide, diclofenac, clofibric acid, and 4-chlorobenzoic acid. Compounds detected monitoring bromine included bromofenac, 4-bromobenzoic acid, bromazepam, and 5-bromouracil. Compounds detected monitoring iodine included 5-iodouracil, 4-iodobenzoic acid, 5-iodo-6-methyluracil, and 5-iodo-2'-deoxyuridine. Direct injection and the use of an Aridus microconcentric nebulizer were compared. The direct injection nebulizer sensitivity was found to be independent of the analyte's structure, but varied with the amount of organic solvent in the matrix. Response factors when using the Aridus microconcentric nebulizer were dependent on the analyte structure, but did not vary significantly with methanol concentrations. It was hypothesized that many of the analyte compounds were partially lost during desolvation in the Aridus nebulization system. Edler, Jakubowski, and Linscheid[94] speciated and quantified melphalan DNA adducts by selectively detecting phosphorus. Shah and Caruso[95] recently published a comprehensive review on the status and application of phosphorus speciation and detection by ICP-MS.

Clearly, a large body of work has been devoted to HPLC-ICP-MS. The majority of this work has been for the analysis of metals, semi-metals, and easy-to-ionize nonmetals such as selenium and arsenic. Fewer studies have been attempted to detect halogens and other heteroatom species. This discussion focuses on current projects under way in our laboratory that will help define the utility of HPLC-USN-MD-ICP-MS detection of nonmetal analytes.

Outline of Current HPLC Experiments Utilizing ICP-MS Detection

Several projects involving HPLC separation and ICP-MS detection of model pharmaceutical compounds are ongoing in our laboratory. The compounds being separated include:

1. isopropyl methanesulfonate (IPMS) and methyl-methionine
2. difluorobenzyl chloride (DFBC) and a bromine-containing API
3. 2,4-difluorobenzyl bromide (2,4-DFBB) and a bromine-containing API
4. 2,6-difluorobenzyl bromide (2,6-DFBB) and a bromine-containing API
5. vitamins B_1 and B_{12}.

The structures of 2,4-DFBB, 2,6-DFBC, vitamin B_1, and methyl-methionine are shown in Figure 85. The structure of vitamin B_{12} is shown in Figure 86. Several of the compounds and chromatographic conditions required for separation are provided by Pfizer Global Research and Development. Structures for DFBC and the bromine-containing API are proprietary and are not shown.

Experimental

HPLC and ICP-MS Instrumentation

A dual pump HPLC (Dynamax Model SD-200, Rainin Instruments,Woburn, MA) was utilized. A six-port injector with a 5 μL sample loop (Rheodyne, Cotati, CA) was used for all analyte injections. A UV-VIS detector (Dynamax Model UV-C, Rainin Instruments,Woburn, MA) was used in series with ICP-MS detection. The ICP-MS was a 27 MHz Fisons (Thermo Electron) Instruments PlasmaQuad II. Ion signals from a Burle (Sturbridge, MA) Channeltron 4870V were acquired utilizing Thermo Electron PlasmaLab software (Version 1.06.007, Ionflight, Boston, MA). Sample introduction was accomplished with a Cetac Industries (Omaha, NE) USN. The nebulized aerosol was directed to a MDX-200 for additional desolvation. A weekly routine calibration of the instrument was performed by continuously nebulizing a peristaltically pumped 10 ppb solution of Li, Mg, Co, In, Pb, Ce, and U in 1% (v/v) nitric acid at a forward power of 1350 W. Tables 24 and 25 summarize the operational parameters.

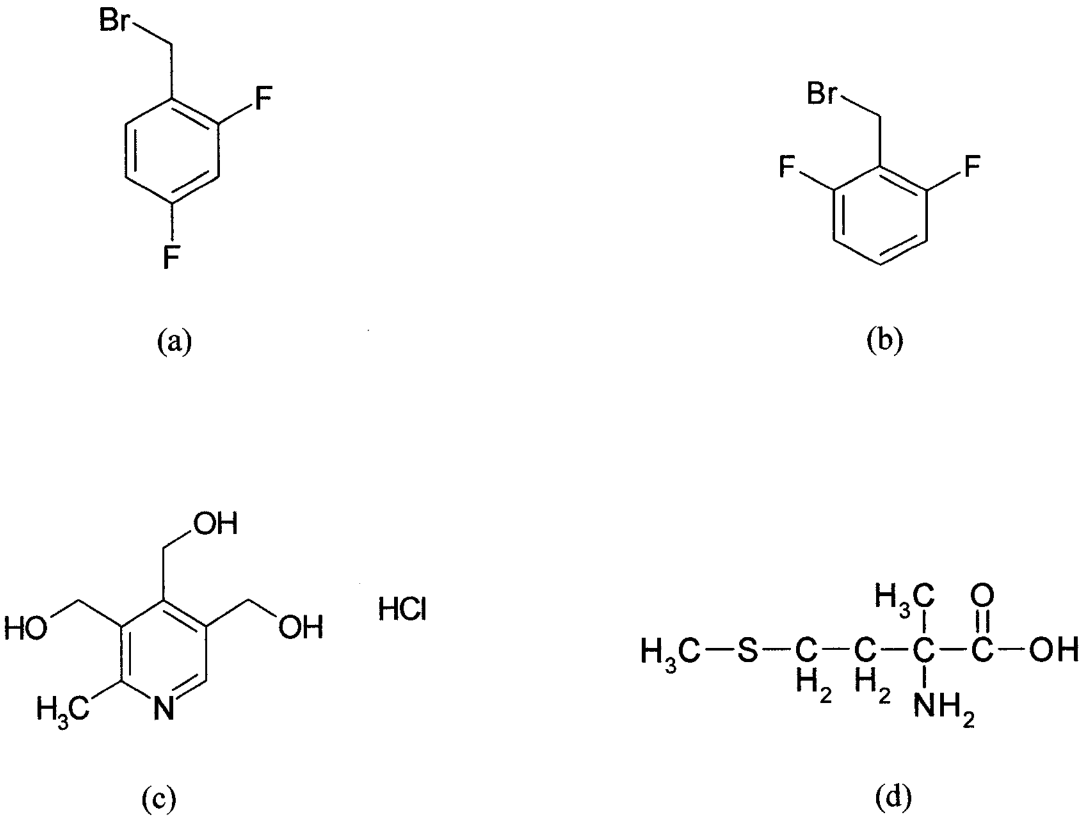
Br
F
F
(a)
Br
F
F
(b)
OH
HO
OH
HCl
H_3C
N
(c)
H_3C
O
H_3C—S—C—C—C—C—OH
H_2
H_2
NH_2
(d)

Figure 85. Structures of (a) 2,4-difluorobenzyl bromide, (b) 2,6-difluorobenzyl bromide, (c) vitamin B_1, and (d) methyl-methionine.

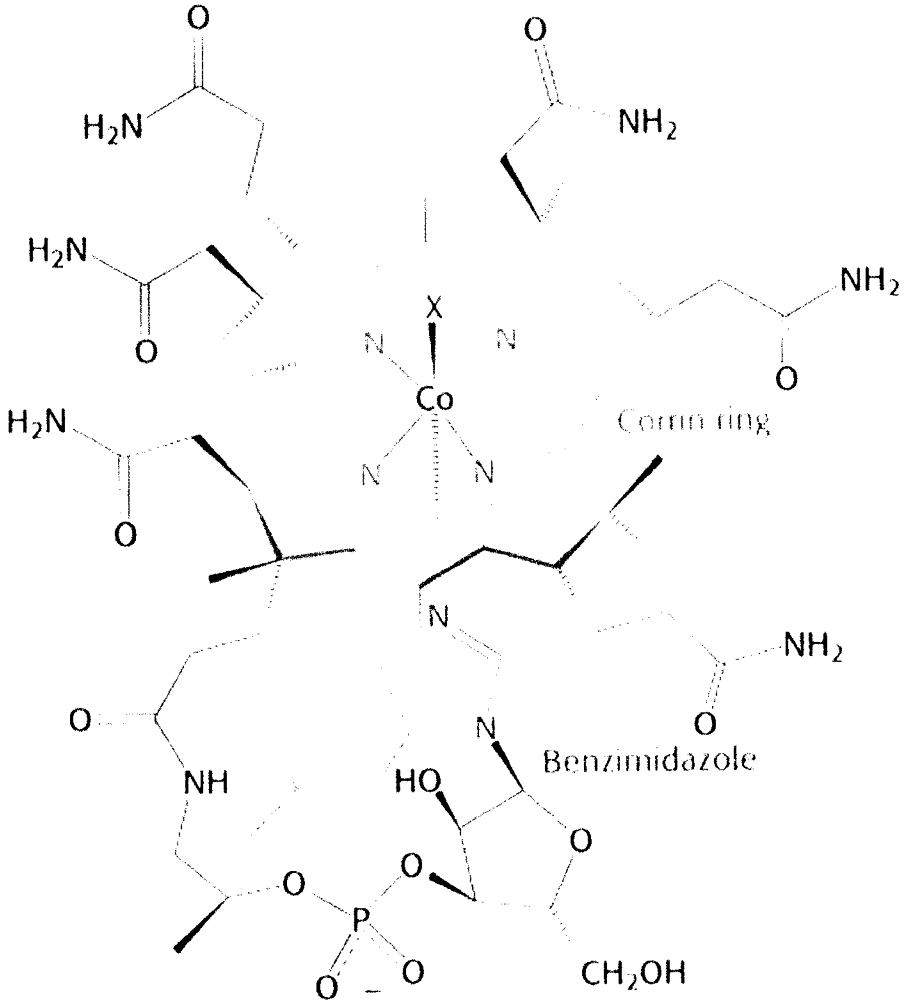
O
H₂N
O
NH₂
H₂N
O
X
N
N
Co
N
N
NH₂
O
H₂N
O
Corrin ring
N
NH₂
O
O
NH
N
Benzimidazole
HO
O
O
O
P
O
O
O
CH₂OH

Figure 86. Structure of vitamin B_{12} where X is a C≡N group.

Table 24. Operating parameters for separation of IPMS and methyl-methionine.

HPLC and USN-MD Settings	
HPLC mobile phase flow rate, mL/min	0.5
Wavelength of UV-VIS Detection, nm	204
Nebulizer gas flow rate, L/min	0.8-1.0
Nebulizer heater temperature, °C	140
Nebulizer condenser temperature, °C	3
Membrane desolvator temperature, °C	160
Membrane desolvator countercurrent flow rate, L/min	1.5
ICP-MS system	
Optimal RF power, W (Daily variable)	490-550 W
Detector	Burle Channeltron 4870V
Outer gas flow rate, L/min	14.0
Intermediate gas flow rate, L/min	0.8
Data acquisition parameters	
Scan mode	Single ion monitor
Dwell time, ms	250
Isotope monitored	^{34}S

Table 25. Operating parameters for the separation of DFBC and DFBB from a bromine-containing API.

HPLC and USN-MD Settings	
HPLC mobile phase flow rate, mL/min	1.0
Wavelength of UV-VIS Detection, nm	220
Nebulizer gas flow rate, L/min	0.8-1.0
Nebulizer heater temperature, °C	140
Nebulizer condenser temperature, °C	3
Membrane desolvator temperature, °C	140
Membrane desolvator countercurrent flow rate, L/min	1.5
ICP-MS system	
Optimal RF power, W (Daily variable)	490-550
Detector	Burle Channeltron 4870V
Outer gas flow rate, L/min	14.0
Intermediate gas flow rate, L/min	0.8
Data acquisition parameters	
Scan mode	Single ion monitor
Dwell time, ms	250
Isotope monitored	^{35}Cl, ^{79}Br

Reagents and Sample Preparation

IPMS, DFBC, and the bromine-containing API were obtained from Pfizer Global Research and Development (PGRD, Ann Arbor, MI). 2,4-DFBB, 2,6-DFBB, methyl-methionine, ammonium hydroxide and formic acid were obtained from Acros Organics (Pittsburgh, PA). Stock solutions were made by dissolving the analytes in appropriate solvents. HPLC grade ACN (Fisher Scientific, Pittsburgh, PA) and 18 MΩ•cm deionized water were used as mobile phase solvents.

Chromatographic Materials and Conditions

Separations of IPMS and methyl-methionine were performed on a diol normal phase column (Develosil 100-5, Japan). Column dimensions were 4.6 x 100 mm and the stationary phase particle size was 5 μm. A mobile phase flow rate of 0.5 mL/min with isocratic conditions was used. The mobile phase consisted of a 20% (v/v) aqueous solution buffered with ammonium hydroxide and formic acid to a pH of 7 and 80% ACN.

Separations of DFBC, 2,4-DFBB and 2,6-DFBB were accomplished on a C_{18} reverse phase column (Chromolith, Merck KGaA, Darmstadt, Germany). Column dimensions were 4.6 x 100 mm with 5 μm stationary phase particle size. A mobile phase flow rate of 1.0 mL/min with isocratic conditions was used. The mobile phase consisted of a 40% (v/v) aqueous solution buffered with ammonium hydroxide and formic acid to a pH of 7 and 60% ACN.

HPLC-ICP-MS Detection of IPMS and Methyl Methionine

HPLC-UV-VIS-ESI-MS

Figure 87 shows an HPLC-UV-VIS chromatogram of a 5 µL injection of a solution containing 5000 ppm IPMS and 400 ppm methyl methionine. Since IPMS contains poor chromophoric moieties, in-series detection by ESI-MS was necessary to identify the analyte peaks and retention times. Data was collected with a Bruker Esquire 3000 quadrupole ion trap mass spectrometer (Bruker Daltonics, Billerica, MA, USA). Standard electrospray conditions were utilized to obtain a sufficient ion signal. Figure 88 displays the data obtained from the ESI-MS detector in three panels. The top panel shows the total ion chromatogram. A large peak with greatest intensity at 7.3-7.5 minutes corresponds well with the peak obtained for methyl methionine in the UV-VIS trace (Figure 87). The major ion peak obtained by continuous mass spectral scans is shown in the middle panel of Figure 88. The most abundant appears at m/z 164.5. This is consistent with a protonated methyl methionine molecule (MW = 163)

A significant increase in the ion count at the expected elution time for IPMS is not observed in the ESI-MS total ion chromatogram (top panel Figure 88). However, the major ion peak observed during this time interval is 122.5 (bottom panel Figure

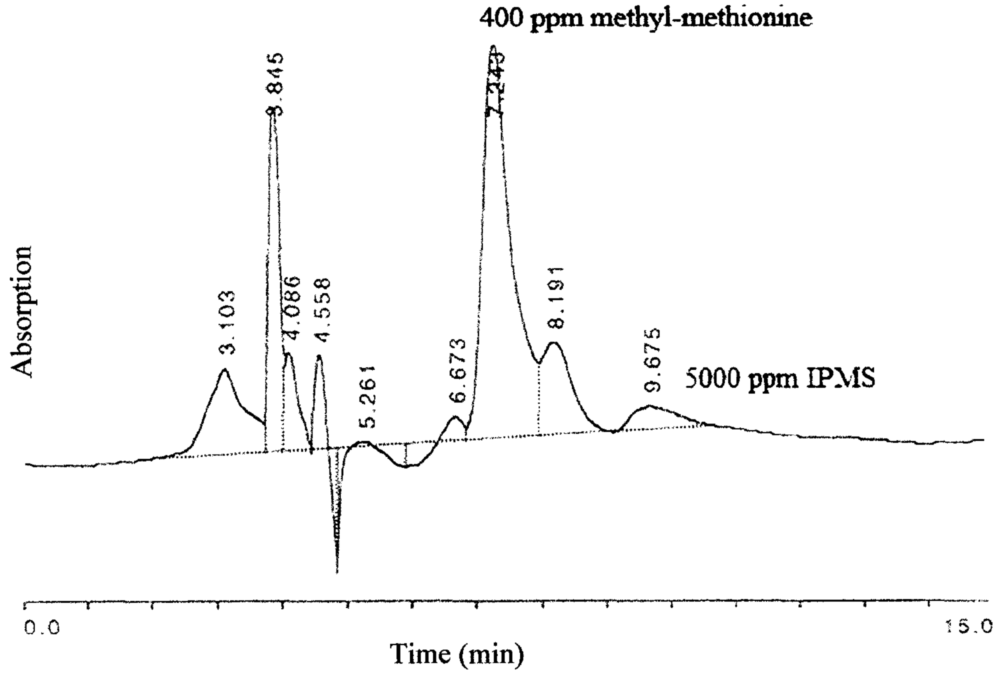

Figure 87. UV-VIS trace of a mixture of 5000 ppm IPMS and 400 ppm methyl methionine. Methyl methionine has been assigned the peak at 7.2 min. and IPMS has been assigned the peak at 9.7 min.

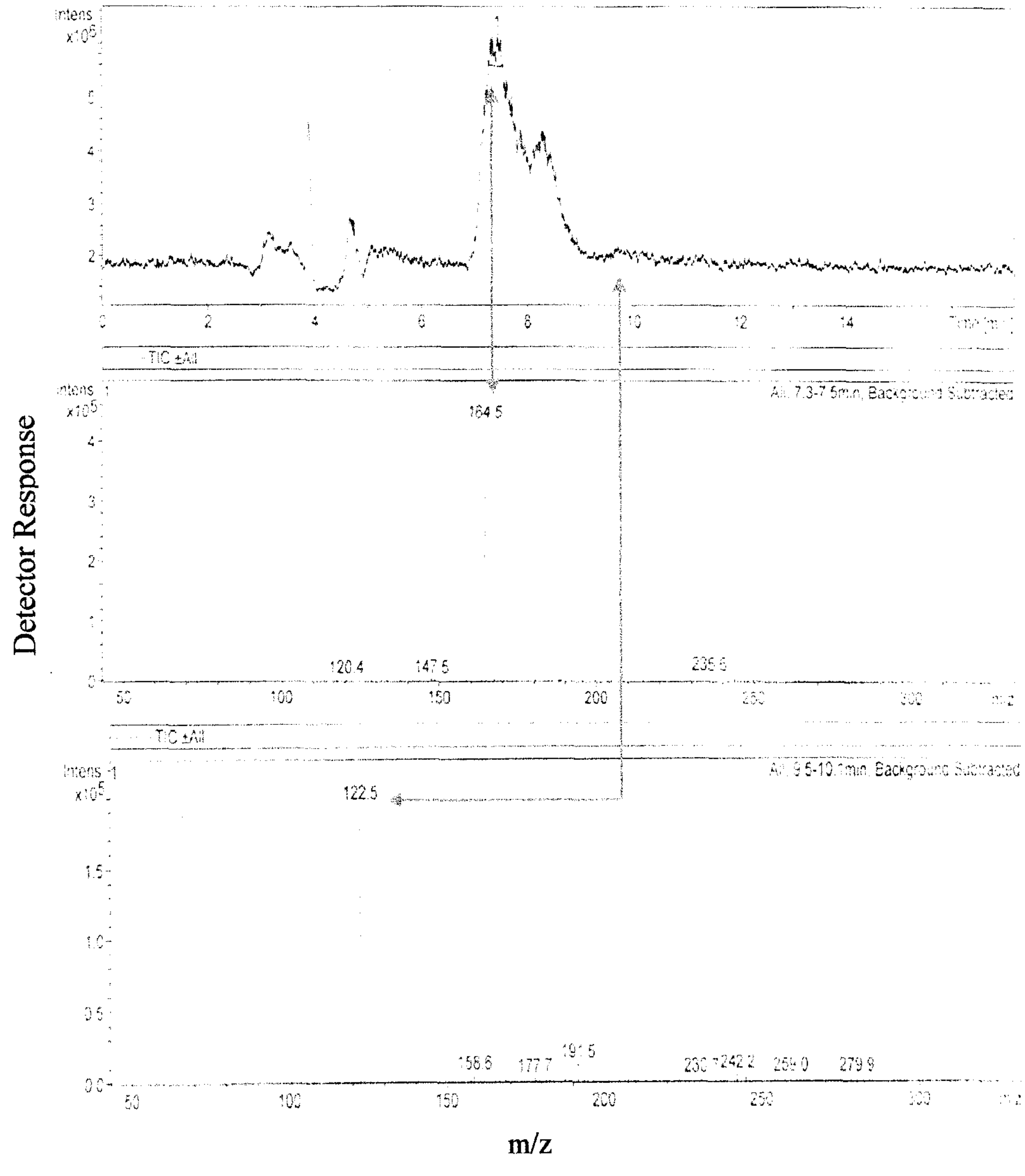

Figure 88. HPLC-ESI-MS trace of a mixture of methyl methionine and IPMS. The top panel is the total ion chromatogram. The middle panel is the mass spectrum obtained for the methyl methionine peak. The bottom panel is the mass spectrum obtained for the IPMS peak

88). This ion peak corresponds to an ion of IPMS with loss of oxygen. IPMS has a molecular mass of 138 amu. The protonated ion peak is not observed. However, loss of oxygen (16 amu) yields $IPMS^{138}$-O^{16} with a molecular mass of 122 amu. For verification, direct injection of IPMS was performed. An identical ion peak was seen (Figure 89).

HPLC-UV-VIS-ICP-MS

Figure 90 shows the ICP-MS signal response to a 5 μL injection of a 25 ppt solution of IPMS eluted under the same conditions as in the HPLC-ESI-MS experiment. Sulfur was monitored as the $^{34}S^+$ isotope. The chromatogram shows a large sulfur signal earlier in the chromatogram. This is likely an impurity in the IPMS sample that has a lower retention index.

Figure 91 shows the ICP-MS signal response to a 5 μL injection of a 400 ppm solution of methyl-methionine. The elution conditions are different than in the HPLC-UV-VIS-ESI-MS trace. However, this chromatogram is included to indicate the relative sensitivity of the ICP-MS towards methyl methionine. It is observed that the net analytical signal for a significantly diluted sample of methyl methionine (400 ppm vs. 5000 ppm) is much higher than obtained for IPMS. These results indicate that it is likely that the high volatility of IPMS is leading to its loss in the desolvation elements of the sample introduction system.

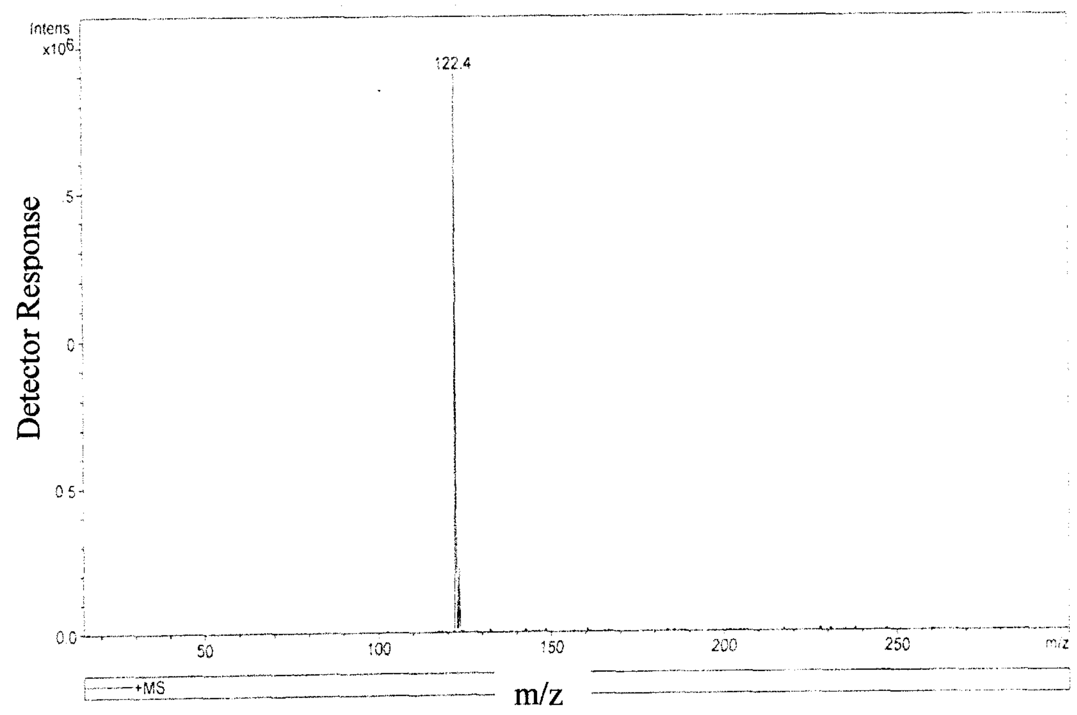

Figure 89. Mass spectrum obtained from direct injection of IPMS into the ESI-MS.

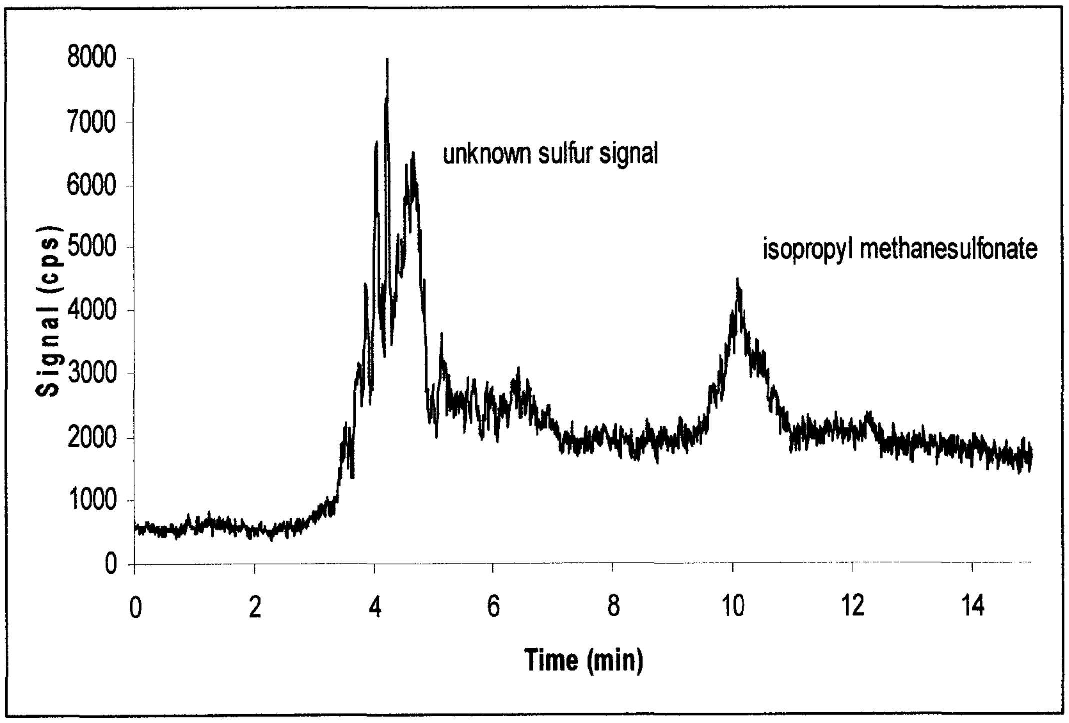

Figure 90. HPLC-ICP-MS trace monitoring $^{34}S^{+}$ for a 5 µL injection of a 25,000 ppm solution of IPMS.

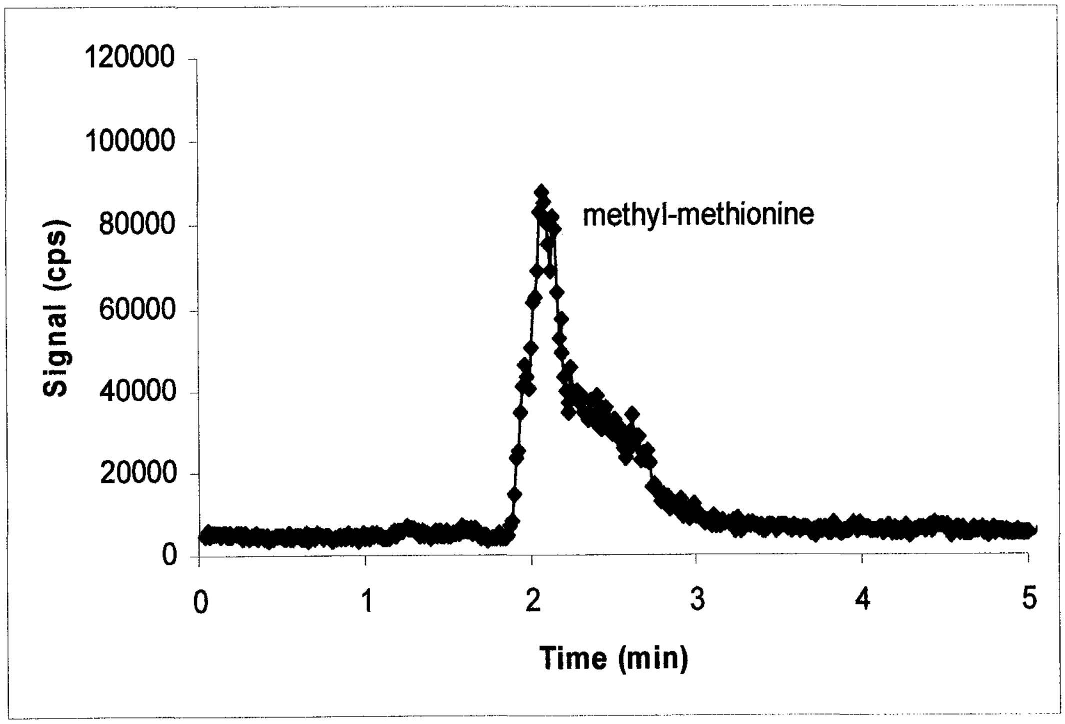

Figure 91. HPLC-ICP-MS trace monitoring $^{34}S^+$ for a 5 μL injection of a 400 ppm solution of methyl methionine.

IPMS and Methyl Methionine Conclusions

A chromatographic method for the separation and detection of IPMS and methyl methionine has been demonstrated. ICP-MS results indicate a decrease in sensitivity for IPMS compared to methyl methionine. A mixture of IPMS and methyl methionine needs to be injected with the method developed with UV-VIS and ESI-MS detection. This will fully demonstrate the capabilities of ICP-MS as a detector for this analyte system. Experiments where the temperature in the sample introduction system is lowered and the nebulizer gas flow is increased should be performed. Under these conditions, the volatile IPMS will be removed less by the desolvating elements of the sample introduction system. This may lead to an increase in the sensitivity of the system to IPMS.

HPLC-USN-MD ICP-MS Analyte Volatility Concerns: DFBC, DFBB, Vitamin B_{12}, and a Bromine-Containing API

Introduction

Experiments with a number of other analyte systems were accomplished in parallel with IPMS and methyl methionine. The results from these initial investigations indicate that sensitive detection of nonmetal-containing analytes is probably linked to the volatility of the molecule. To demonstrate this, several chromatograms of two binary analyte systems are presented. These analyte systems consisted of a bromine-containing API injected with either DFBC, 2,6-DFBB, or 2,4-DFBB.

Results and Discussion

Figure 92 shows the signal response of the UV detector to a 5 µL injection of a 1000 ppm mixture of the bromine-containing API and 2,6-DFBB. Widths at the baseline are approximately 30 seconds or less. Comparing this chromatogram with one obtained with HPLC-USN-MD-ICP-MS (Figure 93) for the same compounds at the same concentrations, it is observed that there is a sharp reduction in ion intensity for 2,6-DFBB as compared to the API.

A similar reduction in sensitivity is observed for DFBC (Figure 94). Table 26 lists the melting points for 2,6-DFBB and DFBC. Both compounds have melting points well below the standard temperature settings of the MD (160 °C) and USN (140 °C). For comparison, the melting point of the API is in the range of 241-245 °C, well above the temperature settings of the MD and USN. Melting points do not provide a direct correlation to a compounds' absolute volatility. However, under standard sample introduction conditions, 2,6-DFBB and DFBC analyte particulates will be present as a liquid while the API will be a solid. The vapor pressure of the 2,6-DFBB and DFBC will be much greater compared to the API. The decreased

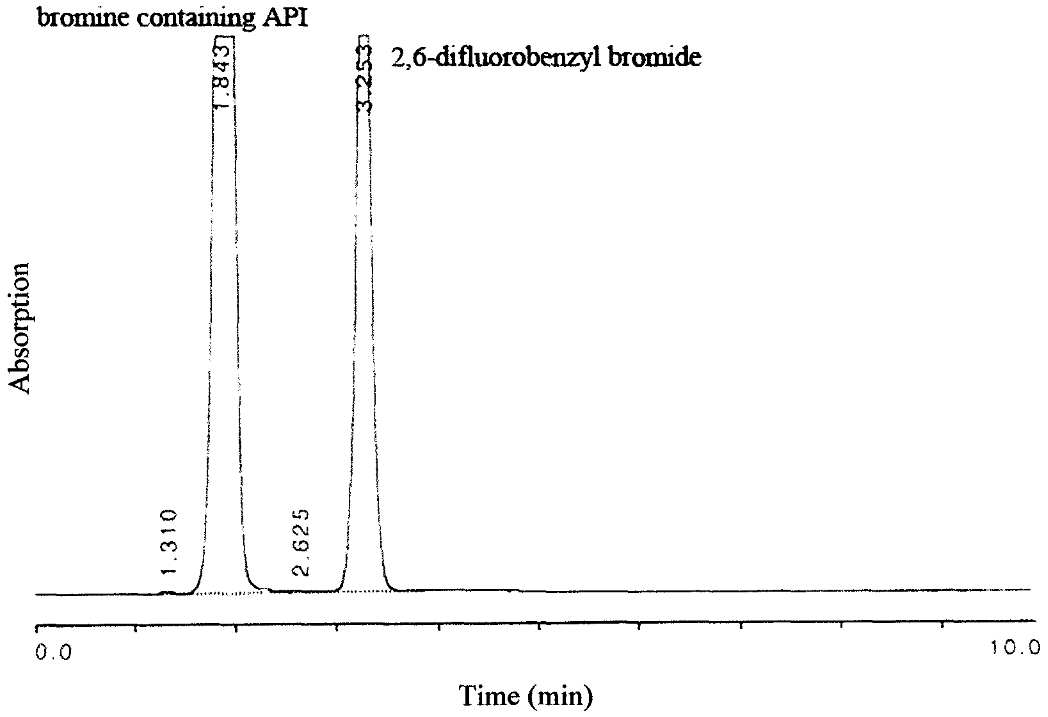

Figure 92. HPLC-UV-VIS trace for a 5 μL injection of a 1000 ppm mixture of the bromine-containing API and 2,6-DFBB.

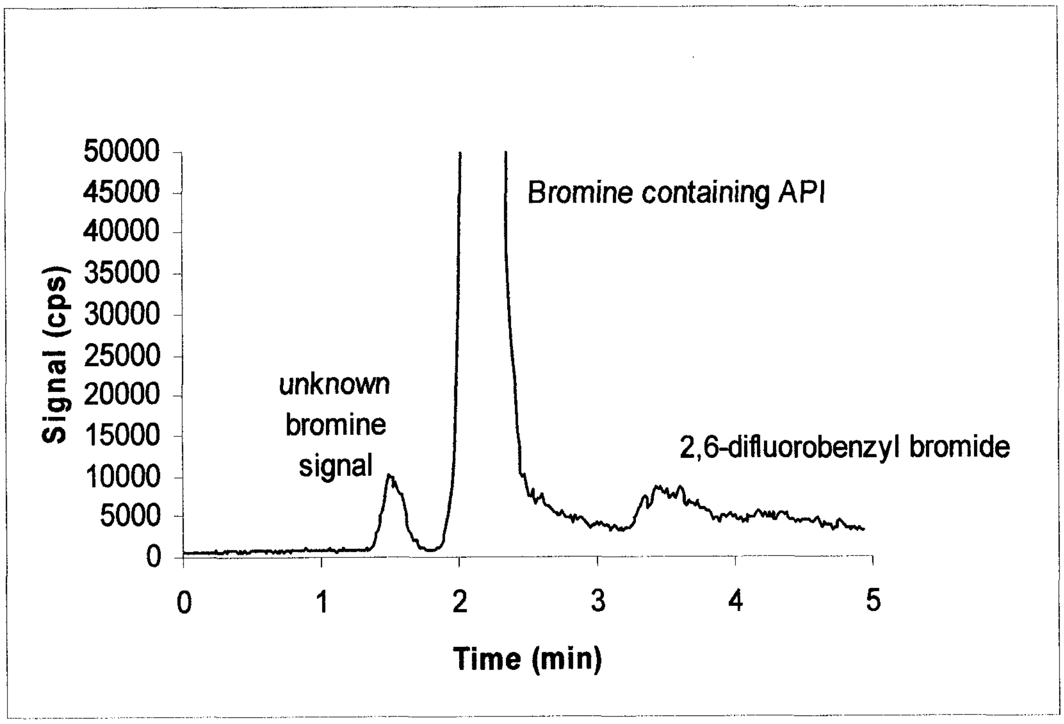

Figure 93. HPLC-ICP-MS trace monitoring $^{79}Br^+$ for a 5 μL injection of a 1000 ppm mixture of the bromine-containing API and 1 ppt 2,6-DFBB.

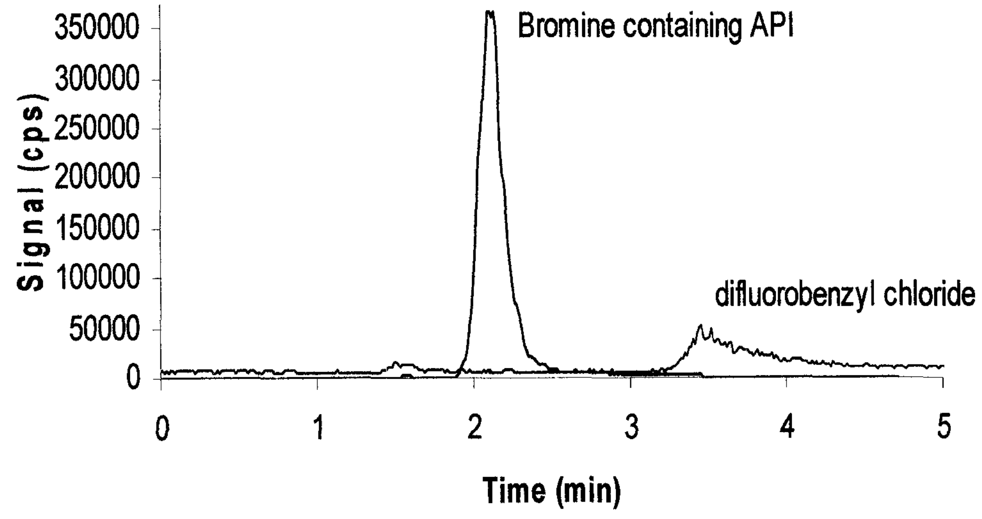

Figure 94. HPLC-ICP-MS trace of 5 μL injection of a 1000 ppm mixture of the bromine-containing API and DFBC. The blue trace corresponds to the $^{79}Br^{+}$ signal. The red trace corresponds to the $^{35}Cl^{+}$ signal.

sensitivity of 2,6-DFBB and DFBC, in comparison to the API, may be caused by the greater volatility of these compounds under MD conditions.

Table 26. Physical properties of select organohalides.

Physical Property	2,6-DFBB	DFBC
Molecular Weight (g/mol)	207.02	162.67
Melting Point (°C)	52-55	34-38

It is apparent from experiments in our laboratory that sensitive nonmetal detection is possible with nonvolatile compounds. It has been shown that there is a large detector response, relative to the volatile analytes, for a 1000 ppm solution of the bromine-containing API. Vitamin B_{12} is also a nonvolatile compound with a melting point of 300 °C. Figure 95 shows an HPLC-ICP-MS chromatogram of a 5 µL injection of a 45 ppm phosphorus solution of vitamin B_{12}. The phosphorus ion signal was monitored. There is a large detector response for this compound. Separation of vitamins B_{12} and B_1 are currently being performed in our laboratory to further demonstrate the utility of this technique.

Discussion of Chromatographic Figures of Merit for ICP-MS Detection

To gauge the performance of the USN-MD-ICP-MS relative to the UV-VIS detector, it is necessary to calculate the pertinent chromatographic figures of merit.

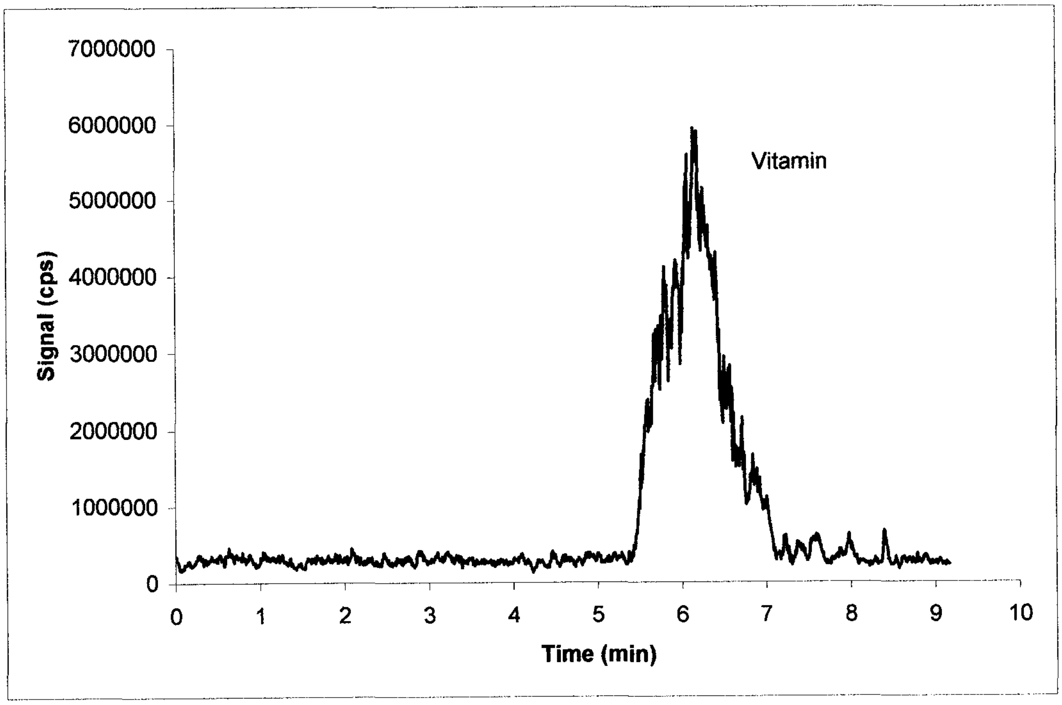

Figure 95. HPLC-ICP-MS trace monitoring $^{31}P^{+}$ for a 5 μL injection of a 45 ppm phosphorus solution of vitamin B_{12}.

The resolution and number of theoretical plates were calculated for the separation of 2,6-DFBB and the bromine-containing API. Additionally, peak tailing factors were calculated for the API and 2,4-DFBB in the ICP-MS chromatograms.

The number of theoretical plates for the UV-VIS chromatograms was calculated by approximating the peak as a triangle. This allowed a direct determination of the peak width at half height for peaks that saturate the detector. For ICP-MS chromatograms, a modified equation[96] for the calculation of the number of theoretical plates was used due to the high degree of peak asymmetry observed for 2,6-DFBB.

$$N = \frac{41.7\left(\frac{t_r}{w_{0.1}}\right)^2}{1.25 + \frac{B}{A}} \qquad (4.1)$$

where t_r is the retention time, $w_{0.1}$ is the peak width at 10% of the peak maximum, B is the width of the right side of the peak, and A is the width of the left side of the peak. Resolution was calculated using the standard resolution equation given previously (Eqn. 1.6). Peak tailing factors were calculated for the API, 2,6-DFBB, and 2,4-DFBB as shown in Figure 9.

Table 27 shows the resolutions, tailing factors, and number of theoretical plates calculated from UV-VIS and ICP-MS chromatograms for 2,6-DFBB. Figures 92 and 93 are representative UV-VIS and ICP-MS chromatograms used for these calculations. Figure 96 highlights the peak tailing observed with all of the volatile analytes in ICP-MS chromatograms.

Table 27. Comparison of select HPLC figure of merit for 2,6-DFBB.

HPLC Figures of Merit	ICP-MS Detection	UV Detection
Resolution	0.6	2.45
Tailing Factor	4.5	1
Number of theoretical plates (N)	30	1800

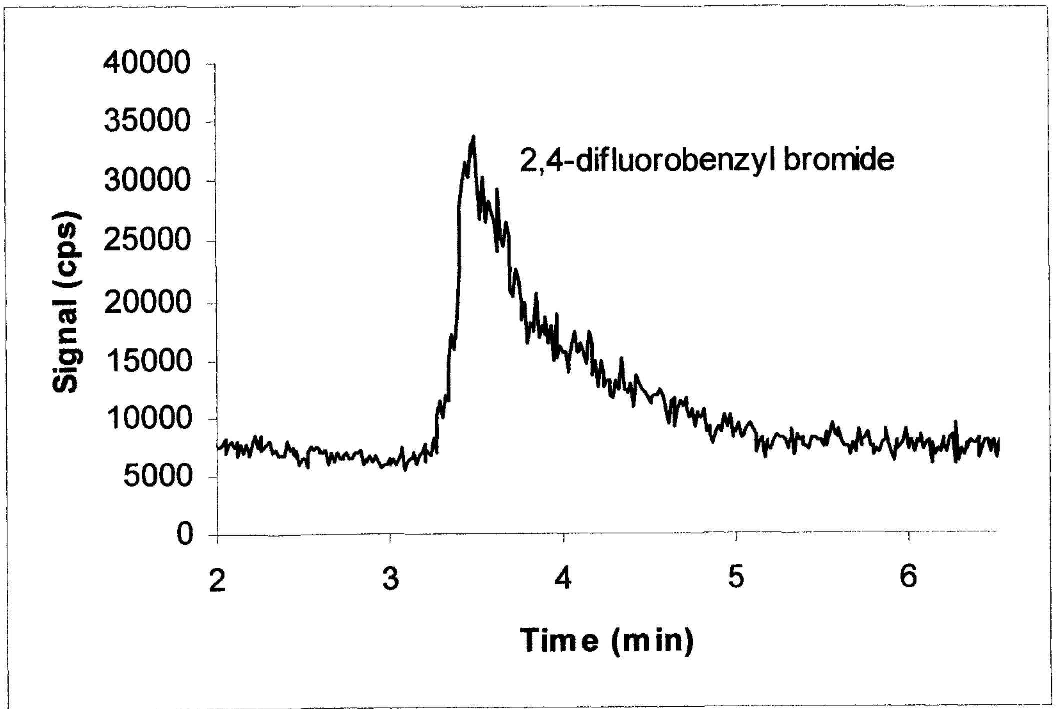

Figure 96. HPLC-ICP-MS trace monitoring $^{79}Br^+$ for a 5μL injection of a 1 ppt solution of the bromine-containing API.

The average number of theoretical plates calculated for 2,6-DFBB from ICP-MS chromatograms was 30. For UV-VIS detection, the number of theoretical plates was 1800. The large difference in plate counts between the ICP-MS and UV trace indicates significant band broadening. This is likely occurring in the sample introduction portion of the ICP-MS system. The average resolution calculated for this separation was 0.6 using the ICP-MS chromatogram. This is not sufficient to provide baseline resolution between two analyte peaks of equal intensity. However, it is observed that baseline resolution is achieved due to the low intensity of the 2,6-DFBB analyte peak. The resolution value, however, indicates that the chromatographic method should be improved to allow for complete separation, especially if sensitivities can be increased for the volatile analytes. Complete separation is desired due to the potential for ionization interferences when analytes co-elute. The resolution obtained with UV-VIS detection was 2.45, more than adequate to achieve baseline resolution. Peak tailing was also observed for all the volatile analytes. Figure 96 shows a zoomed view of the 2,4-DFBB analyte peak, demonstrating the large degree of tailing. The average tailing factor in ICP-MS chromatograms for 2,6-DFBB was 4.5. There was no peak tailing observed in UV-VIS chromatograms. Although not tabulated, the average tailing factor observed for the less volatile API was 1.5 in ICP-MS chromatograms.

Although not shown, resolution and theoretical plate numbers for both UV-VIS and ICP-MS are similar for the separation of the bromine-containing API, 2,4-DFBB, and DFBC.

Conclusion

The model separation systems presented in this dissertation are selected examples of the best results achieved to date. These examples also clearly demonstrate some of the challenges in utilizing HPLC-USN-MD-ICP-MS to detect nonmetal analytes. The results presented do not include failed separation examples, method development to optimize system performance, or other optimization procedures. Likewise, many of these experiments are ongoing and thus quantitative results such as linearity studies, mobile phase composition effects, and detection limit studies are yet to be determined. The data presented in this chapter are qualitative in nature and demonstrate initial results obtained in our laboratory.

Analyte peaks from ICP-MS chromatograms of the API and the model impurities exhibit significant broadening when compared to UV chromatograms. The volatile compounds show great reductions in sensitivities. The ICP-MS chromatographic figures of merit are not currently adequate, especially for volatile analytes. Much of the broadening seen with highly volatile organic impurities is thought to be a function of a combination of the temperature in the “J-tube” (140 °C) and in the membrane desolvator (160°C), and the volumes of the spray chamber, “J-tube,” and condenser region of the ultrasonic nebulizer (approximately 140 mL). It is likely that this combination creates a large dead volume. The aforementioned problems with the USN, coupled with the turbulence of the aerosol stream in the spray chamber and several 180° turns, may lead to significant mixing of the eluent and cause further band broadening.

A volatility study should be performed to clearly define the range of analyte molecules and physical properties that lead to efficient detection of nonmetal heteroatoms. Also, the investigation of alternative nebulizer, spray chamber, and desolvating methods should be performed. It is possible that low volume nebulizers and spray chambers may lead to increased transport efficiencies for volatile analytes. This may lead to beneficial sensitivity enhancements for nonmetal-containing analytes in HPLC-ICP-MS applications.

CHAPTER 5

CONCLUSIONS AND FUTURE DIRECTIONS

Overall Summary

This dissertation reports efforts to improve the analytical performance of USN-MD-ICP-MS as an HPLC detector for the analysis of heteroatom-containing pharmaceutical compounds. There were three core studies conducted in pursuit of this objective. First, an HPLC mobile phase and buffer study was completed. Second, the utility of adding oxygen, nitrogen, and helium as supplemental gases to the nebulizer gas flow was established. Finally, several model heteroatom-containing compounds were speciated and detected by HPLC-USN-MD-ICP-MS.

HPLC Mobile Phase and Buffer Study Conclusions and Suggested Future Directions

The purpose of conducting this study was to determine which common HPLC mobile phases and buffers led to sensitive detection of heteroatoms in pharmaceutical compounds. Specifically, the response of the USN-MD-ICP-MS and AES to phosphorus as phosphomycin was determined. Ultimate detection limits in the hundreds of parts per billion were obtained for AES detection. Signal response as a function of mobile phase composition showed minimal variation. It was determined that HPLC solvent programming can be used with USN-MD-ICP-AES detection.

For ICP-MS, ultimate detection limits in the range of single parts per billion were obtained. Signal response as a function of mobile phase composition showed a large decrease in sensitivity when organic solvent was nebulized. The effects of buffers on the analytical signals were more pronounced in ICP-MS experiments. TBAH and HepS caused the largest signal and detection limit degradations. Isocratic separation conditions are suggested due to the large sensitivity decrease as the amount of organic solvent content is increased.

The scattered behavior of the phosphorus signal to the different mobile phase compositions and buffers in ICP-MS detection indicate that trends in signal and background behavior need to be established for each specific analyte. The background interferences and ionization processes will be different for a chlorine-containing analyte as opposed to a phosphorus-containing analyte. Additionally, a buffer and mobile phase study should be performed with alternative sample introduction methods, such as low flow, high efficiency nebulizers.

Supplemental Nebulizer Gas Addition Conclusions and Future Directions

The addition of supplemental gases to the nebulizer gas flow caused signal depression for nearly all analytes and gases studied. Signal depression is likely due to shifts in the analytical zone of the plasma and plasma cooling, leading to less efficient ionization.

Results for oxygen addition experiments showed signal depression for sulfur-, phosphorus-, and chlorine-containing analytes. Results for fluorine were scattered. Although signal depression was noted for most analytes and oxygen flow rates, detection limits generally remained low. Efficient combustion of deposited carbon was observed when oxygen comprised 6% of the nebulizer gas flow rate.

Addition of nitrogen to the nebulizer gas flow caused a decrease in the S/B ratio for both phosphorus and sulfur analytes. Background ion interferences were greater for phosphorus due to the formation of nitrogen-containing interferences. At higher forward powers, a greater range of nitrogen gas flow rates yielded measurable analytical and background signals.

Addition of helium did not produce any significant signal or detection limit enhancements. It is believed that helium did not become ionized in the argon plasma and did not significantly affect the analytical properties of the plasma.

Suggested future studies include supplementing the auxiliary or coolant gas flow with nitrogen and helium. Increasing the fraction of helium present in the plasma may allow it to be ionized efficiently, allowing a complete investigation into its utility as a supplemental gas. Also, the results presented produced trends consistent with an explanation that the analytical zone of the plasma shifts with supplemental gas addition. However, this shift can be unambiguously demonstrated by imaging the plasma with a hyper-spectral imaging instrument, utilized in our laboratory. This instrument can be used as a plasma diagnostic tool. The regions of the plasma where the maximum ion and excited state atom concentration is located can be visually determined with this instrument. Combining the ion counts obtained from the mass spectrometer with imaging data for different supplemental gases and flow rates will allow for a comprehensive determination of the ionization and excitation processes occurring in the ICP during these experiments.

HPLC-USN-MD-ICP-MS Experiment Conclusions and Future Directions

The separations and detections of a bromine-containing API with, 2,6-DFBB, 2,4-DFBB, and DFBC have been demonstrated. Significant band broadening and sensitivity degradation was noted for ICP-MS chromatograms as compared to UV-VIS chromatograms. This was more pronounced with 2,6-DFBB, 2,4-DFBB, and DFBC. It was observed that analytes with melting points below that found in the sample introduction system had increased tailing, reduced sensitivity, and poor chromatographic figures of merit. It is believed that the deterioration in sensitivity and chromatographic figures of merit is due to a combination of the heating elements within the sample introduction system and the large internal volume of the USN-MD.

Future investigations should include model analyte systems that are lower in volatility to unambiguously show the utility of USN-MD-ICP-MS as a detector for HPLC. A study on the relationship between analyte signal and peak shape with volatility-correlated physical properties should be performed. This will more clearly define which analytes can be sensitively detected with USN-MD-ICP-MS.

The investigation of low flow nebulizers and spray chambers to alleviate analyte loss and band broadening should be performed. The incorporation of low flow nebulizers may allow the complete removal of the MD portion of the sample introduction system due to the lower solvent load on the plasma.

REFERENCES

1. NIST Chemistry WebBook, *http://webbook.nist.gov/chemistry.*
2. J. Ingle and S. Crouch, *Spectrochemical Analysis,* Prentice-Hall, Upper Saddle River, NJ. 1988.
3. Z. Zhang and K. Wagatsuma, *J. Anal. At. Spectrom.* **17** (2002) 699-703.
4. A. Matsumoto and T. Nakahara, *Can. J. of Anal. Sci. Spectrosc.* **49** (2004) 334-345.
5. J. Koch, M. Okruss, J. Franzke, S. V. Florek, K. Niemax and H. Becker-Ross, *Spectrochim. Acta, Part B* **59** (2004) 199-207.
6. J. A. C. Broekaert and V. Siemens, *Spectrochim. Acta, Part B* **59** (2004) 1823-1839.
7. J. W. Carnahan and G. M Hieftje, *Spectrochim. Acta, Part B.* **47** (1992) 731-739.
8. S. Greenfield, I. Jones and C. T. Berry, *Analyst* **89** (1964) 713-720.
9. R. H. Wendt and V. A. Fassel, *Anal. Chem.* **37** (1965) 920-922.
10. R. Thomas, *Spectroscopy* **8** (2) 2003.
11. W. C. Davis, S. S. Vander Pol, M. M. Schantz, S. E. Long, R. D. Day and S. J. Christopher, *J. Anal. At. Spectrom.* **19** (2004) 1546-1551.
12. L. Dussubieux and L. van Zelst, *Appl. Phys. A* **79** (2004) 353-356.
13. R. S. Houk, *Anal. Chem.* **58** (1986) 97A-104A.
14. A. Montaser, *Inductively Coupled Plasma Mass Spectrometry*, Wiley-Inc., USA, 1998.

15. S-A. E. O'Brien, J. A. McLean, B. W. Acon, B. J. Eschelman, W. F. Bauer and A. Montaser, *Appl. Spectrosc.* **56** (2002) 1006-1012.

16. S. Rauch, M. Motelica-Heino, G. M. Morrison and O. F. X. Donard, *J. Anal. At. Spectrom.* **15** (2000) 329-334.

17. S. W. Jenniss, S. A. Katz and R. W. Lynch, *Applications of Atomic Spectrometry to Regulatory Compliance Monitoring* Wiley-VCH, New York, 1997.

18. S. Kozono, S. Takahashi and H. Haraguchi, *Anal. Bioanal. Chem.* **372** (2002) 542-548.

19. J. S. Crighton, J. Carroll, B. Fairman, J. Haines and M. Hinds, *J. Anal. At. Spectrom.* **11** (1996) 461R-508R.

20. F. Vanhaecke, M. Resano and L. Moens, *Anal. Bioanal. Chem.* **374** (2002) 188-195.

21. N. Lewen, S. Mathew, M. Schenkenberger and T. Raglione, *J. Pharm. Biomed. Anal.* **35** (2004) 739-752.

22. J. Huang, X. Hu, J. Zhang, K. Li, Y. Yan and X. Xu, *J. Pharm. Biomed. Anal.* **40** (2006) 227-234.

23. C. J. Duckett, N. J. C. Bailey, H. Walker, F. Abou-Shakra, I. D. Wilson, J. C. Lindon, J. K. Nicholson, *Rapid Comm. Mass Spectrom.*. **16** (2002) 245-247.

24. A. De Kok, M. Hiemstra and U. A. Brinkman, *J. Chromatogr., A* **623** (1992) 265-276.

25. S. Wongyai, *J. Chromatogr., A* **870** (2000) 217-220.

26. P. Manzi, G. Panfili and L. Pizzoferrato, *Chromatographia* **43** (1996) 89-93

27. W. Spivak and M. C. Carey, *Biochem. J.* **225** (1985) 787-805.

28. Q. Hu, G. Yang, J. Yin and Y. Yao, *Talanta* **57** (2002) 751-756.

29. L. Novakova and P. Solich, *J. Chromatogr., A* **1088** (2005) 24-31.

30. I. Baranowska, P. Markowski and J. Baranowski, *Anal. Chim. Acta* **570** (2006) 46-58.

31. C. Camarasu, C. Madichie and R. Williams, *Trends Anal. Chem.* **25** (2006) 768-777.

32. L. Weiyong, *J. Chromatogr., A* **1046** (2004) 297-301.

33. H. Li and G. W. Sluggett, *J. of Pharma. and Biomed. Analysis* **39** (2005) 486-494.

34. D. C. Harris, *Quantitative Chemical Analysis 6th Ed.* W. H. Freeman, New York, 2002.

35. L. L. Ng, *Reviewer Guidance; Validation of Chromatographic Methods* (1994), www.fda.gov/CDER/GUIDANCE/cmc3.pdf

36. http://www.lcresources.com/resources/getstart/t.htm

37. D. A. Skoog, *Principles of Instrumental Analysis* Internation Thomson, 2001.

38. C. R. Cho and R. P. Ashdown, *ICP-MS Application Note* **32** www.varianinc.com.

39. T. W. May and R. H. Wiedmeyer, *At. Spectrosc.* **19** (1998) 150-155.

40. *ICP-MS A Primer*, http://icpms.geology.ucdavis.edu/AgilentICPMSprimer.pdf

41. X. Bu, T. Wang and G. Hall, *J. Anal. At. Spectrom.* **18** (2003) 1443-1451.

42. E. H. Evans, J-C. Wolff and C. Eckers, *Anal. Chem.* **73** (2001) 4722-4728.

43. D. W. Koppenaal, G. C. Eiden and C. J. Barinaga, *J. Anal. At. Spectrom.* **19** (2004) 561-570.

44. C. H. Yang and S. J. Jiang, *Spectrochim. Acta, Part B* **59** (2004) 1389-1394.

45. J. Mora, J. L. Todoli, A. Canals and V. Hernandis, *J. Anal. At. Spectrom.* **12** (1997) 445-451.

46. S. Maestre, J. Mora, J.-L. Todoli and A. Canals, *J. Anal. At. Spectrom.* **14** (1999) 61-67.

47. M. A. Tarr, G. Zhu and R. F. Browner, *Appl. Spectrosc.* **45**, 1424 (1991).

48. K. W. Olsen, W. J. Haas and V. A. Fassel, *Anal. Chem.* **49** (1977) 632-637.

49. H.. G. Infante, G. O'Connor, M. Rayman, R. Wahlen, J. Entwisle, P. Norris, R. Hearn and T. Catterick, *J. Anal. At. Spectrom.* **19** (2004) 1529-1538.

50. W. Tittes, N. Jakubowski, D. Stuwer and G. Tolg, *J. Anal. At. Spectrom.* **9** (1994) 1015-1020.

51. F. Tubaro, F. Barbangelo, R. Toniolo, F. Di Narda and G. Bontempelli, *Ann. Chim. (Rome, Italy)* **89** (1999) 863-872.

52. www.cetac.com

53. K. Kahen, K. Jorabchi and A. Montaser, *J. Anal. At. Spectrom.* **21** (2006) 588-591.

54. D. Das and J. W. Carnahan, *Anal. Chim. Acta* **444** (2001) 229-240.

55. K. Kwok, J. E. Carr, G. K. Webster and J. W. Carnahan, *Appl. Spectrosc.* **60** (2006) 80-85.

56. A. N. Heyrman and R. A. Henry, *Technical Bulletin* http://www.hplcsupply.com/pdf/App_9.pdf

57. "Preparing Buffered Mobile Phases for Reversed Phase HPLC", *Technical Report* http://www.mac-mod.com/pdf/TR-BufferedMP.pdf

58. S. F. Durrant, Fresnius *J. Anal. Chem.* **347** (1993) 389-392.

59. M. Kovačevič, R. Leber, S. D. Kohlwein and W. Goessler, *J. Anal. At. Spectrom.* **19** (2004) 80-84.

60. E. Björn and W. Frech, *Anal. Bioanal. Chem.* **376** (2003) 274-278.

61. I. B. Brenner, A. Zander, M. Plantz and J. J. Zhu, *J. Anal. At. Spectrom.* **12** (1997) 273-279.

62. M. Cai, D. A. Haydar, A. Montaser and A. Mostaghimi, *Spectrochim. Acta, Part B* **52** (1997) 369-386.

63. A. P. Voderheide, J. Meija, M. Montes-Bayón and J. A. Caruso, *Agilent ICP-MS Journal* **16** (2003) 4.

64. D. Beauchemin and J. M. Craig, *Spectrochim. Acta, Part B* **46** (1991) 603-614.

65. A. E. Holliday and D. Beauchemin, *J. Anal. At. Spectrom.* **18** (2003) 1109-1112.

66. N. Fidalgo-Used, M. Montes-Bayón, E. Blanco-González, and A. Sanz-Medel, J. *Anal. At. Spectrom.* **20** (2005) 876-882.

67. S. Branch, L. Ebdon and P. J. Oneill, *J. Anal. At. Spectrom.* **9** (1994) 33-37.

68. J. Wang, E. H. Evans, and J. A. Caruso, *J. Anal. At. Spectrom.* **7** (1992) 929-936.

69. D. Pröfrock, P. Leonhard, S. Wilbur and A. Prange, *J. Anal. At. Spectrom.* **19** (2004) 623-631.

70. G. Xiao and D. Beauchemin, *Can.* J. *Anal. Sci. Spectrosc.* **46** (2001) 28-37.

71. J. W. H. Lam and G. Horlick, *Spectrochim. Acta, Part B* **45** (1990) 1313-1325.

72. N. N. Sesi, A. MacKenzie, K. E. Shanks, P. Yang and G. M. Hieftje, *Spectrochim. Acta, Part B* **49** (1994) 1259-1282.

73. S-H. Nam, W. R. L. Masamba and A. Montaser, *Anal. Chem.* **65** (1993) 2784-2790.

74. S-H. Nam, H. Zhang, M. Cai, J-S. Lim and A. Montaser, *Fresenius J. Anal. Chem.* **355** (1996) 510-520.

75. T. M. Castillano, J. J. Giglio, E. H. Evans and J. A. Caruso, *J. Anal. At. Spectrom.* **12** (1997) 383-385.

76. H. Hayashi, S. Furuzawa,T. Tanaka and M. Hiraide, *J. Anal. At. Spectrom.* **19** (2004) 773-774.

77. D. A. McGregor, K. B. Cull, J. M. Gehlhausen, A. S. Viscomi, M. Wu, L. Zhang and J. W. Carnahan, *Anal. Chem.* **60** (1988) 1089A-1098A.

78. K. J. Jones and J. W. Carnahan, *Spectrochim. Acta, Part B* **47** (1992) 1229-1240.

79. A. P. Vonderheide, M. Montes-Bayón and J. A. Caruso, *J. Anal. At. Spectrom.* **17** (2002) 1480-1485.

80. F. Vanhaecke, S. Saverwyns, G. Wannemacker, L. Moens and R. Dams, *Anal. Chim. Acta* **419** (2000) 55-64.

81. X. Pu, B. Hu, Z. Jiang and C. Huang, *Analyst* **130** (2005) 1175-1181.

82. M. Montes-Bayon, D. Profrock, A. Sanz-Medel and A. Prange, *J. Chromatogr., A* **1114** (2006) 138-144.

83. J. D. Whitely and F. Murray, *Geochem. Exploration Environ. Anal.* **5** (2005) 3-10.

84. R. G. Wuilloud, S. S. Kannamkumarath and J. A. Caruso, *Anal. Bioanal. Chem.* **379** (2004) 495-503.

85. S. Hann, Z. Stefanka, K. Lenz and G. Stingeder, *Anal. & Bioanal. Chem.* **381** (2005) 405-412.

86. E. Bakkaus, R. N. Collins, J. L. Morel and B. J. Gouget, *J. Chromatogr., A* **1129** (2006) 208-215.

87. C. J. Welch, Q. Tu, T. B. Wang, C. Raab, P. Wang, X. J. Jia, X. D. Bu, D. Bykowski, B. Hohenstaufen and M. P. Doyle, *Adv. Synth. Catal.* **348** (2006) 821-825.

88. C. B'Hymer and J. A. Caruso, *J. Chromatogr.*, A **1114** (2006) 1-20.

89. M. Kovačevic, R. Leber, S. D. Kohlwein and W. Goessler, *J. Anal. At. Spectrom.* **19** (2004) 80-84.

90. O. Quiñones, S. A. Snyder, J. A. Cotruvo and J. W. Fisher, *Toxicology* **221** (2006) 229-234.

91. D. D. Richard, B. B. M. Sadi and J. A. Caruso, *J. Anal. At. Spectrom.* **21** (2006) 396-403.

92. P. Marshall, O. Heudi, S. Mckeown, A. Amour and F. Abou-Shakra, *Rapid Commun. Mass Spectrom.* **16** (2002) 220-228.

93. B. P. Jensen, B. Gammelgaard, S. H. Hansen and J. V. Andersen, *J. Anal. At. Spectrom.* **18** (2003) 891-896.

94. M. Edler, N. Jakubowski and M. Linscheid, *J. Mass Spectrom.* **41** (2006) 507-516.

95. M. Shah and J. A. Caruso, *J. Sep. Sci.* **28** (2005) 1969-1984.

96. L. Ohannesian and A. J. Streeter, *Handbook of Pharmaceutical Analysis.* Marcel Dekker Inc. New,York, NY. (2002).